Tailoring *Clostridium ljungdahlii* for Improved Ethanol Production by Genetic Engineering of the Aldehyde:Ferredoxin Oxidoreductase (AOR) and Chemostat Fermentation

Dissertation

der Mathematisch-Naturwissenschaftlichen Fakultät

der Eberhard Karls Universität Tübingen

zur Erlangung des Grades eines

Doktors der Naturwissenschaften

(Dr. rer. nat.)

vorgelegt von

M. Sc. Sarah Schulz

aus Köln

Tübingen

2022

Gedruckt mit Genehmigung der Mathematisch-Naturwissenschaftlichen Fakultät der Eberhard Karls Universität Tübingen.

Tag der mündlichen Qualifikation: 10.10.2022
Dekan: Prof. Dr. Thilo Stehle
1. Berichterstatter/-in: Prof. Dr. Largus T. Angenent
2. Berichterstatter/-in: PD Dr. Evi Stegmann

Für Anja, Herbert, Max und Simon.

ACKNOWLEDGMENTS

ABSTRACT

One of today's major global challenges is the continued global warming and emissions of greenhouse gases. In recent years, the effects of increasing global surface temperatures have become more and more pronounced. Society is facing reoccurring extreme weather events, such as floodings, extreme droughts, and storms. Ecosystems are destroyed and formerly inhabited areas become uninhabitable. To halt the increase of the global temperature and consequently prevent further damage, it is essential to contain greenhouse gas emissions. The most recent report from the Intergovernmental Panel on Climate Change (IPCC) shows that to restrict global warming to 1.5°C, global net-zero carbon dioxide emissions must be achieved in the early 2050s. As a means of achieving that, a transition towards a circular economy is necessary. Synthesis gas fermentation is a very promising technology to recycle gas mixtures containing carbon dioxide (CO_2), hydrogen gas (H_2), and carbon monoxide (CO). Acetogenic bacteria fix the carbon from the gas mixture and convert it to acetate and ethanol. These chemicals can either be used directly, for example, ethanol can be used as a drop-in fuel, or further converted to value-added products for the chemical industry. The process allows for simultaneous recycling of waste gases and the production of platform chemicals or biofuels. Acetogens utilize an ancient linear pathway for carbon fixation, the Wood-Ljungdahl pathway, thriving at the thermodynamic limit of life. The Wood-Ljungdahl pathway produces no net ATP, and energy conservation is facilitated *via* two membrane-bound complexes, a *Rhodobacter* Nitrogen Fixation-like complex (Rnf) and an ATPase. *Clostridium ljungdahlii* is a model acetogen, which has been isolated from chicken yard waste and described in 1993. Since then, researchers have put effort into sequencing and annotating the genome, developing genome editing tools, and optimizing fermentation conditions to achieve maximum production rates of the fermentation products. Recent results show that an aldehyde:ferredoxin oxidoreductase (AOR) is a key enzyme in the ethanol production pathway during autotrophic growth. The genome of *C. ljungdahlii* contains three genes for the AOR, two tungsten-containing variants (CLJU_c20110, CLJU_c20210), and the more oxygen-tolerant molybdenum-containing variant (CLJU_c24130). The AOR reduces acetic acid to acetaldehyde using reduced ferredoxin (Fd_{red}). Acetaldehyde is converted to ethanol by an alcohol dehydrogenase in a thermodynamically favorable reaction, making the AOR reaction a rate-limiting step.

In this dissertation, we focus on elucidating the roles of the two isoforms AOR1 and AOR2 for ethanol production in *C. ljungdahlii.* We present an efficient CRISPR/Cas9 genome editing tool. We apply this tool for the deletion of *aor* genes individually and in combination, and present the reported phenotype changes. Additionally, we conceptualize a system for heterologous and homologous production of AOR enzymes and ferredoxin in *Escherichia coli.* Finally, we present the first characterization of *C. ljungdahlii* wildtype during chemostat fermentation using CO as the sole carbon and energy source. We show that

ethanol production can be enhanced drastically by more than 230% by adding external acetate to the feed medium.

ABSTRACT (GERMAN)

Eine der größten globalen Herausforderungen unserer Zeit ist die anhaltende globale Erderwärmung und der fortwährende Ausstoß von Treibhausgasen. In den letzten Jahren haben sich die Auswirkungen des Anstiegs der globalen Oberflächentemperaturen immer stärker bemerkbar gemacht. Unsere Gesellschaft ist mit immer wiederkehrenden extremen Wetterereignissen wie Überschwemmungen, extremen Dürren und Stürmen konfrontiert. Ökosysteme werden zerstört und ehemals bewohnte Gebiete werden unbewohnbar. Um den Anstieg der globalen Temperatur zu stoppen und damit weitere Schäden zu verhindern, müssen die Treibhausgasemissionen unbedingt eingedämmt werden. Aus dem jüngsten Bericht des *Intergovernmental Panel on Climate Change* (IPCC) geht hervor, dass die Kohlendioxidemissionen bis Anfang der 2050er Jahre weltweit auf Null reduziert werden müssen um die globale Erderwärmung auf 1,5°C zu begrenzen. Um dies zu erreichen ist ein Übergang zu einer Kreislaufwirtschaft erforderlich. Die Synthesegasfermentation ist eine vielversprechende Technologie, um Gasgemische aus Kohlendioxid (CO_2), Wasserstoff (H_2) und Kohlenmonoxid (CO) zu recyceln. Acetogene Bakterien binden den Kohlenstoff aus dem Gasgemisch und wandeln ihn in Acetat und Ethanol um. Diese Chemikalien können entweder direkt verwendet werden, z. B. kann Ethanol als *Drop-in*-Kraftstoff eingesetzt werden, oder sie werden zu höherwertigen Produkten für die chemische Industrie weiterverarbeitet. Das Verfahren ermöglicht die gleichzeitige Verwertung von Abgasen und die Herstellung von Plattformchemikalien oder Biokraftstoffen. Acetogene Bakterien nutzen einen evolutionär ursprünglichen, linearen Stoffwechselweg zur Kohlenstofffixierung, den Wood-Ljungdahl-Weg. Dieser Stoffwechselweg ermöglicht keine Netto-ATP-Produktion, daher werden für die Energieproduktion zwei membrangebundene Komplexe, der *Rhodobacter Nitrogen Fixation-like complex* (Rnf) und eine ATPase, benötigt. *Clostridium ljungdahlii* ist ein Modellorganismus, der 1993 aus Hühnerhofabfällen isoliert und beschrieben wurde. Seitdem haben Forschende das Genom sequenziert und annotiert, gentechnische Werkzeuge entwickelt und die Fermentationsbedingungen optimiert, um maximale Produktionsraten der Fermentationsprodukte zu erzielen. Jüngste Ergebnisse zeigen, dass eine Aldehyd:Ferredoxin-Oxidoreduktase (AOR) ein Schlüsselenzym des Ethanol-Produktionsweges während des autotrophen Wachstums ist. Das Genom von *C. ljungdahlii* enthält drei Gene für die AOR, zwei wolframhaltige Varianten (CLJU_c20110, CLJU_c20210) und die sauerstofftolerantere molybdänhaltige Variante (CLJU_c24130). Die AOR reduziert Essigsäure mit Hilfe von reduziertem Ferredoxin (Fd_{red}) zu Acetaldehyd. Dieses Acetaldehyd wird durch eine Alkoholdehydrogenase in einer thermodynamisch günstigen Reaktion in Ethanol umgewandelt, wodurch die AOR-Reaktion zu einem geschwindigkeitslimitierenden Schritt wird.

Der Fokus dieser Dissertation liegt auf der Entschlüsselung der Rollen der beiden Isoformen AOR1 und AOR2 für die Ethanol Produktion in *C. ljungdahlii*. Wir stellen ein effizientes CRISPR/Cas9-*Genome-*

Editing-Werkzeug vor. Wir nutzen dieses Werkzeug für die Deletion von *aor* Genen einzeln und in Kombination und stellen die beobachteten Veränderungen des Phänotyps vor. Außerdem konzipieren wir ein System für die heterologe und homologe Produktion von AOR-Enzymen und Ferredoxin in *Escherichia coli*. Abschließend präsentieren wir die erste Charakterisierung von *C. ljungdahlii* Wildtyp während einer Chemostat-Fermentation unter Verwendung von CO als einzige Kohlenstoff- und Energiequelle. Wir zeigen, dass die Ethanolproduktion durch die Zugabe von externem Acetat zum Nährmedium drastisch um mehr als 230% gesteigert werden kann.

TABLE OF CONTENTS

LIST OF ABBREVIATIONS

A	adenine (purine nucleobase)
Ac	acetate
ACK	acetate kinase
ACS	CODH/acetyl-CoA synthase complex
ADC	acetone decarboxylase
AdhE	bifunctional aldehyde/alcohol dehydrogenase
ALDC	acetolactate decarboxylase
ALE	adaptive laboratory evolution
ALS	acetolactate synthase
Amp	ampicillin
AOR	aldehyde:ferredoxin oxidoreductase
ATP	adenosin triphosphate
BCD	butyryl-CoA dehydrogenase
2,3-BDO	2,3-butanediol
bp	base pairs
C	cytosine (purimidine nucleobase)
°C	degree Celsius
Cas	CRISPR-associated
CDS	coding sequence
CIP	alkaline phosphatase, calf intestinal
Clr	clarithromycin
Cm	chloramphenicol
CO	carbon monoxide
CO_2	carbon dioxide
CODH	carbon monoxide dehydrogenase
Co-FeS-P	corrinoid iron-sulfur protein
CRISPR	clustered cegularly interspaced short palindromic repeats
CRISPRi	CRISPR interference
CRT	crotonase
CS	counter selection marker
CSTR	continuously stirred tank reactor
CTFA/B	acetoacetyl-CoA:acetate/butyrate-CoA-transferase
dCas9	nuclease-deficient Cas9

dd*Fn*Cas12a	DNase-deactivated *Fn*Cas12a
dH2O	deionized water
DNA	deoxyribonucleic acid
EB	elution buffer
EBT	Environmental Biotechnology
Ery	erythromycin
EtOH	ethanol
F	fructose
FAK	fatty acid kinase
FDH	formate dehydrogenase
Fd_{ox}	oxidized ferredoxin
Fd_{red}	reduced ferredoxin
FeS	iron-sulphur-cluster
F_1F_0 ATPase	F_1F_0 ATP synthase
FRT	flippase recognition target
FTS	formyl-THF synthetase
G	guanine (purin nucleobase)
gDNA	genomic DNA
Gln	glutamine
Glu	glutamic acid
h	hours
H_2	hydrogen
3HB	3-hydroxybutyrate
HBD	3-hydroxybutyryl-CoA dehydrogenase
His	histidine
HPLC	high-performance liquid chromatography
HRT	hydraulic retention time
HydABC	electron-bifurcating Fd_{ox} and NAD^+-dependent [FeFe]-hydrogenase
HytA-E	electron-bifurcating $NADP^+$-dependent [FeFe]-hydrogenase
IDT	Integrated DNA Technologies
IPCC	Intergovernmental Panel on Climate Change
Kan	kanamycin
kb	kilobases
L	liter
LB	lysogeny broth

LDH	lactate dehydrogenase
LHA	left homologous arm
Lys	lysine
M	molar
Mbp	megabasepairs
MBS	multiple-bioreactor system
MCS	multiple cloning site
MFC	mass flow controller
min	minutes
MIT	methyltransferase
µL	microliter
mL	milliliter
mM	millimolar
MPa	megapascal
mRNA	messenger RNA
MTII	methyltransferase II
MTC	methenyl-THF cyclohydrolase
MTD	methylene-THF dehydrogenase
MTF	methyltransferase
MTR	methylene-THF reductase
N_2	nitrogen
NAD(P)H	nicotinamide adenine dinucleotide (phosphate)
Nfn	NADH-dependent Fd_{red}:$NADP^+$ oxidoreductase
nm	nanometer
OD_{600}	optical density at 600 nm
ori	origin of replication
PAM	protospacer adjacent motif
PBS	phosphate saline buffer
PCR	polymerase chain reaction
PFOR	pyruvate:ferredoxin oxidoreductase
Phe	phenylalanine
PMF	the proton motive force
PP	Pressure Plus bottles
ppm	parts per million
Pro	proline

PS	positive selection marker
PTA	phosphotransacetylase
$P_{tetR-01}$	aTc-inducible promoter
PTF	phosphotransferase
RCM	reinforced clostridia medium
RHA	right homologous arm
RNA	ribonucleic acid
Rnf	membrane-associated and energy-conserving Fd_{red}:NAD^+ oxidoreductase
rpm	revolutions per minute
RT	room temperature
SDS-PAGE	sodium dodecyl sulfate–polyacrylamide gel electrophoresis
sec	seconds
Ser	serine
sgRNA	single-guide RNA
Spec	spectinomycin
T	thymine (purimidine nucleobase)
THF	tetrahydrofolate
THL	thiolase
Tm	thiamphenicol
tMFA	presented thermodynamic metabolic flux analysis
Trp	tryptophan
ts-ori	temperature-sensitive ori
WLP	Wood-Ljungdahl pathway
wt	wildtype

LIST OF FIGURES

LIST OF TABLES

CHAPTER 1
Motivation and Objectives

1.1 Motivation

During the last decade, research on the synthesis gas (syngas) fermentation platform has gained increasing momentum as the platform represents an attractive solution to counteract greenhouse gas emissions from industrial processes and waste disposal. In this anaerobic biological process, acetogenic bacteria convert syngas (mixtures of carbon dioxide [CO_2], hydrogen [H_2], and carbon monoxide [CO]) into fermentation products, such as acetate and ethanol, with their metabolism *via* the so-called Wood-Ljungdahl pathway. These products can be used either directly as fuel additives or as raw materials to synthesize higher-value chemicals such as polymers and plastics.

The Environmental Biotechnology Group at the University of Tübingen is looking into different options to improve carbon recycling from waste streams, one of which is the genetic manipulation of acetogenic bacteria for syngas fermentation. These bacteria strive at the thermodynamic limit of life. Therefore, research is focusing on optimizing the energy metabolism of the bacteria themselves rather than introducing heterologous pathways due to the lack of available metabolic energy. One of our goals is to improve the model acetogen *Clostridium ljungdahlii* for higher ethanol production rates from different gas mixtures. Recent results in syngas fermentation with acetogenic bacteria show that the aldehyde:ferredoxin oxidoreductase (AOR) is an enzyme of particular importance to produce ethanol during autotrophic conditions. The AOR is hypothesized to act as a thermodynamic regulator for ethanol production. Even though recent studies clearly offered new insights into the roles of two of the isoforms of AOR, the precise function of the isoforms for autotrophic growth and product formation in *C. ljungdahlii* is yet to be elucidated.

In this dissertation, I focused on the investigation of the role of the two tungsten-containing isoforms of this key enzyme in the metabolism of *C. ljungdahlii.* To this end, I constructed production systems for homologous and heterologous expression of AOR1 and AOR2. I developed a CRISPR/Cas9 system for precise gene deletion in *C. ljungdahlii.* I used this system to target the generation of deletion mutants of *aor1*, *aor2*, and a double deletion mutant of both genes. I investigated the phenotype changes of the successfully generated mutant strains (*aor1*, double deletion) in different batch experiments under heterotrophic and autotrophic growth conditions with different substrate gas mixtures in comparison to *C. ljungdahlii* wildtype (wt). Additionally, I examined the metabolism of *C. ljungdahlii* wt in a chemostat fermentation using CO as the sole carbon and energy source and investigated the impact of the addition of acetate to the medium.

1.2   Organization of this dissertation

Chapter 2 presents a literature review, which gives a detailed overview of the current literature on acetogenic bacteria. Special emphasis was put on: **1)** the anaerobic metabolism of the model acetogen *C. ljungdahlii* and the role of the AOR in ethanol formation; **2)** available genetic tools for metabolic engineering of acetogens; **3)** the enzymatic properties of the aldehyde:ferredoxin oxidoreductase; and **4)** chemostat fermentations as a tool to investigate acetogenic bacteria. In Chapter 3, the methods developed in this dissertation are described in detail and the required bacterial strains, DNA molecules, and equipment are listed. The design of the production systems for the production of AOR and the CRISPR/Cas9 system for gene deletion is described in this chapter. Methods for genetic modifications of *C. ljungdahlii* are described in detail, as well as the process conditions for the chemostat fermentations. Chapter 4 describes the results of the laboratory work of this dissertation, which are discussed and put into perspective in Chapter 5. Chapter 6 gives a conclusion and outlook for future work. Supplemental material can be found in chapter 7. This chapter includes further experiments on: **1)** the analysis of the produced AOR enzymes from Chapter 4 in an enzyme activity assay; and **2)** the production of ferredoxin for the activity assay. Besides that, we describe the problems during the design and cloning of the CRISPR/Cas9 system, especially for the deletion of *aor2.*

CHAPTER 2
BACKGROUND AND LITERATURE REVIEW

2.1   Synthesis gas fermentation

Effective and sustainable new techniques to reduce greenhouse gas emissions are needed to counteract progressive global warming. syngas fermentation is a promising process for carbon recovery from gaseous waste streams (Figure 1). In this process, microbes fix the carbon and energy from carbon dioxide (CO_2)-, hydrogen (H_2)-, and carbon monoxide (CO)-containing gas mixtures (synthesis gas/syngas) into organic compounds such as acetate and ethanol (Daniell *et al.*, 2012). The variety of possible substrates of the biocatalyst poses a significant advantage here, ranging from steel mill off-gases to gasified agricultural and municipal waste (Molitor *et al.*, 2016b). Consequently, the technology does not rely on agricultural land or expensive feedstock. The products of syngas fermentation can be used directly as fuel additives or further processed into value-added chemicals and fuels (Daniell *et al.*, 2012).
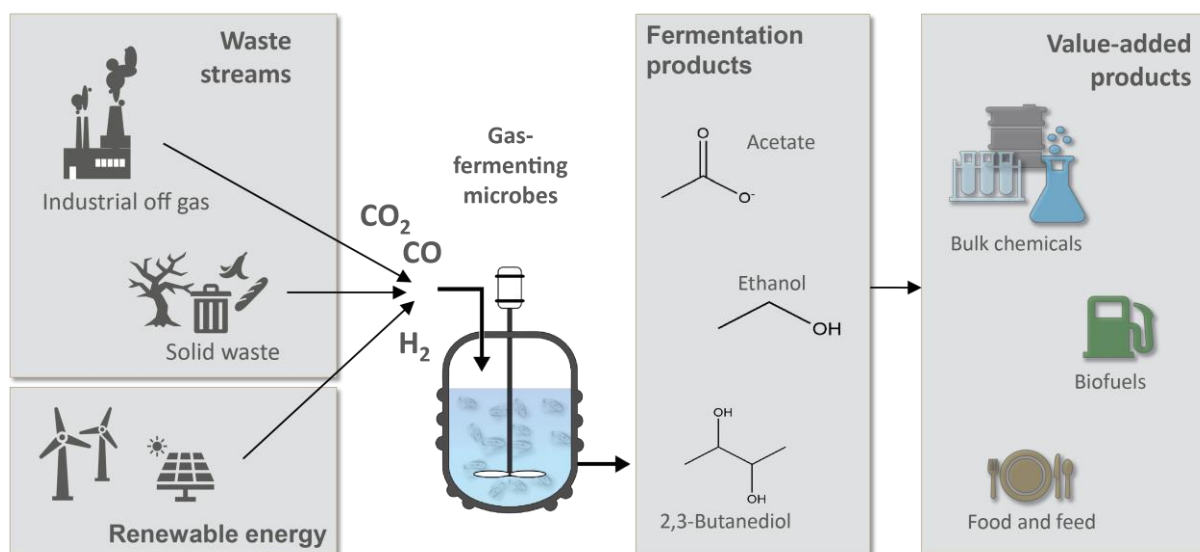
Figure 1: Syngas fermentation overview. Waste streams (solid or gaseous) are captured and converted to fermentation products (acetate, ethanol, and 2,3-butanediol) by gas-fermenting microbes using renewable electricity to power the fermentation. Fermentation products can later be converted into value-added products, such as bulk chemicals for industry, biofuels, and even food or animal feed.

2.2   The metabolism of the model acetogen *Clostridium ljungdahlii*

Clostridium ljungdahlii is a model microbe for syngas fermentation. It is a strict anaerobic acetogenic bacterium originally isolated from chicken yard waste (Tanner *et al.*, 1993). Both heterotrophic growth on sugars and organic compounds, and autotrophic growth on H_2/CO_2, CO, or syngas are possible (Figure 2) (Köpke *et al.*, 2010). During autotrophic growth, the carbon is fixed into biomass and

converted to the main fermentation products acetate and ethanol *via* acetyl-CoA as the central intermediate in the Wood-Ljungdahl Pathway (WLP) (reductive acetyl-CoA pathway) (Figure 2) (Daniell *et al.*, 2012). Unlike many better-known representatives of this genus, such as *Clostridium perfringens* or *Clostridioides difficile*, the microbe is not pathogenic, making it a suitable production strain for biotechnology. The 4.6 Mbp genome has been sequenced, which is a prerequisite for establishing a genetic system (Köpke *et al.*, 2010).

Figure 2: Overview of metabolic pathways and energy conservation in *C. ljungdahlii* when growing autotrophically with gases (CO or H₂/CO₂). ACS, acetyl-CoA synthase; AOR, aldehyde:ferredoxin oxidoreductase; CODH, carbon monoxide dehydrogenase; Co-FeS-P, corrinoid iron-sulfur protein; FDH, formate dehydrogenase; Fdox, oxidized ferredoxin; Fdred, reduced ferredoxin; F1F0 ATPase, F1F0 ATP synthase; HydABC, electron-bifurcating Fdox and NAD+-dependent [FeFe]-hydrogenase; HytA-E, electron-bifurcating NADP+-dependent [FeFe]-hydrogenase; Nfn, NADH-dependent Fdred:NADP+ oxidoreductase; Rnf, membrane-associated and energy-conserving Fdred:NAD+ oxidoreductase; THF, tetrahydrofolate.

2.2.1 Wood-Ljungdahl Pathway

The WLP is considered the evolutionary oldest metabolic pathway for CO_2 fixation, and it is the basis for syngas fermentation with Clostridia (Latif *et al.*, 2014). Ragsdale *et al.* (2008) give a detailed description of the pathway and highlight its discovery and elucidation. The linear process is divided into two branches, the carbonyl and the methyl branch. Initially, CO_2 is reduced to formate in the

methyl branch. This reduction is catalyzed by a formate dehydrogenase (FDH, gene cluster CLJU_c06990) and a hydrogenase (HytBCDE$_1$AE$_2$, gene cluster CLJU_c07030-07080). The electrons from H$_2$ are transferred to CO$_2$ *via* electron bifurcation with NADPH and reduced ferredoxin (Fd$_{red}$) (Mock *et al.*, 2015; Richter *et al.*, 2016; Wang *et al.*, 2013a). Formate and tetrahydrofolate (THF) are converted to formyl-THF by the formyl-THF synthetase (FTS) while consuming ATP. The bifunctional formyl-THF cyclohydrolase (MTC)/methenyl-THF dehydrogenase (MTD) first reduces formyl-THF to methenyl-THF and later to methylene-THF while eliminating water and consuming NADPH (Figure 3).
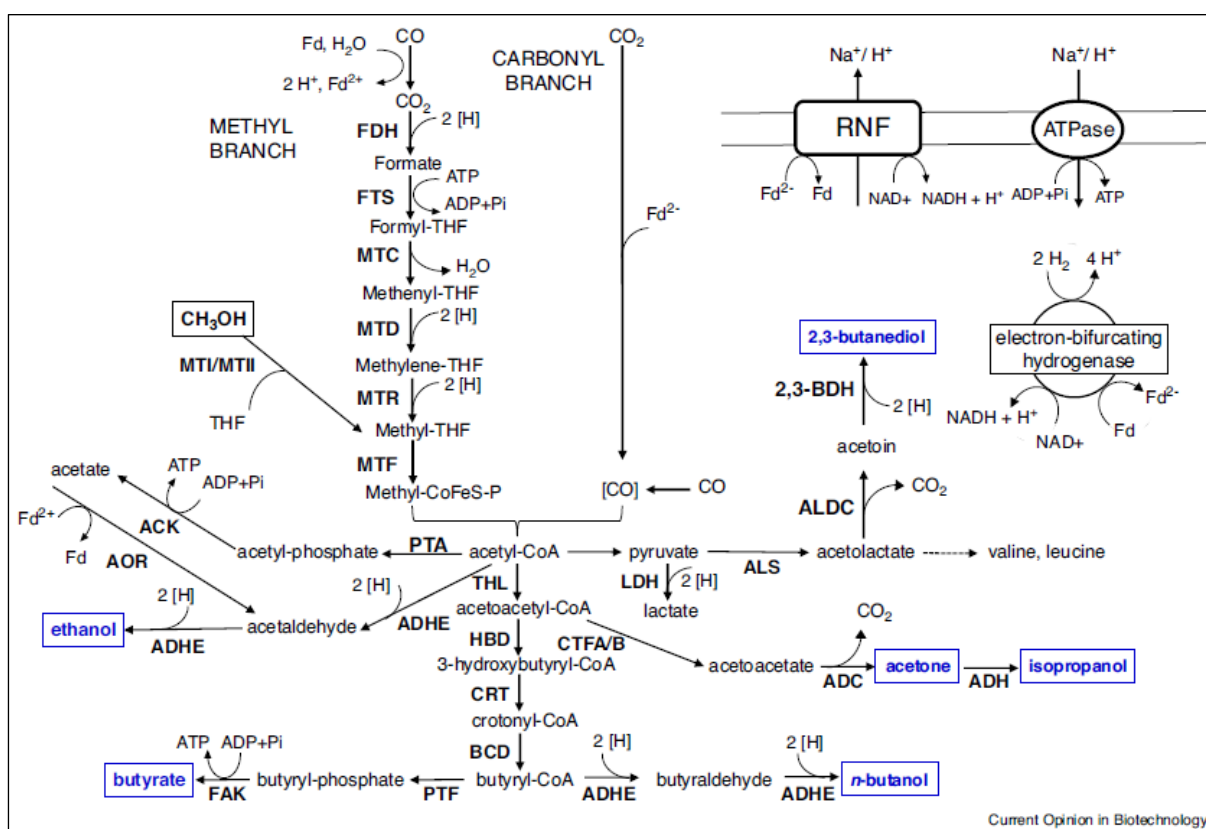
Figure 3: Wood-Ljungdahl pathway of acetogens with possible products (blue boxes). Comment on the figure: Fd^{2-} (Fd$_{red}$) is formed in the reaction of CO to CO2; Fd^{2-} (Fd$_{red}$) is consumed to reduce acetate to acetaldehyde. ACK, acetate kinase; ACS, CO dehydrogenase/acetyl-CoA synthase; ADC acetone decarboxylase; ADHE, aldehyde/alcohol dehydrogenase; ALDC, acetolactate decarboxylase; ALS, acetolactate synthase; AOR, aldehyde:ferredoxin oxidoreductase; BCD, butyryl-CoA dehydrogenase; CoFeS-P, corrinoid iron–sulphur protein; CRT, crotonase; CTFA/B, acetoacetyl-CoA:acetate/butyrate-CoA-transferase; FAK, fatty acid kinase; Fd2+, oxidized ferredoxin; Fd^{2-}, reduced ferredoxin; FDH, formate dehydrogenase; FTS, formyl-THF synthetase; HBD, 3-hydroxybutyryl-CoA dehydrogenase; LDH, lactate dehydrogenase; MTI, methyltransferase I; MTII, methyltransferase II; MTC, methenyl-THF cyclohydrolase; MTD, methylene-THF dehydrogenase; MTF, methyltransferase; MTR, methylene-THF reductase; PFOR, pyruvate:ferredoxin oxidoreductase; PTA, phosphotransacetylase; PTF, phosphotransferase; RNF, Rnf complex THF:tetrahydrofolate; THL, thiolase, 2,3-

BDH: 2,3-butanediol dehydrogenase; 2 [H], reducing equivalents (e.g. NADH or NADPH). Source: (Humphreys *et al.*, 2018).

Methylene-THF is reduced to methyl-THF by a heterodimeric methylene-THF reductase (MTR). The electron donor for this reaction is still unclear, but recent reports indicate the physiological electron donor could be Fd_{red}, possibly *via* coupling with the Rnf complex (Oppinger *et al.*, 2022; Yi *et al.*, 2021). In the last step, a methyl transferase catalyzes the transfer of the methyl group from methyl-THF to a corrinoid iron-sulphur protein (CoFeS-P). In the carbonyl branch, CO_2 is reduced to CO by a bifunctional CO dehydrogenase (CODH)/acetyl-CoA synthetase (ACS) (Liew *et al.*, 2016a). The CO is subsequently fused to the methyl group (previously bound to CoFeS-P) and condensed to acetyl-CoA with coenzyme A (CoA). During growth with CO, CODH also catalyzes the oxidation of CO to CO_2 to feed into the methyl branch while producing Fd_{red} (Liew *et al.*, 2016a).

Acetyl-CoA can subsequently be used for biomass production or converted to fermentation products of which acetate (simultaneously produces one ATP) and ethanol are the most prominent ones. 2,3-butanediol is also naturally produced in small amounts. Other possible products that can be produced with engineered strains are *n*-butanol (Köpke *et al.*, 2010), acetone (Banerjee *et al.*, 2014; Hoffmeister *et al.*, 2016; Philipps *et al.*, 2019), isopropanol (Bengelsdorf *et al.*, 2016; Philipps *et al.*, 2019), butyrate (Ueki *et al.*, 2014), mevalonate and isoprene (Diner *et al.*, 2018), 3-hydroxybutyrate (3HB) (Woolston *et al.*, 2018), butyric acid (Huang *et al.*, 2019; Zhao *et al.*, 2019), and isobutanol (Hermann *et al.*, 2021) (Figure 3, not showing all products). Recently, Liew *et al.* (2022) achieved the first carbon negative production of the industrially important chemicals acetone and isopropanol at industrial scale.

2.2.2 Energy conservation and electron bifurcation

The WLP does not generate an excess of ATP because the ATP generated *via* acetate formation is required to activate formate to formyl-THF. Energy conservation is facilitated through the Rnf complex (ferredoxin:NAD^+ oxidoreductase), which is a membrane-bound enzyme complex (Tremblay *et al.*, 2012). The Rnf complex transports either protons (H^+) or sodium ions (Na^+) across the membrane (H^+ in *C. ljungdahlii*) while transferring electrons from Fd_{red} to NAD^+. The resulting proton gradient drives an ATP synthase, which catalyzes ATP production. Therefore, the Rnf complex is essential for autotrophic growth (Klask *et al.*, 2022; Tremblay *et al.*, 2012; Westphal *et al.*, 2018). It has recently been shown that the Rnf complex of *Acetobacterium woodii* also catalyzes the reverse reaction, reducing Fd by transferring electrons from NADH to oxidized Fd (Westphal *et al.*, 2018). This enables growth on energy-low substrates, such as ethanol and lactate, because it provides the Fd_{red} necessary for the WLP.

The proton translocation *via* the Rnf not only results in the production of cellular energy as ATP but also affects the cellular redox balance significantly. Recent literature suggests that the redox balance or thermodynamic control is responsible for cellular regulations rather than gene expression or post-transcriptional regulations (Demmer *et al.*, 2015; Mahamkali *et al.*, 2020; Mock *et al.*, 2015; Nagarajan *et al.*, 2013; Richter *et al.*, 2016). Besides the Rnf-complex, other electron-bifurcating hydrogenases modulate the redox balance of the cell. Many of these enzymes utilize flavin-based electron bifurcation for flexible conversion of reducing equivalents to maintain redox homeostasis (Demmer *et al.*, 2015; Schuchmann *et al.*, 2018; Schuchmann *et al.*, 2014; Wang *et al.*, 2013a; Wang *et al.*, 2013b). The Nfn (NADH-dependent Fd_{red}:$NADP^+$ oxidoreductase) transfers electrons from Fd_{red} and NADH to $NADP^+$ and has recently been shown to play a crucial role in regulating the redox balance (Demmer *et al.*, 2015; Mahamkali *et al.*, 2020; Marcellin *et al.*, 2016; Mock *et al.*, 2015). Furthermore, Wang *et al.* (2013a) have shown that the formate dehydrogenase, which catalyzes the initial reduction of CO_2 in the WLP, can form a complex with an $NADP^+$-dependent hydrogenase to directly reduce CO_2 with electrons from H_2. This complex consists of seven subunits and can catalyze a variety of reversible reactions: **1)** coupled reduction of Fd and $NADP^+$ with H_2; **2)** coupled reduction of Fd and $NADP^+$ with formate; **3)** reduction of CO_2 with H_2 to formate; and **4)** reduction of methyl viologen with H_2, formate, and NADPH. Finally, the HydABC reversibly transfers electrons from 2 H_2 to Fd and NAD^+ (Nagarajan *et al.*, 2013; Schuchmann *et al.*, 2012, 2014; Wang *et al.*, 2013b). The overall redox homeostasis is a complex interplay and crucial for cell growth and ethanol formation.

2.2.3 Ethanol formation and aldehyde:ferredoxin oxidoreductase (AOR)

The acetyl-CoA produced in the WLP is converted to acetate while producing ATP. This reaction is facilitated by the phosphotransacetylase (PTA) and the acetate kinase (ACK) *via* acetyl phosphate as an intermediate. There are two possible pathways for ethanol formation, the direct route *via* acetaldehyde, which utilizes a bifunctional aldehyde/alcohol dehydrogenase (AdhE), and the indirect route *via* acetate (Liew *et al.*, 2017; Richter *et al.*, 2016). In the indirect route, undissociated acetic acid from the PTA/ACK reactions is further reduced to acetaldehyde by the aldehyde:ferredoxin oxidoreductase (AOR), which requires Fd_{red} as a co-substrate. At an intracellular pH of 6, 95% of the acetate is present in the dissociated form. The undissociated form, acetic acid, can diffuse freely over the membrane and dissociates inside the cell (pK_a acetic acid/acetate 4.8). To make the AOR-reaction thermodynamically feasible, high intracellular substrate concentrations (acetic acid and Fd_{red}) and low product concentrations (acetaldehyde) are necessary (Richter *et al.*, 2016). An alcohol dehydrogenase converts acetaldehyde to ethanol in a thermodynamically favorable reaction, keeping the product concentration of the AOR low (Richter *et al.*, 2016). Recent studies have shown that the indirect route

is mainly responsible for ethanol production under autotrophic conditions, whereas the activity of AdhE was hardly detectable (Liew *et al.*, 2017; Richter *et al.*, 2016).

The AOR is highly dependent on the cell's redox state, as Fd_{red} is required to reduce the substrate acetic acid. When CO is the substrate for ethanol production, Fd can directly be reduced during the oxidation of CO to CO_2. In contrast to that, the redox potential of H_2 does not suffice for the direct reduction of Fd. As a result, ethanol production from H_2/CO_2 gas mixtures remains challenging. In recent findings by Zhu *et al.* (2020), the specific activity of AOR in cell extract of *C. ljungdahlii* grown in fed-batch mode with pH and pressure control (pH 6, 0.1 MPa) on CO reached 6.7 U/mg, compared to 2.5 U/mg on H_2/CO_2. Therefore, improving ethanol production from H_2/CO_2 is necessary because when using CO-rich gases, 2/3 of the carbon from CO ends up as a CO_2 surplus of the fermentation (Molitor *et al.*, 2017). In fact, Mahamkali *et al.* (2020) have shown that co-feeding H_2 in continuous oscillating CO fermentation can improve the re-assimilation of dissipated CO_2 during peak growth phases. Here, CO_2 dissipation was reduced by 1/3 when using a high H_2-CO gas mixture (H_2:CO 3:1). The presented thermodynamic metabolic flux analysis (tMFA) by Mahamkali *et al.* (2020) shows that ethanol production during growth with CO and H_2 is thermodynamically only feasible *via* AOR.

Several studies have been conducted to elucidate the influence of the enzymes related to ethanol production under different growth conditions. Various gene deletions greatly influence ethanol production in *C. autoethanogenum*, which is a close relative to *C. ljungdahlii* (Liew *et al.*, 2017). Deleting the *adhE* genes individually led to an increase of the ethanol titer by 154-183% with CO. A single deletion of *aor1* resulted in reduced growth with CO and about 43% lower ethanol titers. In comparison, single deletion of *aor2* increased ethanol titers by 170%. Simultaneous inactivation of both isozymes AOR1 and AOR2 led to incapability to reduce carboxylic acids to their corresponding alcohols and reduced the ethanol titer (Liew *et al.*, 2017). These findings have been partly confirmed in *C. ljungdahlii* by Liu *et al.* (2020). A double deletion strain of *adhE1* and *adhE2* showed impaired growth and substrate consumption in mineral medium with fructose as a carbon source. The strain was not able to produce ethanol under these conditions. An *adhE1* mutant, however, produced more ethanol than the wt, which is in accordance with the findings for *C. autoethanogenum* (Liew *et al.*, 2017; Liu *et al.*, 2020). During fed-batch cultivation on syngas (controlled pH and gas pressure) with the double deletion strain, Liu *et al.* (2020) observed ethanol production during the exponential growth phase and re-oxidization during the stationary phase. Transcriptomic data showed strong up-regulation of *aor2* in the stationary phase, supporting the hypothesis that AOR2 is part of the ethanol-oxidizing pathway (Liu *et al.*, 2020). Transcriptomic data and evaluation of growth and product formation showed that AOR2 converted acetate to acetaldehyde in CO fermentation but catalyzed the reverse reaction during H_2 fermentation (Zhu *et al.*, 2020). Even though recent studies offered new

insights into the roles of the two isoforms of AOR, the precise function of both isoforms for autotrophic growth and product formation in *C. ljungdahlii* is yet to be elucidated.

To date, the highest ethanol concentration with *C. ljungdahlii* was achieved in a continuously stirred tank reactor (CSTR) with a gas mixture of H_2, CO, CO_2, and argon (20/55/10/15, volume-%). The culture produced 48 g L^{-1} with a molar ratio of ethanol/acetate >20 (Phillips *et al.*, 1993). An ethanol production rate of 0.37 g L^{-1} h^{-1} was achieved in a bubble column reactor at atmospheric pressure with 60% CO, 35% H_2, and 5% CO_2 (Richter *et al.*, 2013). The company IneosBio achieved rates of up to 10 g L^{-1} h^{-1} for ethanol production in a pressurized CSTR fed with CO and H_2 (Gaddy *et al.*, 2014) (non-peer-reviewed patent). Currently, syngas fermentations achieve stable ethanol production rates of 8 g L^{-1} h^{-1} in a lab-scale CSTR under atmospheric pressure (Molitor *et al.*, 2016b).

2.3 Genetic engineering of acetogens

2.3.1 Existing essential tools for the genetic system

For further elucidation of the metabolism of acetogens and improvements of ethanol production rates, efficient, reproducible, and reliable genetic tools are needed. A widely-used tool for inserting foreign DNA into *C. ljungdahlii* is the *E. coli-Clostridium* shuttle-vector system pMTL80000 (Figure 4) (Heap *et al.*, 2009). The modular system has been tested in various clostridial species. It contains different origins of replication (ori) for Gram$^+$ bacteria (pBP1, pCB102, pCD6, and pIM13) and Gram$^-$ bacteria (ColE1, p15a, with or without *traJ* region for conjugation). Additionally, several selection markers (resistance genes for *catP*-chloramphenicol/thiamphenicol, *ermB*-erythromycin, *tetA*-tetracycline, *aad9*-spectinomycin) and five application modules are included for the plasmids (MCS (Figure 4 B), *catP* reporter gene, spacer, and two expression constructs with different clostridial promoters, P_{fdx} and P_{thl}) (Heap *et al.*, 2009).
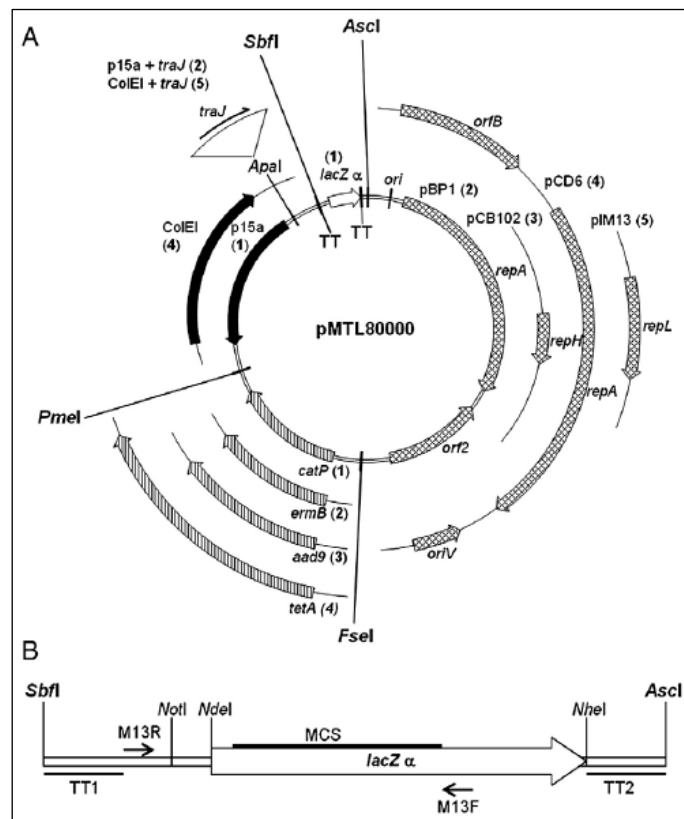
Figure 4: A) Scheme of modular pMTL80000 shuttle plasmids. B) MCS module. Source: (Heap *et al.*, 2009).

The modules are flanked by recognition sites for the rare eight-cutting restriction enzymes *Asc*I, *Fse*I, *Pme*I, and *Sbf*I, which enables simple replacement of individual modules and construction of new vectors (Figure 4A). The system is, therefore, easily expandable with new customized modules. The plasmids can be constructed and multiplied in *E. coli* and afterwards introduced into the specific target microbe. One option for that is conjugation (plasmids carrying the *traJ* region). Here, the plasmid is transferred into *Clostridium* by an *E. coli* donor strain (Liew *et al.*, 2017; Mock *et al.*, 2015; Purdy *et al.*, 2002). A second method is the transformation *via* electroporation (Köpke *et al.*, 2010; Leang *et al.*, 2013; Molitor *et al.*, 2016a).

Besides the tools included in the modular system by Heap *et al.* (2009), various other genetic tools have been established in Clostridia. Molitor *et al.* (2016a) have developed a temperature-sensitive origin (pWV01ts) and a fluorescence marker for anaerobic systems. The temperature-sensitive ori was replicated at 30°C and could be cured from transformants by passaging and incubating the culture at 37°C.

Expanding the choice of promoters for gene expression is necessary to improve genetic tools and fine-tune genome editing tools such as CRISPR-Cas. A lactose-inducible promoter was established (Banerjee *et al.*, 2014; Hartman *et al.*, 2011), but others have reported it to have a high background activity, which is fatal for CRISPR applications (Woolston *et al.*, 2018). Other inducible promoters for Clostridia

include an arabinose- (Zhang *et al.*, 2015), a laminaribiose- (Mearls *et al.*, 2015), a D-xylan- (P_{1133}) (Teng *et al.*, 2015), a xylose- (Nariya *et al.*, 2011), and an anhydrotetracycline (aTc)-inducible promoter (Dong *et al.*, 2012). As the aTc promoter enabled stringent regulation and high expression on induction, it has been further improved and applied in various applications (Nagaraju *et al.*, 2016; Wasels *et al.*, 2017; Woolston *et al.*, 2018). In addition to the inducible promoters, the toolkit for constitutive promoters has also been extended. Characterized constitutive promoters include a shortened version of the thiolase promoter described by Heap *et al.* (2009), the mini-P_{thl} (Woolston *et al.*, 2018), a small RNA promoter (Wang *et al.*, 2016), an engineered P4 (Woolston *et al.*, 2018), and a synthetic promoter (Xia *et al.*, 2020). Recently, a promoter screening was performed by Zhao *et al.* (2019), and Mordaka *et al.* (2018) tested and compared promoters with regard to their stringency.

2.3.2   Tools for gene deletions, insertions, and alterations

A frequently used tool for stable genetic manipulation in acetogens is the ClosTron tool (Heap *et al.*, 2010; Heap *et al.*, 2007), based on bacterial group II introns (Ll. LtrB intron from *Lactococcus lactis*). Targeted homologous recombination inserts an intron at the desired position on the genome that carries an antibiotic resistance marker. This inactivates the target gene and allows easy mutant selection (Heap *et al.*, 2007). Further development now enables marker recycling from the genome to introduce multiple gene deletions in one strain (Heap *et al.*, 2010). Recycling selection markers is essential in Clostridia, as only a few of the common markers work in Clostridia. A further possibility for marker-less chromosomal modifications (deletions and insertions) is double-crossover allelic exchange (Al-Hinai *et al.*, 2012). The target microbe is transformed with a plasmid carrying homologous regions flanking a flippase recognition target (FRT) flanked thiamphenicol resistance gene (Th^r-FRT) (Schlake *et al.*, 1994). The homologous regions recombine with the up-and downstream regions of the target gene in a first recombination event, replacing the target gene with the thiamphenicol resistance that can be selected for. The second recombination event is triggered by the expression of an FLP recombinase from a second unstable plasmid. This triggers recombination of the FRT regions and excision of the antibiotic resistance gene from the chromosome (Al-Hinai *et al.*, 2012). Even though the marker is recycled in this method, a cloning scar is left on the chromosome. A similar system was developed by Philipps *et al.* (2019). They use a *Himar1* transposase gene controlled by a xylose-inducible promoter– repressor system flanked by ITRs. The antibiotic marker gene *ermC* is flanked by FRT sites to facilitate subsequent marker removal (Philipps *et al.*, 2019).

2.3.3   Marker-less and scar-free genome editing with *Triple-Cross*

LanzaTech has developed a similar tool that does produce a cloning scar, called the *Triple-Cross* method (Walker *et al.*, 2015). The produced clones are easily selectable without the need for extensive

screenings as required for classical crossover techniques (Chapter 2.3.2). The method is based on three recombination events between a plasmid and the chromosome of the target microbe (Figure 5).
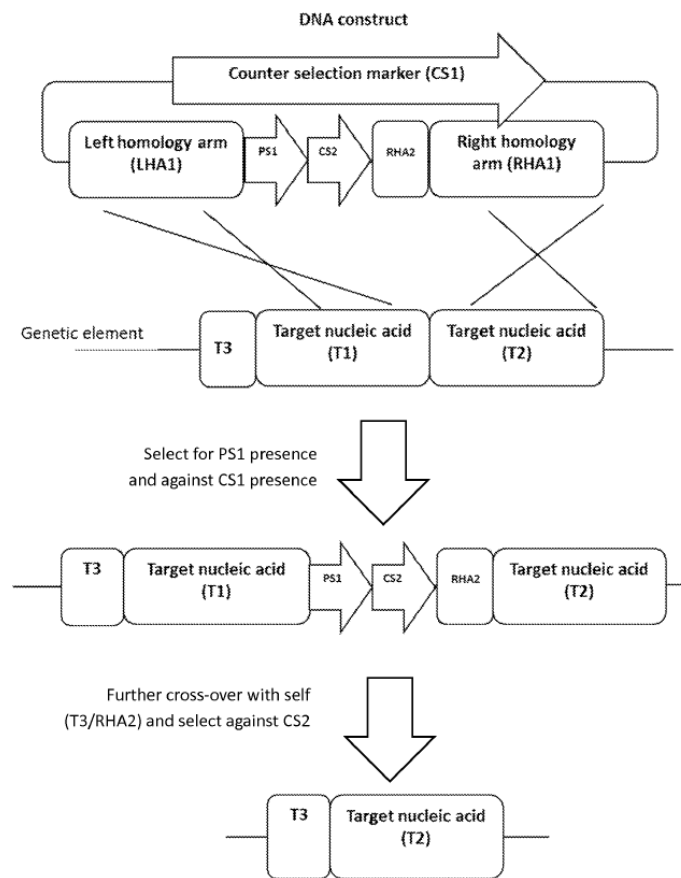
Figure 5: Schematic overview of the *Triple-Cross* Method as designed by (Walker *et al.*, 2015).

The plasmids carry three regions (LHA1, RHA1, RHA2) that are homologous to the bacterial chromosome, as well as one positive (PS1) and two negative selection markers (CS1, CS2). The region LHA1 is homologous to the target gene, while the regions RHA1 and RHA2 are homologous to the upstream and downstream regions of the target gene (Walker *et al.*, 2015). After transforming the target microbe with the corresponding plasmid, the first two spontaneous recombination events are favored by selection pressure for PS1 and against CS1. PS1 is an antibiotic resistance, without which the microbe would not be viable if selected. CS1 is a toxin gene only expressed when a regulated promoter is induced and is, therefore, lethal for the bacterium if the plasmid is still present in the cell. This ensures that only those mutants that have integrated the LHA1 to RHA1 region into their genome through two recombination events survive. Bacteria in which the third recombination event has occurred are selected using CS2. After recombination of RHA2 and T3, the intermediate region is completely removed from the genome. What remains is an exact deletion of the desired region without leaving markers or scars (Walker *et al.*, 2015). This enables the successive deletion of multiple

genes in one strain. The tool is not limited to gene deletions, but it can be used for other purposes, such as insertions, as well (Walker *et al.*, 2015).

2.3.4   CRISPR techniques

A prominent tool for marker-less and scar-free genome editing is the CRISPR-Cas technique (Doudna *et al.*, 2014; Jinek *et al.*, 2012; Knott *et al.*, 2018). The system enables targeted and efficient genome editing with relatively low effort. It requires a plasmid that contains sequences for a single-guide RNA (sgRNA) to target the genomic DNA, which is a Cas nuclease to cleave the targeted DNA sequence, and homologous repair templates to facilitate the desired edits (Knott *et al.*, 2018) (Figure 6).
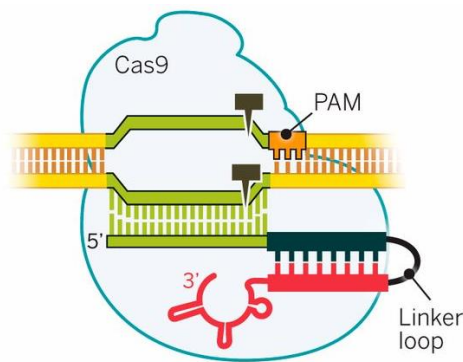
Figure 6: Structure of *S. pyogenes* Cas9 guided to the target sequence by sgRNA (Doudna *et al.*, 2014).

The CRISPR/Cas9-technique has recently been used to successfully manipulate *C. ljungdahlii* by Huang *et al.* (2016a). The efficient creation of gene deletion mutants with CRISPR-Cas is highly dependent on the promoters used for the expression of *cas9* and the sgRNA (Huang *et al.*, 2016a). After screening of heterologous promoters, the authors chose two constitutive promoters for the expression of *cas9* and the sgRNA, P_{thl}, and $P_{araE,}$ respectively. The system was tested on four target genes, all achieving >50% deletion efficiency, although they observed mixed populations as well (Huang *et al.*, 2016a). Woolston *et al.* (2018) developed an inducible repression system that enables multiplex gene silencing based on a nuclease-deficient Cas9 (dCas9). The dCas9 does not cleave the DNA but blocks transcription, therefore, repressing the gene product. Woolston *et al.* (2018) controlled the dCas9 with an anhydrotetracycline-inducible promoter P_{2tetO1} (Dong *et al.*, 2012). For expression of the sgRNA, they used an engineered P4 promoter (Xu *et al.*, 2015) and a multiplexing design that facilitated easy addition of multiple target fragments (Woolston *et al.*, 2018). Multiplexed silencing of *aor2* and *pta* improved titers and yields in a 3-hydroxybutyrate (3HB) production strain (Woolston *et al.*, 2018).

A similar system was developed by Zhao *et al.* (2019). They used Cas12a instead of Cas9, because Cas12a finds TTN (N being any nucleotide) instead of NGG (Cas9) as the protospacer adjacent motif (PAM). Owing to the fact that *C. ljungdahlii* has an A-T-rich genome, the authors could greatly enhance

the number of possible editing sites (approximately 830.000 sites compared to 240.00 sites for Cas9) (Zhao *et al.*, 2019). In the first two attempts to generate edited mutants with a sgRNA that targets *pyrE,* no colonies were generated due to inefficient DNA repair. A pre-treatment of the cells used for transformation (OD_{600} 0.4-0.6) with 1.25 weight-% glycine and 0.3 M sucrose, combined with a prolonged recovery period (20h), increased transformation efficiency greatly (tested with pMTL83151, the basis for the editing plasmid, which was constructed in this study). This improved transformation protocol achieved efficient gene deletion of four different target genes (*pyrE*, *pta*, *ctf*, and *adhE1*). By introducing a mutation to Cas12a reported previously (Li *et al.*, 2018), a DNase-deactivated *Fn*Cas12a (dd*Fn*Cas12a) was used to generate a gene regulation CRISPRi system. The system was successfully applied to re-distribute carbon flux towards butyric acid in a previously constructed butyric acid-producing strain (Huang *et al.*, 2019; Zhao *et al.*, 2019).
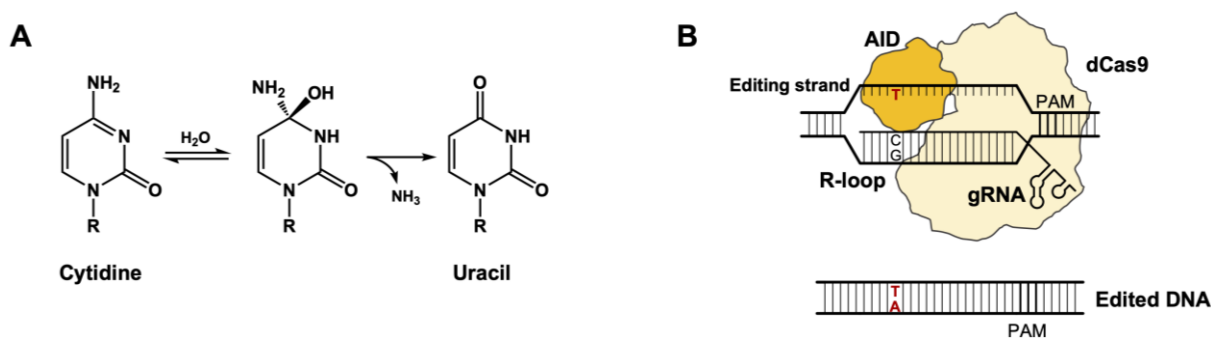
Figure 7: Design of a base-editing tool in *C. ljungdahlii*. A) Chemistry of deamination process converting cytidine to uracil. B) Mechanism of base editing. dCas9 binds to the target DNA. Activation-induced cytosine deaminase deaminates the Cs in the single-strand DNA on the editing strand, resulting in C-to-T single-nucleotide variations in the genome (Xia *et al.*, 2020).

Based on the CRISPR/Cas9 system, a base-editing system at one-nucleotide resolution for *C. ljungdahlii* was recently developed in our group and with me as a co-author (Xia *et al.*, 2020). It combines a dCas9 with an activation-induced cytidine deaminase, thus, enabling cytosine (C) to thymine (T) substitutions without generating a double-strand break in the DNA (Figure 7). Therefore, the system is not relying on repair mechanisms, which greatly enhances an efficient generation of mutants. Computational analysis showed that 99.69% (4,171 out of 4,184) of the genes can be edited (Xia *et al.*, 2020). The system was successfully applied to generate premature STOP-codons in *adhE1*, *adhE2*, *aor1*, and *aor2*, thus, allowing evaluation of the re-distribution of carbon fluxes in disruption mutants (Xia *et al.*, 2020).

2.4   Enzymatic properties of AOR

2.4.1   Characteristics of AOR

The structure of the AOR from *C. ljungdahlii* has not been resolved, yet. White *et al.* (1991); White *et al.* (1993) purified and described two AOR enzymes from *Clostridium formicoaceticum*, which is a mesophilic acetogenic microbe able to grow autotrophically on CO or H_2/CO_2 (Andreesen *et al.*, 1970; Diekert *et al.*, 1978; Lux *et al.*, 1992). Both enzymes reduced different carboxylic acids to their corresponding aldehydes (White *et al.*, 1991; White *et al.*, 1993). One major difference between the two isolated AORs was that one AOR was tungsten- (W-) containing (White *et al.*, 1991), while the other one contained molybdenum (Mo) (White *et al.*, 1993). The W-containing AOR was shown to be very oxygen labile, while the other one was only moderately oxygen-sensitive (Huber *et al.*, 1994). The W-containing AOR consisted of two identical subunits of about 67 kDa (White *et al.*, 1991). In enzyme assays with different artificial electron donors, tetramethylviologen (TMV) (E_0' = -550 mV) was the best co-substrate to reduce carboxylic acids.
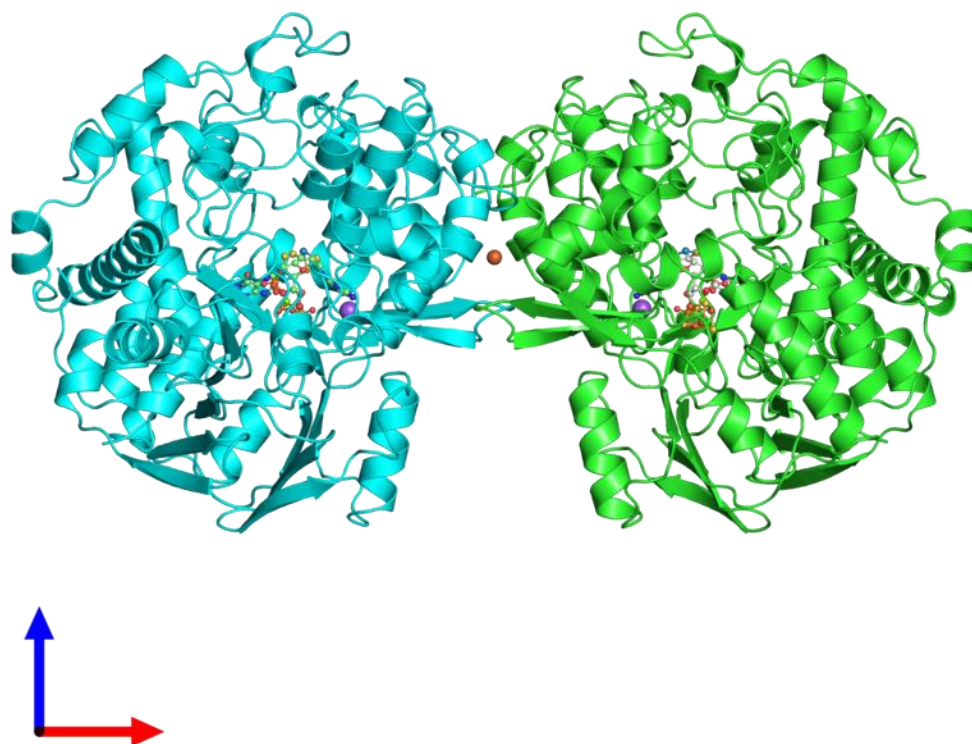
Figure 8: Structure of the AOR from *P. furiosus* colored by chain and viewed from the front (Chan *et al.*, 1995) (figure downloaded from PDBe 29.06.2020).

Chan *et al.* (1995) have characterized the AOR from the hyperthermophilic archaeon *Pyrococcus furiosus* (Figure 8)*.* This enzyme is, like the one from *C. ljungdahlii*, a W-containing AOR (purple in Figure 8). The authors used crystallization and x-ray diffraction to analyze the enzyme's structure at 2.3 Å

resolution. The enzyme consists of two identical 66 kDa subunits, each containing a [4Fe-4S] cluster (red and yellow in Figure 8) and a W-atom, which is bound by two molybdopterin molecules *via* dithiolene sulfurs (Chan *et al.*, 1995; Kramer *et al.*, 1987). A central Fe-atom is coordinated by both subunits (Chan *et al.*, 1995) (central red atom in Figure 8). In a detailed sequencing analysis of the *aor* gene from *P. furiosus,* the enzyme's primary structure has been elucidated, which allowed the accurate identifications of the amino acids binding the ligands (Kletzin *et al.*, 1995).

2.4.2 Purification of AOR

To examine enzymes *in vitro*, it is necessary to disrupt the cells and use the cell extract or further purified enzymes for enzyme assays. Strategies to purify native enzymes with traditional biochemical methods typically require a large amount of cell material as an input, are time-consuming, and are cumbersome to optimize. This can be partly overcome by heterologous (*e.g.*, in *E. coli*) or homologous (in the native host) production of enzymes. To further facilitate the purification, one popular system is using a StrepTag II, which can be fused to the enzyme genetically. StrepTag II is a short amino acid sequence consisting of eight amino acid-residues (Trp-Ser-His-Pro-Gln-Phe-Glu-Lys) (Schmidt *et al.*, 2007). It naturally binds to streptavidin, which allows the simple purification of tagged proteins *via* affinity chromatography (Schmidt *et al.*, 2007). A modified streptavidin called Strep-Tactin binds the tag with high affinity. It is used as column material bound to sepharose (Schmidt *et al.*, 2007). Huang *et al.* (2012) have shown that the system works to purify anaerobic enzymes from acetogenic microbes. They produced a Strep-tagged Nfn complex in *E. coli* and used the purified enzyme for activity assays. Girbal *et al.* (2005) also purified a Fe-only hydrogenase from *Clostridium acetobutylicum via* a StrepTag. Stefan Petschak, a master's student in our lab, showed that production and purification of the *C. ljungdahlii* AOR *via* StrepTag are possible from *E. coli* and *C. ljungdahlii* (Petschak, 2019). Although purification was possible, the AOR produced in *E. coli* seemed not to be catalytically active (Petschak, 2019). *E. coli* seemed to be lacking specific maturation systems to produce functional AOR *in vivo*.

2.4.3 Activity assay

For the characterization of AOR enzyme activities, an anaerobic spectrophotometric activity assay has been established previously (Heider *et al.*, 1995; Huber *et al.*, 1995; Mock *et al.*, 2015; Wang *et al.*, 2013a; Whitham *et al.*, 2015). This assay is based on measuring the change in light absorbance properties during the reduction of methyl or benzyl viologen as an artificial electron acceptor. It is carried out in the direction of the oxidation of acetaldehyde to acetate. Zhu *et al.* (2020) and Liu *et al.* (2020) have replaced the artificial electron acceptors with the natural substrate ferredoxin, which can also be followed spectrophotometrically in the AOR activity assay. For this purpose, *C. autoethanogenum* ferredoxin was heterologously produced in *E. coli* as described previously (Demmer

et al., 2015; Huang *et al.*, 2016b; Nakamura *et al.*, 1999). In addition to the spectrophotometric measurements, the concentrations of acetate and acetaldehyde can be measured *via* HPLC (Huber *et al.*, 1995). Furthermore, the activity of the AOR can be investigated in the direction that is important under physiological conditions for *C. ljungdahlii* (reduction of acetic acid to acetaldehyde). However, due to the thermodynamic relationships, this assay is less trivial compared to the non-physiological direction. It is necessary to keep the concentration of the product of the AOR reaction (acetaldehyde) low, to make the reaction thermodynamically feasible, and allow for the determination of the AOR-specific enzyme parameters. For this purpose, the acetaldehyde can be reacted to ethanol in a favorable reaction either with purified alcohol dehydrogenase (ADH) or with AOR-free *C. ljungdahlii* cell extract, which also contains ADH and NAD(P)H. To keep the co-substrate level (Fd$_{red}$) high, the reduction of Fd is achieved using CODH or *C. ljungdahlii* cell extract and CO in a separate or coupled reaction, as described by Wang *et al.* (2013a) and Demmer *et al.* (2015). Appropriate controls cover parameters, such as the background activity of ferredoxin in the cell extract. The ADH reaction is thermodynamically favorable and occurs at a significantly higher rate. Therefore, the AOR reaction can be considered the rate-determining step.

2.5 Bioreactor studies

It is essential to characterize recombinant strains and biotechnological production hosts in more detail in bioreactor studies. Examining their performance with regards to ethanol production rates and long-term genetic stability during syngas fermentation produces important data for later applications as possible production strains. The multiple-bioreactor system (MBS) developed by Klask *et al.* (2020) in our group offers a convenient platform to test and compare new strains easily. It comprises six identical 1-L bioreactors and can be run in batch or continuous mode (Figure 9). The system is autoclavable and offers automated temperature and pH control. It has proven to be a robust system, which facilitates replicable cultures and has recently been upgraded by adding microflowmeters to the gas lines. This will also facilitate the monitoring of gas consumption, enabling a more exact carbon balance.
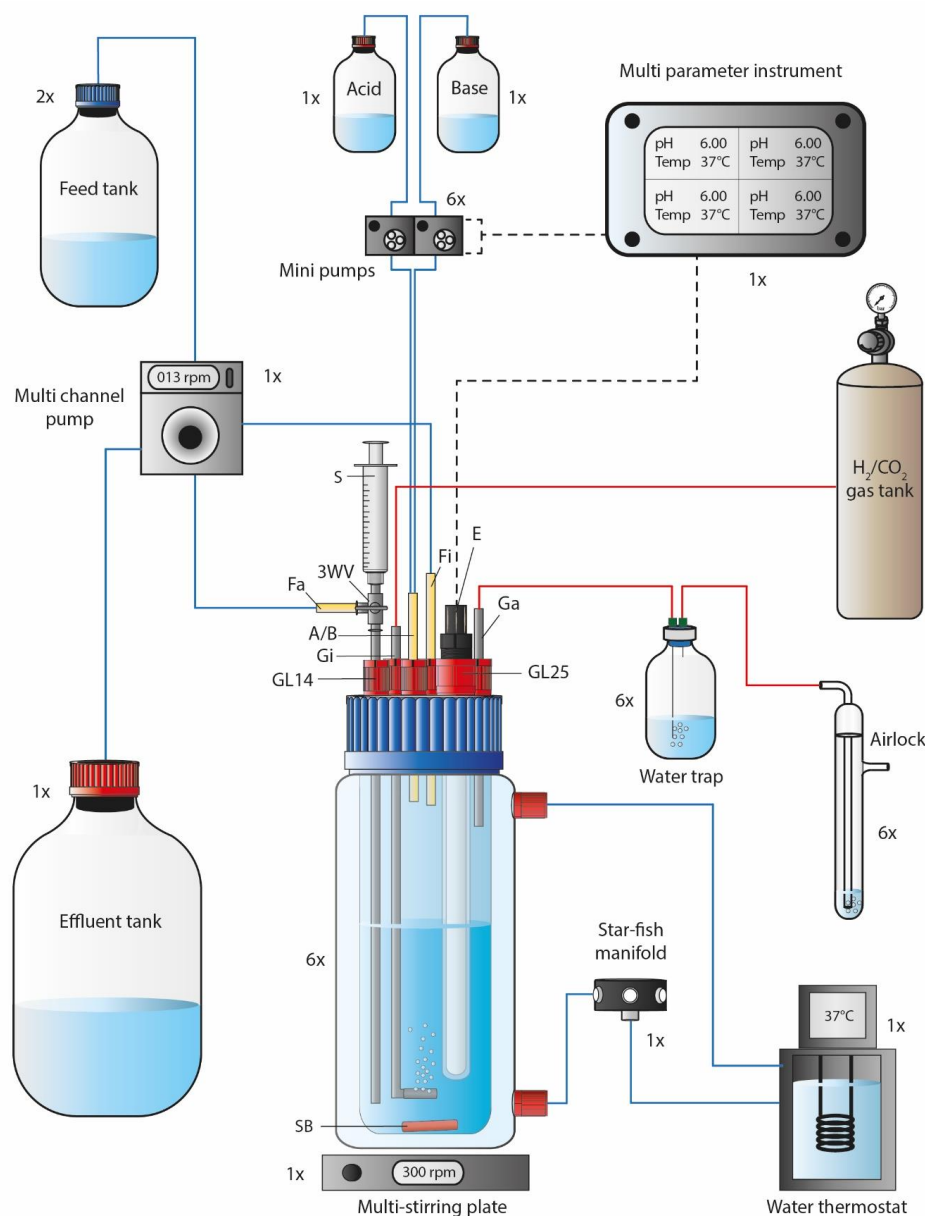
Figure 9: Flow chart of a single bioreactor operated in the MBS. 1x, 2x, and 6x next to each unit in the figure describe the quantity required to operate six bioreactors simultaneously. Abbreviations: A/B, Acid and/or base feed line; E, pH/pt1000 electrode; Fa, medium feed-out line; Fi, medium feed-in line; Ga, gas-out line; Gi, gas-in line; GL14, screw joint connection size 14; GL25, screw joint connection size 25; rpm, revolutions per minute; SB, stirring bar; 3WV, three-way valve. Blue lines indicate liquid transfer, red lines contain gas, and dotted black lines provide electric power or signals (Klask *et al.*, 2020).

The performance of the strains must be tested with different substrate gas compositions, including H_2/CO_2, pure CO, and different syngas mixtures. It is essential to test a variety of gas mixtures because ethanol production *via* the AOR is highly dependent on the redox equivalents present in the cell. The redox state itself is dependent on the gas composition. We have, therefore, acquired a second convenient bioreactor system in our lab. The Sartorius Stedim Biostat® B-DCU system is equipped with

four stainless steel 2-L bioreactors (pressurizable to 2 bar), each controlled by a supply tower (Figure 10). A control tower (Figure 10 A) enables the individual or parallel operation of the four reactors and enables a wide set of automation possibilities, including temperature and pH control, programmable protocols to ramp up process conditions, automated gassing rate and medium exchange, and culture volume control with antifoam addition. This system offers a more secure set-up when working with the toxic gas mixtures containing CO, due to the stainless steel vessels and included safety features.
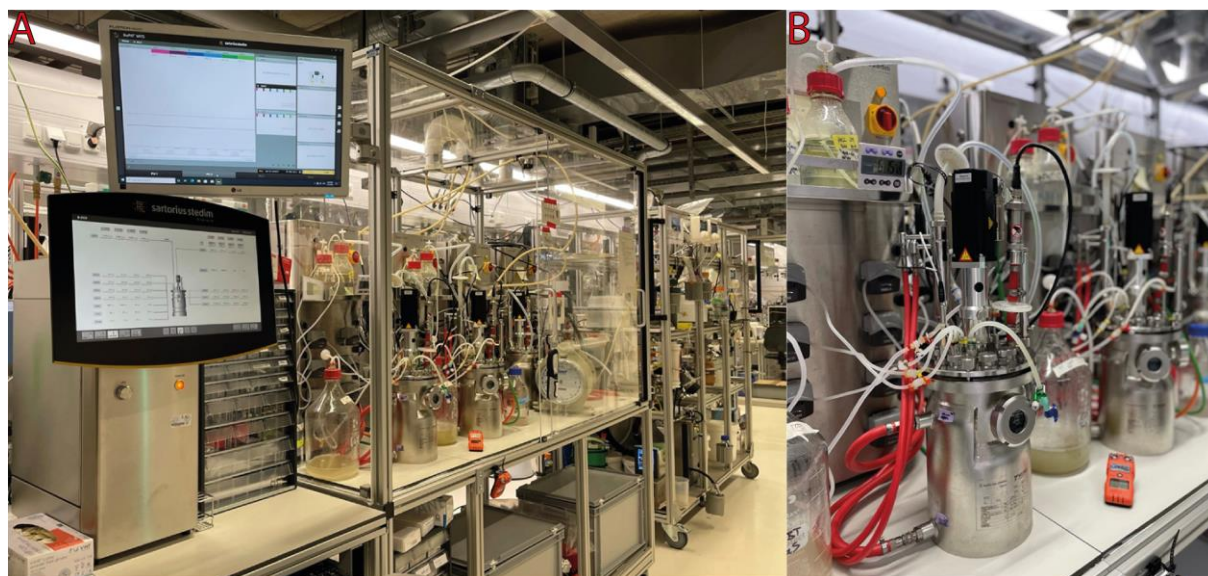
Figure 10: The Sartorius Stedim Biostat® B-DCU system during operation. A) Control tower, BioPat MFCS software, and four supply towers with stainless steel bioreactors in a self-built fume hood. B) Close-Up of one stainless steel 2-L bioreactor during operation.

Characterizing new strains in chemostat fermentations offers important advantages over batch fermentations as they represent a more robust fermentation system. They offer sampling during steady-state conditions, which is important to gain a better understanding of the metabolic functions of enzymes. This gives the opportunity to conduct omics experiments, such as proteomics and transcriptomics, as well as community analysis in open microbiome processes. Additionally, pH control has been shown to be of vital importance for the characterization of *C. ljungdahlii* by preventing acid crashes or enabling growth with certain substrates, such as nitrate as N-source (Klask *et al.*, 2020).

CHAPTER 3
MATERIALS AND METHODS

3.1   Bacterial strains and cultivation conditions

For this study, exclusively *E. coli* and *C. ljungdahlii* strains were used. *E. coli* TOP10 (Invitrogen, Carlsbad, USA) was used for general cloning purposes and plasmid methylation. *E. coli* NEB stable (New England Biolabs, Frankfurt, Germany) was used to assemble CRISPR/Cas9 plasmids or other hard-to-assemble constructs. *E. coli* C41 (DE3) and *E. coli* BL21 were used for heterologous production of clostridial ferredoxins and AOR enzymes. *C. ljungdahlii* DSM 13528 (ATCC 55383) was obtained from DSMZ. *C. ljungdahlii* QX5 (*aor1* Gln267*) and QX6 (*aor2* Gln267*) were constructed by Dr. Pengfei Xia in the Environmental Biotechnology Group (EBT) (Xia *et al.*, 2020).

E. coli was routinely cultivated in lysogeny broth (LB), which contained (per liter): 10 g tryptone; 5 g yeast extract; and 5 g sodium chloride. The medium was supplemented with appropriate amounts of chloramphenicol (Cm) (30 µg/mL), ampicillin (Amp) (100 µg/mL), kanamycin (Kan) (50 µg/mL), erythromycin (Ery) (400 µg/mL in plates, 250 µg/mL in liquid medium), or spectinomycin (Spec) (60 µg/mL) to select for transformants and maintain plasmids in *E. coli*. Liquid cultures were agitated at 150 rpm (Lab companion ISS-7100R, Jeio Tech, Republic of Korea) and incubated at 37°C. The solidified medium was prepared by adding 1.5 weight-% agar to the medium and plates were incubated without agitation at 37°C (Incubator IN260, Memmert, Schwabach, Germany).

C. ljungdahlii was routinely cultivated under strictly anaerobic conditions at 37°C without agitation. Reinforced Clostridial Medium (RCM) was used for general propagation and contained (per liter): 5 g fructose; 3 g yeast extract; 10 g meat extract; 10 g peptone; 5 g sodium chloride; 1 g soluble starch; 3 g sodium acetate; 4 mL resazurin-solution (0.025 vol-%); and 0.5 g L-cysteine HCl. Standard cultivations were conducted in 50 mL RCM aliquots in 100-mL serum bottles. All growth experiments were performed with the minimal medium PETC, which contained (per liter): 1 g yeast extract; 1 g ammonium chloride; 0.1 g potassium chloride; 0.2 g magnesium sulfate heptahydrate; 0.8 g sodium chloride; 0.1 g potassium dihydrogen orthophosphate; 0.02 g calcium chloride dihydrate; 4 mL resazurin-solution (0.025 vol-%); 10 mL trace element solution (100x); 10 mL Wolfe's vitamin solution (100x); 10 mL reducing agent (100x); and 20 mL of fructose/2-(N-morpholino)ethanesulfonic acid (MES) solution (50x). The trace element solution was prepared as 100x stock solution containing (per liter): 2 g nitrilotriacetic acid (NTA); 1 g manganese sulfate monohydrate; 0.8 g ammonium iron(II) sulfate hexahydrate; 0.2 g Cobalt(II) chloride hexahydrate; 0.0002 g zinc sulfate heptahydrate; 0.2 g Copper(II) chloride dihydrate; 0.02 g Nickel(II) chloride hexahydrate; 0.02 g sodium molybdate dihydrate; 0.02 g sodium selenate; and 0.02 g sodium tungstate. The pH of the trace element solution

was adjusted to 6.0 after adding NTA. The solution was autoclaved and stored at 4°C. Wolfe's vitamin solution was prepared aerobically containing (per liter): 2 mg biotin; 2 mg folic acid; 10 mg pyridoxine-hydrochloride; 5 mg thiamin-HCl; 5 mg riboflavin; 5 mg nicotinic acid; 5 mg calcium pantothenate; 5 mg p-aminobenzoic acid; 5 mg lipoic acid; and 0.1 mg cobalamin. The vitamin solution was sterilized by sterile filtration (pore size 0.2 μm), sparged with sterile N_2, and stored at 4°C. The 50x fructose/MES solution contained (per 100 mL): 25 g fructose; and 10 g MES. The pH was adjusted to 6.0 with potassium hydroxide. The 50x fructose/MES solution was sterilized by sterile filtration (pore size 0.2 μm), sparged with sterile N_2, and stored at room temperature (RT). For autotrophic growth experiments, the fructose was omitted in the MES solution. The reducing agent contained (per 100 mL): 0.9 g sodium hydroxide and 4 g L-cysteine hydrochloride. The reducing agent was prepared with anaerobic water in an anaerobic workbench (Workstation LABmaster Pro, which was equipped with Gas Purifier MB20/MB200 G, MBraun, Garching, Germany), autoclaved, and stored at RT. For chemostat fermentations, the amount of L-cysteine hydrochloride was doubled. Heterotrophic cultivations with fructose were conducted in 100 mL medium aliquots in 240-mL SB. Pre-cultures were grown in 50 mL PETC medium in 100-mL SB. The medium was supplemented with appropriate amounts of thiamphenicol (Tm) (5 μg/mL) or clarithromycin (Clr) (5 μg/mL) when necessary. Autotrophic cultivations with H_2/CO_2 (80:20, vol-%) or CO (100 vol-%) were performed in 100 mL PETC medium without fructose in 1-L Pressure Plus (PP) bottles (SCHOTT AG, Mainz, Germany). Cultures were incubated at 37°C and agitated at 150 rpm for proper gas-liquid mass transfer. Expression of the genes controlled by an anhydrotetracycline (aTc)-inducible promoter was induced with 100 ng/mL aTc.

All antibiotic stock solutions were stored at -20°C unless otherwise indicated. Stock solutions (1000x) for Amp (100 mg/mL), Kan (50 mg/mL), and Spec (60 mg/mL) were prepared with sterile water. Stocks (1000x) for Cm (30 mg/mL) were prepared with 70 vol-% ethanol. Ery stocks (100 mg/mL) were always prepared freshly with ethanol. Tm stocks (25 mg/mL) were prepared with DMSO (100 vol-%) and diluted 1:10 with sterile water *prior* to addition to the medium. A sterile syringe was used to transfer the diluted Tm solution into the culture bottles. For Clr stocks (2.5 mg/mL), water was adjusted to pH 2.0 to dissolve the clarithromycin. After dissolving, the solution was carefully adjusted to pH 6.0 and sterile filtered for storage. Stock solutions for aTc (100 mg/mL) were prepared with Dimethylsulfoxid (DMSO) (100 vol-%) and diluted 1:100 with sterile water.

3.2   Plasmid and primers used in this study

All plasmids and primers (Integrated DNA Technologies (IDT), Coralville, United States) are listed in tables 1-2.

Table 1: List of Plasmids used in this study.

Plasmid name	Description	Reference
pMTL83151	Broad host spectrum shuttle vector	(Heap *et al.*, 2009)
pMTL8315tet	pMTL 83151 with inducible aTc Promoter $P_{tetR-01}$	(Klask, 2021)
pASK-IBA3C	*E. coli* expression vector with an aTc-inducible promoter and C-terminal StrepTag	IBA Lifesciences
pASK-IBA3C_*aor1*	*E. coli* expression vector for aTc-inducible expression of *aor1*-StrepTag	This study
pASK-IBA3C_*aor2*	*E. coli* expression vector for aTc-inducible expression of *aor2*-StrepTag	This study
pASK-IBA3C_*fd1*	*E. coli* expression vector for aTc-inducible expression of *fd1*-StrepTag	(Petschak, 2019)
pASK-IBA3C_*fd2*	*E. coli* expression vector for aTc-inducible expression of *fd2*-StrepTag	(Petschak, 2019)
pMTL8315tet-*aor1*-Strep	*C. ljungdahlii* expression vector for aTc-inducible expression of *aor1*-StrepTag	This study
pMTL8315tet-*aor2*-Strep	*C. ljungdahlii* expression vector for aTc-inducible expression of *aor2*-StrepTag	This study
pMTLCas9	*E. coli – C. ljungdahlii* shuttle vector with aTc-inducible *cas9* gene	Supplied by Prof. Dr. Xia (unpublished work)
pTargetF	Plasmid containing P_{J23119} for sgRNA cassette	(Jiang *et al.*, 2015)
pgRNA_*aor1*	Plasmid containing sgRNA cassette for *aor1*	This study
pgRNA_*aor2*	Plasmid containing sgRNA cassette for *aor2*	This study
pMTLCas9-*aor1*	CRISPR plasmid for deletion of *aor1*	This study
pMTLCas9-*aor2*-STEP1	STEP1 Gibson Assembly for *aor2* deletion	This study
pMiniT2.0_donor-*aor2*	Sub-cloning of homologous repair DNA for *aor2* deletion	This study
pMTLCas9-*aor2*	CRISPR plasmid for deletion of *aor2*	This study
pANA1	Methylation plasmid with Φ3T methyltransferase	(Molitor *et al.*, 2016a)
pMTLts	Temperature-sensitive *E. coli – C. ljungdahlii* shuttle vector with pWV01ts (ts-ori)	(Molitor *et al.*, 2016a)
pMUT2ts	Temperature-sensitive *E. coli – C. ljungdahlii* shuttle vector with pWV01ts (ts-ori) and error-prone Polymerase IV	(Schulz, 2015)

Table 2: List of primers used in this study.

Name	Purpose	Sequence (5' – 3')	Reference
SaS-038	pASK-IBA3C_*aor1*	ATGGTAGGTCTCAAATGTATGGTTATGATG GTAAAGTATTAAGA	This study
SaS-039	pASK-IBA3C_*aor1*	ATGGTAGGTCTCAGCGCTGAACTTACCTAT ATATTCATCTAATCC	This study
SaS-040	pASK-IBA3C_*aor2*	ATGGTAGGTCTCAAATGTACGGATATAAGG GTAAGGTATTAAG	This study
SaS-041	pASK-IBA3C_*aor2*	ATGGTAGGTCTCAGCGCTAAGCTTACCTAC GTATTCATCTAATC	This study
SaS-042	Sequencing of pASK-IBA3C vectors	GAGTTATTTTACCACTCCCT	IBA Lifesciences
SaS-043	Sequencing of pASK-IBA3C vectors	CGCAGTAGCGGTAAACG	IBA Lifesciences
SaS-057	QuikChange pMTLts #2	CGAAATCCTGTAACAATAGAAAGCG	This study
SaS-058	QuikChange pMTLts #2	CGCTTTCTATTGTTACAGGATTTCG	This study
SaS-059	QuikChange pMTLts #4	GGATTTTTATTATATCCTGACTCAATTCC	This study
SaS-060	QuikChange pMTLts #4	GGAATTGAGTCAGGATATAATAAAAATCC	This study
SaS-062	pMTL8315tet-*aor1/2*-Strep	GCGTGACGTCGACTCTAGAGTTATTTTTCG AACTGCGG	This study
SaS-064	pMTL8315tet-*aor2*-Strep	ATAAACTTGAATTTGAAATAGAGGAGGTTA AGAATGTACGGATATAAGGGTAAG	This study
SaS-072	pMTL8315tet-*aor1*-Strep	ATAAACTTGAATTTGAAATAGGAGGTTAAG AATGTATGGTTATGATGGTAAAG	This study
SaS-085	pgRNA_*aor1*	GCTGGTGAACGATTGTCTCTGTTTTAGAGC TAGAAATAGC	This study
SaS-086	pgRNA_*aor1*	AGAGACAATCGTTCACCAGCGCTAGCATTA TACCTAGGAC	This study
SaS-120	pgRNA_*aor2*	AGTACAGCTGTTCCGTATGTGTTTTAGAGC TAGAAATAGC	This study
SaS-121	pgRNA_*aor2*	ACATACGGAACAGCTGTACTGCTAGCATTA TACCTAGGAC	This study
EBT-PFX-049	Sequencing pgRNA constructs	CTTTGAGTGAGCTGATACCG	Supplied by Prof. Dr. Xia
EBT-PFX-088	Amplification of sgRNA cassette	GGCTCACCTTCGGGTGGGCCTTTCTGCGTT ACCGCATATGCTGGATCCTT	(Xia *et al.*, 2020)
EBT-PFX-089	Amplification of sgRNA cassette	ACGTTGTAAAACGACGGCCAGTGCCGAGCT CTGCAGGTCGACTCTAGAGAAT	(Xia *et al.*, 2020)
SaS-077	LHA1	GAGGATCTGAATAGCGCCGTCGACTAAATA GGAATCCTGATATTATTATATTTGGG	This study
SaS-078	LHA1	CTTTCTAGTTTACCGAATCAAATGAAATTC CTCCTCATATAAATGT	This study
SaS-079	RHA1	CATTTATATGAGGAGGAATTTCATTTGATT CGGTAAACTAGAAAG	This study

SaS-080	RHA1	ACGTTGTAAAACGACGGCCAGTGCCGAGCT CTAACATTTACGGGTATTTGC	This study
SaS-101	Screening for Δ*aor1*	GCACAATCTCCTGCAA	This study
SaS-106	Screening for Δ*aor1*	CCAGCTATATACCATATCTTG	This study
SaS-109	Screening for Δ*aor1*	GATTGCTGATTCTTGGAAG	This study
SaS-110	Screening for Δ*aor1*	GCCTTTTAACTTTTATCTGATG	This study
SaS-162	STEP1 Gibson Assembly for *aor2* deletion	ACGTTGTAAAACGACGGCCAGTGCCGAGCT GTCGACTCTAGAGAATTCAAAAAAAGC	This study
SaS-102	LHA2	GAGGATCTGAATAGCGCCGTCGACTAAATG TGTTATGACTAGAGAATGCG	This study
SaS-082	LHA2	CTAATCTCTAATTAATCAAAAAAAACCCTC CTAAAAAATTGATTA	This study
SaS-083	RHA2	ATTTTTTTAGGAGGGTTTTTTTTGATTAAT TAGAGATTAGACTTCATG	This study
SaS-084	RHA2	ACGTTGTAAAACGACGGCCAGTGCCGAGCT GTGGAACTATTTCATACTCACT	This study
SaS-124	Overlap extension PCR for repair DNA	GAGGATCTGAATAGCGCCG	This study
SaS-125	Overlap extension PCR for repair DNA	ACGTTGTAAAACGACGGCC	This study
Sas-174	Flip donor for STEP 2 Gibson Assembly for *aor2* deletion	ACGTTGTAAAACGACGGCCAGTGCCGAGCT AGTGGTACAGGTAAAGAAATCTTTG	This study
Sas-175	Flip donor for STEP 2 Gibson Assembly for *aor2* deletion	CGAGTCGGTGCTTTTTTTGAATTCTCTAGA GTGGAACTATTTCATACTCACTAGAG	This study
SaS-129	screening for pMTLCas9-*aor* plasmids	CTCTGCCAAGCAAATATGTG	This study
SaS-130	screening for pMTLCas9-*aor* plasmids	GGACTAGCCTTATTTTAACTTGC	This study
EBT-PFX-121	Sequencing pMTLCas9-*aor*	CTCGAGTAAGGATCTCCAGGCA	Supplied by Prof. Dr. Xia
SaS-103	Sequencing pMTLCas9-*aor*	GAGTCAGAGTTGCTTG	This study
SaS-104	Sequencing pMTLCas9-*aor*	TGCTTGGCGCAATAC	This study
SaS-105	Sequencing pMTLCas9-*aor*	CCAAAGGAATCGAAAAGG	This study
SaS-115	Sequencing pMTLCas9-*aor*	CCTCCACAGCCTACAAC	This study
SaS-103	Screening for Δ*aor2*	GAGTCAGAGTTGCTTG	This study
SaS-104	Screening for Δ*aor2*	TGCTTGGCGCAATAC	This study
SaS-105	Screening for Δ*aor2*	CCAAAGGAATCGAAAAGG	This study
SaS-108	Screening for Δ*aor2*	CAGTAAGACTCAAAACTCC	This study

fdhA_fwd	Strain-specific primer for *C. ljungdahlii*	AGTGCAGCGTATTCGTAAGG	(Molitor *et al.*, 2016a)
fdhA_rev	Strain-specific primer for *C. ljungdahlii*	TAATGAGCCACGTCGTGTTG	(Molitor *et al.*, 2016a)
M13F	Sequencing	CAGGAAACAGCTATGACC	IDT
M13R	Sequencing	TGTAAAACGACGGCCAGT	IDT

3.3 Molecular methods for genetic modification of *E. coli*

3.3.1 PCR amplification with Q5® Hot Start High-Fidelity Polymerase

All DNA amplification for cloning purposes were performed with Q5® Hot Start High-Fidelity Polymerase (NEB, Frankfurt, Germany). Primers were designed with SnapGene (GSL Biotech LLC, San Diego, USA) and annealing temperatures were calculated with NEB TmCalculator. The reactions were set up on ice (Table 3). Master mixes were prepared for all PCRs to minimize pipetting errors and the individual reactions were aliquoted into 0.2-mL PCR tubes. Amplifications were performed in a Mastercycler Pro S (Eppendorf, Hamburg, Germany) (Table 4). Subsequently, the products were pooled, purified *via* QIAquick PCR Purification Kit (Qiagen, Hilden, Germany), and eluted in 40 µL elution buffer (EB) twice. Successful amplifications were controlled *via* agarose gel electrophoresis (Chapter 3.3.12). DNA concentration of the eluted product was determined with a Nanodrop spectrophotometer (NP80, Implen, Munich, Germany) or estimated *via* gel electrophoresis.

Table 3: Reaction setup for DNA amplification with Q5® Hot Start High-Fidelity Polymerase.

Component	Amount
5x Q5® Reaction Buffer	10 µL
dNTP mix (10 mM)	1 µL
Forward Primer (10 µM)	2.5 µL
Reverse Primer (10 µM)	2.5 µL
Template DNA (ca. 1-10 ng)	1 µL
Q5 Polymerase	0.5 µL
Nuclease-free water	32.5 µL
Total reaction volume	50 µL

Table 4: PCR conditions for Q5® Hot Start High-Fidelity Polymerase.

Step	Temperature	Time	# cycles
Initial Denaturation	98°C	2 min	1
Denaturation	98°C	10 sec	
Annealing	50-72°C	30 sec	35
Extension	72°C	20-30 sec/kb	
Final Extension	72°C	2 min	1
Hold	4-10°C	∞	∞

3.3.2 Overlap extension PCR

Overlap extension PCR is commonly used to fuse DNA fragments *in vitro*. First, the target fragments were extended by amplification with primers containing overhangs homologous to the other fragment. Second, the fragments were fused by an overlap PCR with only the outside primers (Table 5). The overlap PCR was first set up without the primers and placed into a Mastercycler Pro S. The first 10 cycles were run without primers at an annealing temperature of 60°C. For the second phase, primers were added and the last 25 cycles were run at an annealing temperature of 72°C.

Table 5: Conditions for overlap extension PCR Q5® Hot Start High-Fidelity Polymerase.

Step		Temperature	Time	# cycles
	Initial Denaturation	98°C	2 min	1
1 (no primers)	Denaturation	98°C	10 sec	
	Annealing	60°C	90 sec	10
	Extension	72°C	2 min	
	Denaturation	98°C	10 sec	
	Annealing	72°C	90 sec	25
2 (add primers)	Extension	72°C	2 min	
	Final Extension	72°C	2 min	1
	Hold	4-10°C	∞	∞

3.3.3 Restriction/Ligation cloning

PCR fragments designated for restriction/ligation cloning were digested with 1 µL restriction enzyme for 1 h at the optimal temperature of the respective restriction enzyme (commonly 37°C) in the PCR buffer after amplification. Digestion of plasmid DNA was set up in CutSmart Butter (10x) (NEB, Frankfurt, Germany) and incubated for 15 min for control digests or 1-3 h for cloning purposes (Table

6). For vector backbones, Calf Intestinal Alkaline Phosphatase (CIP) (NEB, Frankfurt, Germany) was added to remove phosphate residues to prevent re-ligation. Restriction digests were heat-inactivated, if necessary, purified *via* QIAquick PCR Purification Kit (Qiagen, Hilden, Germany), and eluted in 40 µL EB twice. DNA concentration of the eluted product was determined with a Nanodrop spectrophotometer (NP80, Implen, Munich, Germany) or estimated *via* gel electrophoresis.

Table 6: Setup of restriction digest reactions with NEB restriction enzymes.

Component	For cloning Incubation 1-3 h	Control digests Incubation for 15 min
10x CutSmart Buffer	5 µL	1 µL
DNA	1-2 µg	1 µL
Enzyme I	1 µL	0.2 µL
Enzyme II	1 µL	0.2 µL
Alkaline Phosphatase, Calf Intestinal (CIP) (only for vector backbones)	1 µL	-
Nuclease-free water	To 50 µL	To 10 µL
Total reaction volume	50 µL	10 µL

T4 DNA Ligase (NEB, Frankfurt, Germany) was used for sticky-end and blunt-end cloning of inserts into linearized vectors after restriction digests. Reactions were set up in a total reaction volume of 20 µL and at a molar ratio of 1:3 (vector:insert). The reactions were mixed carefully by pipetting up and down and incubated at room temperature for 15 min to 2 h. The ligase was heat-inactivated for 10 min at 65°C and kept on ice *prior* to the transformation of *E. coli* with 10 µL of the ligation mixture.

3.3.4 Sub-cloning with NEB® PCR Cloning Kit

Sub-cloning of fragments from genomic DNA (gDNA) of *C. ljungdahlii* was used for convenient amplification from a vector and preservation of hard-to-clone fragments. The NEB® PCR Cloning Kit (NEB, Frankfurt, Germany) was used in all cases (Table 7). First, the supplied linearized vector (pMiniT2.0), the insert, and nuclease-free water were mixed in a total reaction volume of 5 µL. Second, the Cloning Mix 1 and 2 were added and the reaction was incubated at RT for 15 min. The ligation was cooled down on ice for 2 min and 5 µL of the ligation was used to transform *E. coli* TOP10.

Table 7: Setup of sub-cloning reactions with the NEB® PCR Cloning Kit

Step	Component	Amount
1	Linearized pMiniT2.0 Vector (25 ng/µL)	1 µL
	Insert	1-4 µL
	Nuclease-free water	To 5 µL
2	Cloning Mix 1	4 µL
	Cloning Mix 2	1 µL
	Total reaction volume	10 µL

3.3.5 Gibson Assembly® with the NEBuilder® HiFi DNA Assembly Kit

The NEBuilder® HiFi DNA Assembly Kit was used for assembly for multi-fragment constructs. The insert fragments were prepared by amplification with Q5® Hot Start High-Fidelity Polymerase. The vector DNA was prepared by restriction digestion with a single cutter and CIP for 3 h or overnight. All fragments were purified *via* the QIAquick PCR Purification Kit (Qiagen, Hilden, Germany), eluted in 40 µL EB twice and the DNA concentrations were calculated *via* gel electrophoresis. For assembly, the linearized vector, inserts, and the master mix were mixed with nuclease-free water in a total reaction volume of 20 µL (Table 8). The reaction was incubated at 50°C for 60 min in a Mastercycler Pro S (Eppendorf, Hamburg, Germany). 10 µL of the reaction was used for transformation of self-prepared or commercial NEB® Stable Competent *E. coli* (High Efficiency) cells. Colonies were screened by colony PCR after 16-24 h (Chapter 3.3.9).

Table 8: Setup of Gibson Assembly® reactions with the NEBuilder® HiFi DNA Assembly Kit

Component	2-3 Fragments	>3 Fragments
DNA molar ratio (vector:insert)	1:2 (1:3)	1:1
NEBuilder Master Mix	10 µL	10 µL
Linearized vector (~100 ng)-	1-2 µL	1-2 µL
Insert I	X µL	X µL
(Insert II)	X µL	X µL
Nuclease-free water	To 20 µL	To 20 µL
Total reaction volume	20 µL	20 µL

3.3.6 Site-directed mutagenesis with the QuikChange® II Kit

QuikChange® II (Agilent, Santa Clara, USA) is a kit used for site-directed mutagenesis and was used to restore the point mutations in pMTLts. The DNA amplification was performed with *PfuUltra* High-

Fidelity DNA polymerase (Agilent, Santa Clara, USA). The primers were designed and annealing temperatures were calculated with the QuikChange Primer Design tool (Agilent, Santa Clara, USA). The reactions were set up on ice (Table 9). Master mixes were made for all PCRs to minimize pipetting errors and the individual reactions were aliquoted into 0.2-mL PCR tubes. The amplifications were performed in a Mastercycler Pro S (Eppendorf, Hamburg, Germany) (Table 10). Subsequently, the products were digested with *Dpn*I and 10 µL of the reaction were used for transformation of *E. coli* for nick repair.

Table 9: Reaction setup for DNA amplification with *PfuUltra* High-Fidelity DNA polymerase.

Component	Amount
10x Reaction Buffer	5 µL
dNTP mix (10 mM)	1 µL
Forward Primer (10 µM)	1.25 µL
Reverse Primer (10 µM)	1.25 µL
Template DNA (ca. 2-100 ng)	2 µL
Q5 Polymerase	1 µL
Nuclease-free water	38.5 µL
Total reaction volume	50 µL

Table 10: PCR conditions for *PfuUltra* High-Fidelity DNA polymerase.

Step	Temperature	Time	# cycles
Initial Denaturation	95°C	30 sec	1
Denaturation	95°C	30 sec	
Annealing	50-68°C	1 min	12
Extension	68°C	1 min /kb	
Final Extension	68°C	2 min	1
Hold	4-10°C	∞	∞

3.3.7 Preparation of chemically competent *E. coli* cells (Sambrook *et al.*, 1989), modified by Christian Klask (2017)

To prepare competent *E. coli* cells, an overnight culture was used to inoculate 100 mL LB medium in a 500-mL baffled flask (start OD_{600} ~0.05-0.1). The culture was incubated for about 1-1.5 h at 37°C with agitation. Cells were harvested at an OD_{600} of 0.3-0.5 by centrifugation at 3,750 x g for 15 min at 4°C (Centrifuge 5920 R, rotor S-4x1000, Eppendorf, Hamburg, Germany) in sterile 50-mL falcon tubes. The

pelleted cells were placed on ice and kept on ice for the remaining steps. Cells were resuspended gently in 50 mL ice-cold 100 mM $CaCl_2$-solution and incubated for 15-30 min. The cells were washed a second time before gently resuspending in 8 mL of ice-cold 100 mM $CaCl_2$ solution with 25 vol-% glycerol. After 20 min incubation on ice, the cells were aliquoted into 1.5-mL tubes (100 µL/tube) and frozen in liquid nitrogen for storage at -80°C for up to three months.

3.3.8   Chemical transformation of competent *E. coli* cells

For chemical transformation of *E. coli*, an aliquot of 100 µL cell suspension was thawed on ice. The cells were mixed with 5 µL NEB® PCR Cloning Kit ligation reaction, 10 µL T4 DNA ligase ligation reaction, 10 µL NEBuilder® HiFi DNA Assembly Kit reaction, or 1-2 µL purified plasmid DNA by swirling with the pipette tip and incubated on ice for 30 min. Afterward, the cells were treated with heat shock at 42°C for 45 sec and cooled down on ice for 2 min. For cell recovery, 900 µL SOC medium was added and the tube was incubated at 37°C for 1 h. The cells were harvested by centrifugation at 13,000 rpm for 3 min (Centrifuge 5427 R, rotor FA-45-24-11-Kit, Eppendorf, Hamburg, Germany) and the supernatant was discarded. Afterward, the cells were resuspended in the remaining ~90 µL of SOC medium and plated on pre-warmed LB plates containing the respective selective antibiotics. Plates were incubated at 37°C for 16-24 h until colonies formed.

3.3.9   Colony PCR with Phire Plant Direct PCR Master Mix

Screenings of colonies on selective plates and liquid cultures were performed with the Phire Plant Direct PCR Master Mix (ThermoFisher Scientific, Waltham MA, USA). Primers were designed with SnapGene and the annealing temperatures were calculated with ThermoFisher Scientific T_m Calculator. The reactions were set up on ice (Table 11). Master mixes were made for all PCRs to minimize pipetting errors and the individual reactions were aliquoted into 0.2-mL PCR tubes. For screenings of colonies on selective plates, sterile toothpicks were used to pick the colony, re-streak it onto a fresh selective plate, and dabbed into the aliquoted master mix in a 0.2-mL PCR tube. For screening of liquid cultures, 1 µL of DNA, isolated by lysing the cells (Chapter 3.8.3) or gDNA isolation (Chapter 3.3.11), was added to the aliquoted master mix. The amplifications were performed in a Mastercycler Pro S (Eppendorf, Hamburg, Germany) (Table 11). The products were analyzed *via* agarose gel electrophoresis (Chapter 3.3.12). For subsequent Sanger sequencing, the PCR products were pooled, purified *via* QIAquick PCR Purification Kit (Qiagen, Hilden, Germany), and eluted in 40 µL EB twice (Chapter 3.3.13).

Table 11: Reaction setup for DNA amplification with the Phire Plant Direct PCR Master Mix.

Component	Amount
2x Phire Plant Direct PCR Master Mix	10 µL
Forward Primer (10 µM)	0.8 µL
Reverse Primer (10 µM)	0.8 µL
Template DNA/colony from plate	1 µL / -
Nuclease-free water	To 20 µL
Total reaction volume	20 µL

Table 12: PCR conditions for DNA amplification with the Phire Plant Direct PCR Master Mix.

Step	Temperature	Time	# cycles
Initial Denaturation	98°C	5 min	1
Denaturation	98°C	5 sec	
Annealing	50-72°C	5 sec	35
Extension	72°C	20 sec/kb	
Final Extension	72°C	2 min	1
Hold	4-10°C	∞	∞

3.3.10 Plasmid isolation

Isolation of plasmid DNA from liquid culture for screening was performed with an alkaline lysis protocol adapted from Sambrook *et al.* (1989) (Klask, 2021). Recombinant *E. coli* strains were grown in 5 mL LB medium overnight and cells were harvested at 17,900 x g for 3 min. The supernatant was discarded and the cell pellet was resuspended in 150 µL P1 buffer (Table 13) by vortexing. The cells were lysed by adding 150 µL P2 buffer (Table 13) and inverting 5 times. For protein precipitation, 250 µL P3 buffer (Table 13) was added, the tubes were inverted 5 times, and centrifuged at 17,900 x g for 10 min. During centrifugation, aliquots of 500 µL isopropanol in 1.5-mL tubes were prepared for each of the samples. 500 µL supernatant was carefully removed and transferred to the isopropanol for DNA precipitation. The supernatant was discarded after pelleting the DNA by centrifugation at 17,900 x g for 3 min. The DNA pellets were washed twice with 500 µL ice-cold ethanol 70 vol-% (without resuspension). The supernatant was removed carefully and the DNA was dried at 50-65°C for 10 min. The plasmid DNA was resuspended in 30 µL EB. Buffer P1 was stored at 4°C *prior* to use to maintain RNAse activity, buffers P2 and P3 were stored at RT. The eluted plasmid DNA concentration was determined with a Nanodrop spectrophotometer (NP80, Implen, Munich, Germany) or estimated *via* gel electrophoresis.

Table 13: Buffers for plasmid isolation with alkaline lysis (Klask, 2021).

Buffer	Component	Concentration
P1 – Resuspension buffer (stored at 4°C)	Tris	50 mM
	EDTA	10 mM
	RNAseA	100.0 µg/mL
	pH (with HCl)	8.0
P2 – Lysis buffer	NaOH	200 mM
	SDS	1 vol%
P3 – Neutralization/Protein precipitation buffer	Sodium acetate	2.55 M
	pH (with acetic acid)	4.8

For isolation of highly pure plasmid DNA for sequencing or cloning purposes, QIAprep Spin Miniprep Kit (Qiagen, Hilden, Germany) was used according to the manufacturer's protocol and DNA was eluted in 50 µL EB twice. For isolation of low-copy and single-copy plasmids, the QIAprep® Spin Midiprep protocol was applied, using double amounts of buffers P1, P2, and N3.

3.3.11 gDNA isolation with the NucleoSpin Microbial DNA Mini kit

For isolation of gDNA from liquid cultures, the NucleoSpin Microbial DNA Mini kit (Macherey-Nagel, Düren, Germany) was used. Depending on the optical density of the culture, 0.5-1.5 mL cell suspension was harvested at 17,900 x g for 5 min. The supernatant was discarded and the cell pellet was resuspended in 100 µL BE buffer and transferred into a supplied MN tube Type B (with lysis matrix beads). The lysis conditions were adjusted by adding 40 µL MG buffer and 10 µL liquid Proteinase K. The tubes were placed into a FastPrep-24™ 5G beating grinder and lysis system, which was equipped with a QuickPrep™ 24 x 2 mL Sample Holder (MP Biomedicals™). The lysis was achieved in two cycles at 6.5 m/sec for 30 sec (rest time 300 sec). The beads and foam were displaced from the screwcap by centrifugation at 11,000 x g for 30 sec. The DNA binding conditions were adjusted by adding 600 µL MG buffer, mixing by vortexing, and centrifugation at 11,000 x g for 30 sec. The DNA-containing supernatant (~550 µL) was carefully removed from the tube, transferred to a supplied NucleoSpin® Microbial DNA Column, and bound to the column by centrifugation at 11,000 x g for 30 sec. First, the membrane was washed with 500 µL BW buffer and the collection tube containing the flowthrough was replaced by a fresh collection tube. Second, the membrane was washed with 500 µL B5 buffer, the flowthrough was discarded, and the membrane was dried by centrifugation at 11,000 x g for 30 sec. The gDNA was eluted from the membrane with 100 µL BE. The DNA concentration of the eluted product was determined with a Nanodrop spectrophotometer (NP80, Implen, Munich, Germany) or estimated *via* gel electrophoresis. The gDNA was diluted 1:100 for subsequent use in PCRs.

3.3.12 Agarose gel electrophoresis

Agarose gel electrophoresis was used for the separation and identification of DNA fragments and the calculation of concentrations. All agarose gels were prepared by dissolving 1 weight-% agarose in 100 mL 1x TAE buffer (Table 14). After cooling down, the DNA staining agent Midori Green Advance DNA Stain (Biozym, Hessisch Oldendorf, Germany) was added, and the mixture was poured into a gel tray, which was equipped with a suitable comb. After solidification of the gel for 20 min at RT, PerfectBlue Gelsystems (VWR, Bruchsal, Germany) for electrophoresis were filled with 1x TAE. The gel was placed into the system, samples were loaded onto the gel, and electrophoresis was run at 130-140 V for 30-45 min. Samples were mixed with the Purple (6X) Gel Loading Dye (NEB) and the GeneRuler 1 kb DNA Ladder, ready-to-use (ThermoFisher Scientific, Waltham MA, USA) was applied as a size and concentration standard. The DNA was visualized by illumination with an UV light and an ethidium bromide filter in a UVP ChemStudio Plus Gel Documentation System (Analytik Jena, Jena, Germany).

Table 14: Components for TAE buffer.

Component	Amount for 50x TAE	Concentration in 1xTAE
Tris	242 g	40 mM
EDTA	18.61 g	1 mM
Glacial acetic acid	57.1 mL	
$H_2O_{millipore}$	To 1000 mL	

3.3.13 Sanger sequencing

To prove the correct assembly of plasmid constructs or genomic deletions, samples were sequenced by Sanger sequencing. Highly pure DNA was analyzed at the genomics center of the Max-Planck Institute for Biology Tübingen or by an external company (GeneWiz Inc., Leipzig, Germany). Sequencing reads were mapped to plasmid/genome sequences with SnapGene.

3.3.14 Long-term storage of *E. coli* strains

For long-term storage of recombinant *E. coli* strains, 2-mL screwcap vials containing 500 µL glycerol solution 80 vol-% were prepared and sterilized by autoclaving. Cryo stocks were prepared by mixing 1 mL of an overnight culture of the recombinant strain with the glycerol solution. The cryo stocks were mixed by vortexing, incubated on ice for 30 min, barcoded, and stored at -80°C. All strains were kept in duplicates and added to the database of the Environmental Biotechnology Lab.

3.4 Design and construction of vectors for production of clostridial proteins in *E. coli*

For heterologous production of clostridial proteins in *E. coli*, the commercial expression vector pASK-IBA3C (IBA Lifesciences, Göttingen, Germany) consisting of ColE1 and F1 origin of replication, *CamR*, an inducible tetracycline-promoter system, and a multiple cloning site (MCS) with a C-terminal Strep-tag®II was used. To produce AOR enzymes, the target genes *aor1* (CLJU_c20110) and *aor2* (CLJU_c20210) were amplified from gDNA of *C. ljungdahlii* and inserted in pASK-IBA3C by restriction/ligation cloning with *Bsa*I using primers SaS-038-041 (Table 2).

3.5 Design and construction of vectors for overproduction of clostridial proteins in *C. ljungdahlii*

To produce the enzymes AOR1 and AOR2 in *C. ljungdahlii*, vectors with an inducible expression system based on an anhydrotetracycline-inducible promoter ($P_{tetR-01}$) by Dong *et al.* (2012) and Woolston *et al.* (2018) were designed. The *aor* genes were fused to a C-terminal StrepTag to facilitate straightforward enzyme purification *via* affinity chromatography (Figure 11). pMTL8315tet, containing ColE1 and *traJ*, pCB102, *catP*, and $P_{tetR-01}$ (Klask, 2021) served as the backbone. Plasmids pMTL8315tet-*aor1*-Strep and pMTL8315tet-*aor2*-Strep were assembled by insertion of the respective *aor* gene and the fused StrepTag (PCR amplified with primers SaS-062 and SaS-072/SaS-064 (Table 2) from pASK-IBA3C_*aor1* or pASK-IBA3C_*aor2*, respectively) with Gibson Assembly at the *Bam*HI restriction site.
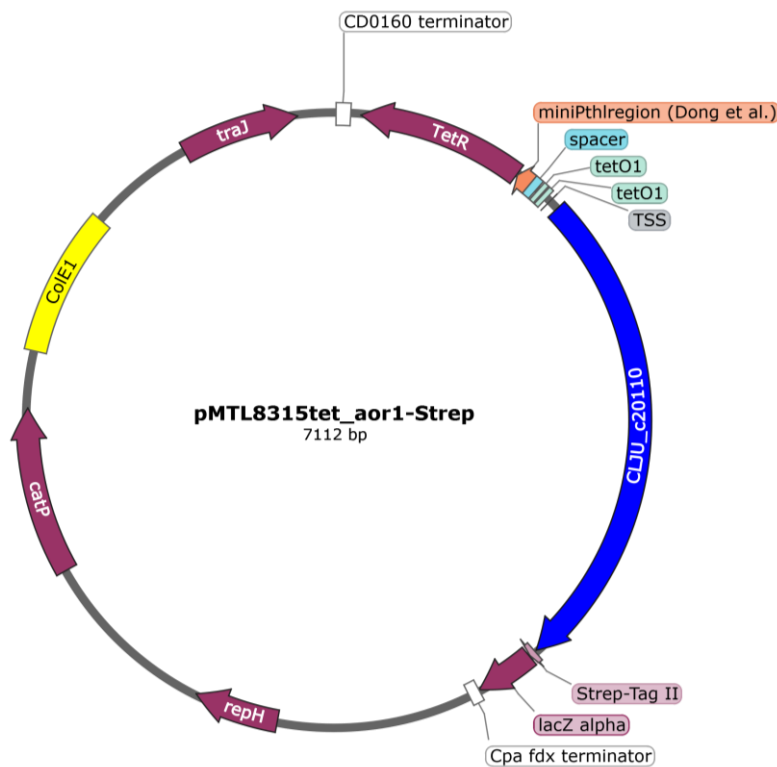
Figure 11: Plasmid map of *aor1* expression system pMTL8315tet-aor1-StrepTag. The plasmid consists of a pMTL8315tet backbone (Klask, 2021) and *aor1* controlled by P$_{tetR-01}$ (Dong *et al.*, 2012; Woolston *et al.*, 2018) and fused with a C-terminal StrepTag II**.**

3.6   *Triple-Cross* **method for genome editing in** *C. ljungdahlii*

An adapted *Triple-Cross* method for *aor* deletions was designed during my master's thesis (Schulz, 2018). The original design by Walker *et al.* (2015) (Chapter 2.3.3) was adapted by exchanging the marker for CS1 with the temperature-sensitive ori pWV01ts from pMTLts (Table 1). The *mazF* toxin gene was chosen as counter-selection maker CS2. All incubations with strains carrying pMTLts or pMUT2ts were performed at 30°C (permissive temperature) and plasmid isolations were performed *via* Midi prep protocol.

3.7   **Design and construction of a CRISPR/Cas9 system for genome editing in** *C. ljungdahlii*

To construct a functional CRISPR/Cas9 system for the deletion of both *aor* genes in *C. ljungdahlii*, a multi-step cloning strategy was developed. The system was inspired by the base-editing system that was previously designed by Prof. Dr. Pengfei Xia in the EBT lab (Xia *et al.*, 2020). The Plasmid pMTLCas9 (supplied by Prof. Dr. Xia, unpublished work) served as the vector backbone (Table 1). It contained P$_{tetR-01}$-*cas9* in a pMTL84422 backbone (Heap *et al.*, 2009; Woolston *et al.*, 2018) and was linearized by digestion with *Sal*I and CIP overnight. For the sgRNAs, we chose multiple possible target sequences

(protospacer) for each isoform; one at the beginning of the CDS of the gene and one in the middle (Table 15).

Table 15: Single guide RNAs used for CRISPR edits in *C. ljungdahlii*.

sgRNA	PAM	Sequence (5' – 3')	Target	Successful CRIPSR edit?
sgRNA1.1	AGG	GTTACTAAAGCACCGCTTAC	*aor1* after 13 %	No
sgRNA1.2	AGG	GCTGGTGAACGATTGTCTCT	*aor1* after 27 %	Yes
sgRNA2.1	AGG	GGAAACAGATTCGAGAGCTA	*aor2* after 25 %	No
sgRNA2.2	TGG	ACATACGGAACAGCTGTACT	*aor2* after 39 %	No
sgRNA2.3	TGG	AGTACAGCTGTTCCGTATGT	*aor2* after 39 %	Yes
sgRNA2.4	AGG	ATGTACTATTGCAGCAGCTA	*aor2* after 57 %	No

The expression of the sgRNA is controlled by a synthetic constitutive promoter (P_{J23119}) (Jiang *et al.*, 2015), which has been shown to work in different Clostridia strains (Li *et al.*, 2016; Li *et al.*, 2019; Schmitz *et al.*, 2019). The protospacer region in the construct was exchanged by inverse PCR of the template plasmid pTargetF (Table 1). The 20-bp protospacer sequences were added to the primers as overhang during inverse PCR (Table 2). The PCR products were digested with *Dpn*I for 1 h to remove template DNA and *E. coli* TOP10 was transformed with the digested product, forming plasmids pgRNA_*aor1* and pgRNA_*aor2*. The *aor*-targeting sgRNA expression cassettes were amplified from pgRNA_*aor1/2* with Gibson overhangs. Homologous regions LHA1 and RHA1 served as repair template DNA for genome editing after the CRISPR event and were chosen as the up- and downstream regions (about 1 kb) of the target gene. Both regions were amplified from gDNA of *C. ljungdahlii* with Gibson primers (Table 2). The digested backbone pMTLCas9, sgRNA1.2 (Table 15), LHA1, and RHA1 were assembled with Gibson Assembly, resulting in pMTLCas9-*aor1* (Figure 12). Correct assembly of the plasmid was screened *via* colony PCR (Table 2) and verified *via* Sanger sequencing.
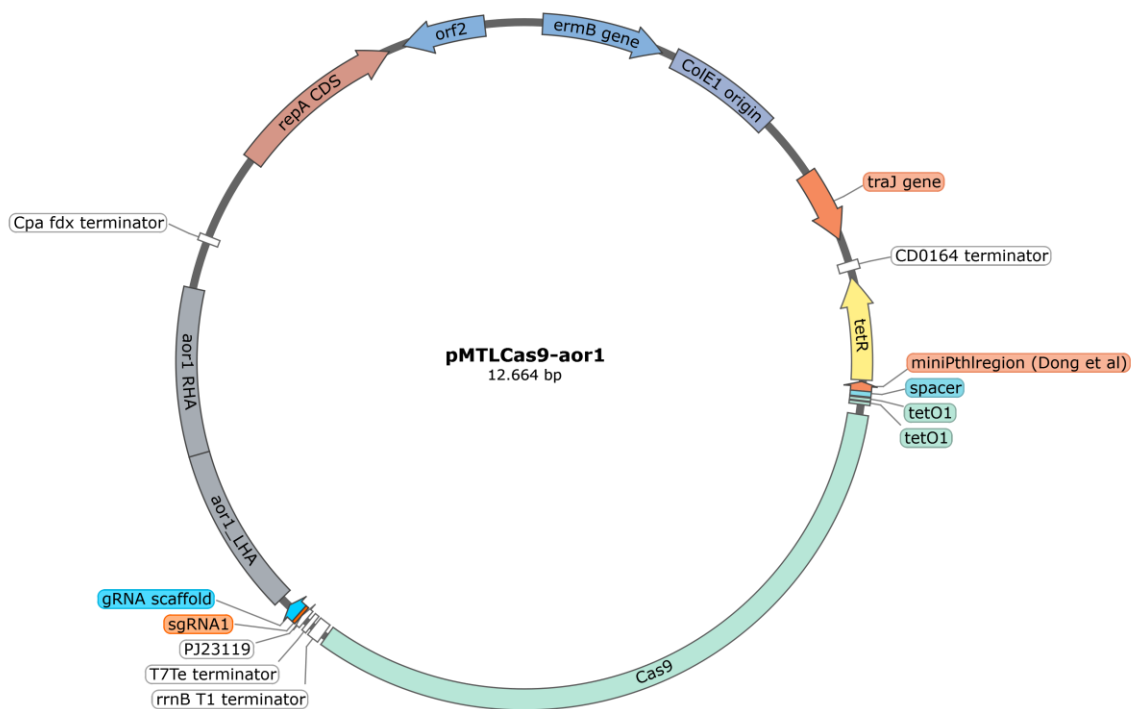
Figure 12: Plasmid map of pMTLCas9-*aor1* for deletion of *aor1* in *C. ljungdahlii*. The plasmid consists of pMTLCas9 backbone, homologous repair DNA LHA1 and RHA1, and the sgRNA1.2 cassette.

Assembly of the pMTLCas9-*aor2* appeared less trivial and was performed in two successive Gibson assemblies. First, the digested backbone pMTLCas9 and the sgRNA2.3 (Table 15) were fused, recovering the *Sal*I restriction site (Table 2) and resulting in pMTLCas9-*aor2*-STEP1. To generate the homologous repair DNA, LHA2 and RHA2 were amplified from the gDNA of *C. ljungdahlii.* The two fragments were fused by overlap extension PCR (Chapter 3.3.2) and the product was sub-cloned into pMiniT2.0 (Chapter 3.3.4), resulting in pMiniT2.0_donor-*aor2*. The donor sequence was amplified, flipped with Gibson primers (Table 2), and purified. For the final assembly of plasmid pMTLCas9-*aor2,* pMTLCas9-*aor2*-STEP1 was digested with *Sal*I and CIP overnight, purified, and fused with the donor-*aor2*-fragment by Gibson Assembly. Correct assembly of the plasmid was screened *via* colony PCR (Table 2) and verified *via* Sanger sequencing.

3.8   Molecular methods for genetic modification of *C. ljungdahlii*

3.8.1   Plasmid methylation

C. ljungdahlii possesses a very efficient defensive restriction system against foreign DNA. To enhance transformation efficiencies, plasmids were methylated with a site-specific methylation pattern (Molitor *et al.*, 2016a). This *in vivo* methylation was achieved *via* co-transformation of *E. coli* TOP10 with the target plasmid and a methylation plasmid pANA1 (Table 1). The plasmid contained a gene for

the methyltransferase that produces the specific methylation pattern. The methylated plasmids were isolated from liquid culture and tested for successful methylation by test digestions with *Hae*III. The restriction enzyme *Hae*III cleaves only the unmethylated plasmids, whereas the methylation pattern protects the plasmids from cleavage.

3.8.2   Electroporation of *C. ljungdahlii* cells

The transformation protocol for *C. ljungdahlii* was adopted from Molitor *et al.* (2016a). Cells were grown in liquid culture (100 mL culture volume) until early exponential phase (OD$_{600}$ ~0.2-0.4). The culture was transferred into an anaerobic workbench (Workstation LABmaster Pro, which was equipped with Gas Purifier MB20/MB200 G, MBraun, Garching, Germany) and transferred into sterile 50-mL Falcon tubes (kept in anaerobic workbench for at least 48 h *prior* to use). Cells were harvested at 4°C in a pre-cooled centrifuge at 3,750 x g for 15 min (Centrifuge 5920 R, rotor S-4x1000, Eppendorf, Hamburg, Germany) and transferred back into the anaerobic workbench immediately to minimize oxygen exposure. All further steps were performed in the anaerobic workbench at <0.5 ppm oxygen while keeping the cells on ice. The supernatant was discarded, and the cells were re-suspended in 10 mL ice-cold anaerobic 10 volume-% glycerol. The cell suspension was aliquoted into sterile 1.5-mL tube (max. 10 reactions in total), and the cells were spun down in a mySPIN™ 12 Centrifuge (ThermoFisher Scientific, Waltham MA, USA). The cells were washed with 1 mL ice-cold anaerobic 10 volume-% glycerol each two more times and re-suspended in 200 µL ice-cold anaerobic 10 volume-% glycerol. The cells were mixed with ≥2 µg methylated plasmid DNA and transferred to a pre-chilled electroporation cuvette (gap-size 0.2 cm). After the electroporation (2.5 kV, 600 Ω, 10 µF), the cells were quickly transferred into pre-warmed (37°C) 5 mL RCM in Hungate tubes without antibiotics. After 16-24 h of regeneration at 37°C, the cells were plated. Freshly prepared anaerobic RCM agar was transferred into the anaerobic workbench and cooled down to approximately 45-35°C. For each plate, 25 mL agar medium containing the respective antibiotics were mixed with 100 µL recovered culture and poured into a petri dish. The plates were incubated at 37°C for up to 14 days until single colonies were obtained. Using a sterile pipette tip, colonies were picked into liquid selective medium. After 1-2 days of incubations, the strains were verified *via* colony PCR with strain-specific and plasmid-specific primers (Table 2). As an additional control, the plasmid was isolated from liquid recombinant *C. ljungdahlii* culture and *E. coli* was re-transformed with the isolated plasmid DNA.

3.8.3   CRISPR/Cas9 genome editing in *C. ljungdahlii*

For genome editing of *C. ljungdahlii* with the developed CRISPR/Cas9 system (Chapter 3.7), the transformation protocol (Chapter 3.8.2) was adapted. After the electroporation, cells were recovered in the unselective medium for 24h, and the cells were then transferred into liquid selective medium.

When growth was observed, the cells were transferred into selective medium containing 100 ng/mL aTc for induction overnight. The cells were plated in a dilution series (undiluted to $1:10^6$ dilution) on selective plates. Single colonies were picked into 5 mL selective medium and screened for pMTLCas9 presence with colony PCR. To this end, a 200-500 µL sample was taken from the liquid culture, harvested at 11,000 x g for 3 min, resuspended in 100 µL NaOH (0.1 M), and boiled at 95°C for 10 min in a thermoblock (ThermoMixer C, Eppendorf, Hamburg, Germany). After cooling down, 1 µL of the sample was used for colony PCR with Phire Plant Master Mix. Positive clones were screened for deletion events with colony PCR from liquid culture or isolated gDNA (Table 2). Successful gene deletion was verified *via* Sanger sequencing.

3.8.4 Plasmid curation from *C. ljungdahlii*

After successful generation of *aor* deletion mutants of *C. ljungdahlii,* the recombinant strains were cured of the CRISPR plasmid as these pose a metabolic burden. The recombinant strains were transferred multiple times in unselective medium (at least 3 successive transfers) before plating on unselective RCM plates in a dilution series. Single colonies were screened for presence of pMTLCas9 with colony PCR. If the plasmid was not present anymore, the strain was inoculated into selective and unselective medium. Recombinant strains were considered plasmid-free if the colony PCR did not give a signal for pMTLCas9 and the strain lost the ability to grow in selective medium.

3.8.5 Whole-genome sequencing with Oxford Nanopore MinION sequencing

For whole-genome sequencing with Oxford Nanorpore, gDNA was isolated from 4 mL culture with the NucleoSpin Microbial DNA Mini kit (Macherey-Nagel, Düren, Germany) (Chapter 3.3.11). An additional RNAse digest was added after the cell lysis and the centrifugation to dry the columns was extended to 1 min. The gDNA was eluted with pre-heated elution buffer. Nanopore sequencing was performed as described previously (Fink, 2021).

3.8.6 Long-term storage of *C. ljungdahlii* strains

For long-term storage of *C. ljungdahlii* strains, glass vials containing 3 mL anaerobic 75 vol-% glycerol were sterilized by autoclaving. A culture of the respective strain was inoculated in RCM medium and incubated at 37°C overnight. The culture was grown to a high cell density (OD_{600} ≥1). The culture was transferred into an anaerobic workbench (Workstation LABmaster Pro, which was equipped with Gas Purifier MB20/MB200 G, MBraun, Garching, Germany) and transferred into a sterile 50-mL Falcon tube (kept in an anaerobic workbench for at least 48 h *prior* to use). Cells were harvested at 4°C in a pre-cooled centrifuge at 3,750 x g for 15 min (Centrifuge 5920 R, rotor S-4x1000, Eppendorf, Hamburg, Germany) and transferred back into the anaerobic workbench immediately to minimize oxygen

exposure. All further steps were performed on ice in the anaerobic workbench at <0.5 ppm oxygen. The supernatant was discarded, and the cells were re-suspended in fresh medium to an OD_{600} 5-10. For each cryo stock, 2 mL of the concentration cell suspension was added to the glycerol vial sterilely. The suspension was mixed by vortexing, incubated on ice for 30 min, and frozen at -80°C. All strains were kept in triplicates, barcoded, and added to the database of the Environmental Biotechnology Lab.

3.9   Growth experiments with *C. ljungdahlii* strains in batch

Phenotypical characterizations of recombinant *C. ljungdahlii* strains were performed in growth experiments with PETC medium in batch cultivations. For heterotrophic experiments, the strains were grown with 5 g/L fructose in 100 mL medium in 240-mL serum bottles. For autotrophic experiments, the strains were grown in 100 mL medium in 1-L PP bottles with agitation for proper gas-liquid mass transfer. Pre cultures were grown in 100 mL PETC medium with fructose to exponential phase (OD_{600} ~0.6-0.9) overnight. The OD_{600} of each pre-culture was measured in a BioMate™ 160 UV/VIS-Spectrophotometer (ThermoFisher Scientific, Waltham MA, USA), and the culture was transferred into an anaerobic workbench. The cells were transferred into sterile 50-mL Falcon tubes (kept in an anaerobic workbench for at least 48 h *prior* to use), harvested at RT at 3,750 x g for 15 min (Centrifuge 5920 R, rotor S-4x1000, Eppendorf, Hamburg, Germany), and transferred back into the anaerobic workbench immediately to minimize oxygen exposure. The supernatant was discarded and the cells were re-suspended in fresh PETC medium to an OD_{600} 5-10 and transferred into sterile anaerobic Hungate tubes with a syringe. The medium was prepared as described in chapter 3.1, and the appropriate antibiotics were added if necessary. For autotrophic cultivations, the headspace of the culture bottles was exchanged with H_2/CO_2 (80:20, vol-%) or CO (100 vol-%) at 1 bar overpressure by vacuum/gassing cycles for 40 sec three times. The cultures for the growth experiments were inoculated to a start-OD_{600} of 0.05-0.1 in triplicates outside the anaerobic workbench. Heterotrophic cultivations were incubated at 37°C without agitation, taking samples once or twice per day. Autotrophic cultivations were incubated at 37°C with agitation at 150 rpm (Ecotron incubator shaker, Infors HT, Bottmingen, Switzerland) and samples were taken once a day. For each sampling point, a 2 mL sample was taken from each culture from which 1 mL was used for OD_{600}- and pH-measurements and 1 mL was used to determine products *via* high-performance liquid chromatography (HPLC). OD_{600} was measured in a 2-mL disposable cuvette in a spectrophotometer (light path 1 cm) and samples were diluted with 100 mM phosphate saline buffer (PBS) if OD_{600} >0.4. Before pH measurements, the pH-meter was calibrated by 3-point-calibration every day (pHenomenal® 1100LB, which is equipped with the electrode LS221, VWR, Bruchsal, Germany). For product determination, 1 mL of the sample was centrifuged at 17,900 x g for 5 min to pellet the cells. The supernatant was transferred into fresh 1.5-

mL tubes and stored at -20°C. For HPLC analysis, samples were thawed at 37°C for 10 min in a thermoblock, mixed by vortexing, centrifuged at 17,900 x g for 5 min, and the supernatant (≥ 600 µL) was transferred into HPLC vials. Samples were randomized and fructose, acetate, ethanol, and 2,3-butanediol were measured with a Shimadzu LC20 system (Shimadzu, Kyōto, Japan) as described previously (Klask *et al.*, 2020).

3.10 Protein-biochemical methods

3.10.1 Production of clostridial proteins in *E. coli*

To produce clostridial proteins in *E. coli*, *E. coli* BL21 or *E. coli* C41 (DE3) was transformed with the production plasmids pASK-IBA3C carrying the respective gene (Chapter 3.4). The recombinant strains of *E. coli* carrying these plasmids were generated and validated *via* colony PCR. To produce clostridial ferredoxins, the strains were co-transformed with iron-sulphur-cluster (FeS) production plasmids (Table 1) (Keßler, 2021). Cultivations, protein purification, and analysis *via* SDS-PAGE and Western Blot were performed as described in Keßler (2021). Enzyme activity of AOR was determined in an anaerobic activity assay in a plate reader (Supplemental S1).

3.10.2 Homologous expression of AOR in *C. ljungdahlii*

To produce AOR in *C. ljungdahlii*, the wt strain was transformed with the production plasmids pMTL8315tet-*aor1/2* (Chapter 3.5). The recombinant strains of *C. ljungdahlii* carrying these plasmids were generated and validated *via* colony PCR. To produce AOR, the cultures were induced with 100 ng/mL aTc from the beginning of the experiment. Since we saw an inhibiting effect on growth from this concentration, the inducer concentration was reduced to 25 ng/mL aTc for the following experiments. The equivalent amount of DMSO was added to the uninduced control cultures. Cells were harvested after the experiment was finished, the cells were lysed in two cycles at 6.5 m/sec for 30 sec (rest time 300 sec) in a FastPrep-24™ 5G beating grinder, and the supernatant was used for affinity chromatography using a Strep-Tactin®XT Superflow® gravity flow column (IBA Lifesciences, Göttingen, Germany). Protein purification and analysis *via* SDS-PAGE and Western Blot were performed as described in Keßler (2021).

3.11 Chemostat fermentations

3.11.1 Preparations for chemostat fermentations

The chemostat fermentations in this study were conducted in a Sartorius Stedim Biostat® B-DCU system (Sartorius, Göttingen, Germany) with 2-L working volume stainless steel reactors (pressurizable to 2 bar overpressure). The customizable reactor lid was equipped with the following instruments and ports: **1)** stirring unit (motor attached to a stirring shaft equipped with two impellers); **2)** combined redox- and pH electrode (EasyFerm Plus, 225 mm, Hamilton, Reno, USA); **3)** temperature sensor; **4)** level sensor; **5)** foam sensor; **6)** sparger with 20 µm pore size; **7)** pressure sensor; **8)** exhaust cooler; **9)** waste port; **10)** sample port; **11)** 4-fold liquid port to feed fresh medium, base, acid, and antifoam; and **12)** inoculation port. Additional ports in the lid were sealed with blind plugs. Each vessel was equipped with a heating jacket connected to the supply tower. Each supply tower was equipped with eight individually controllable pumps, gas supply *via* a mass flow controller (MFC), and a pressure regulation system. All supply towers and process parameters were controlled *via* a control unit. Automation and data acquisition of temperature, stirring, pH-control, foam- and reactor volume, pressure, and feeding rates of correction liquids and the medium was controlled at the control tower *via* BioPAT® MFCS 4 software (Sartorius, Göttingen, Germany). Scales were connected to the supply towers and used for gravimetric medium feed. To prepare the reactors for fermentation, 2 L PETC medium containing 1 g/L yeast extract was prepared (without buffer, vitamins, reducing agent) and filled into the vessel. The lid was attached and the height of the level- and antifoam sensors were adjusted (level sensor barely touching the liquid, foam sensor ~2-4 cm higher). The pH/redox electrode was calibrated and attached to the lid. Masterflex C-Flex ULTRA pump tubing was chosen as tubing formulation due to its high oxygen tightness. Tubing size 14 was used for the 4-fold liquid port and tubing size 16 was used for the sample port, the waste port, and the sparger. Luer connectors were attached to all tubing for liquid handling, secured with zip-ties, and covered with luer plugs. A Midisart® 2000 sterile filter (pore size 0.2 µm, Sartorius) was attached upstream of the sparger and on the exhaust cooler. To sterilize the reactors by autoclaving, the filters, stirring shaft, cable connectors, and temperature sensor port were covered with aluminum foil. Tubing connected to tubes reaching into the liquid was clamped to prevent liquid from leaking out. Correction liquids (HCl 2M, KOH 2M, and antifoam 100x) were prepared and autoclaved. After autoclaving, sterile tops with tubing were attached to the bottles. After autoclaving, the reactor vessel was connected to N_2 gassing and the MES buffer, vitamins, and cysteine were added. The correction liquids were connected to the vessel sterilely, the pH electrode was connected, the pH was adjusted to 5.9, and the pH control was started. The exhaust cooler and heating jacket were connected to the supply tower, the temperature sensor was attached to the port, and

temperature control was set to 37°C. Stirring was set to 500 rpm. The off-gas was connected to the supply tower and the pressure sensor, the level sensor, and the foam sensor were connected. A sterile three-way stopcock (Discofix® C, B. Braun SE, Melsungen, Germany) was attached sterilely at the sample port. A sterile waste bottle (PP or DURAN® Protect bottles) was attached sterilely at the waste port. A sample was taken out, the pH was measured externally, and the pH electrode was re-calibrated. To test the sterility of the system, the completed setup was run for 3 days before inoculation.

3.11.2 Inoculation and batch phase

Before inoculation, the feed-gas was switched to CO (100 vol-%) at a rate of 0.062 L/min and the reactors were gassed overnight to check for CO leakage. Antifoam control was started to prevent heavy foam formation from clogging the waste line. A pre-culture of *C. ljungdahlii* wt was grown in 100 mL PETC medium with fructose to mid-exponential phase (OD_{600} ~0.5-0.9) overnight. The inoculation port was sterilized with ethanol 70 vol-% and the culture was used to inoculate the reactors directly with a syringe (inoculum 1 vol-%). An initial sample was taken, which marked the timepoint zero of the batch phase. For each sampling, 10 mL dead volume was taken out and discarded before a 3-mL sample was retrieved. The sample was split into two 1.5-mL samples, one for OD_{600}- and pH-measurements, the other one for HPLC analysis. Samples were treated as described above (Chapter 3.9). The fermentation was kept in batch phase until the OD_{600} reached ~0.9-2.

3.11.3 Continuous phase

As soon as the reactors reached an OD_{600} ~0.9-2, the fermentation was switched to continuous mode of operation (process time ~500 h). For this, 5 L of PETC medium containing 1 g/L yeast extract was prepared, autoclaved, gassed with N_2, and the supplements (MES, vitamins, cysteine) were added for each reactor. After the medium was reduced completely, the medium-feed bottles were placed on the scale and the feed lines were connected to the 4-fold liquid port. The reactor volume was maintained at 2 L by activating level control and gravimetric medium feed was set to a hydraulic retention time (HRT) of 8 days (dilution factor of 0.125). The cells were slowly adapted to higher dilution factors, the pH was reduced to 5.7, and yeast extract was decreased over time. After about 1000 h, the medium was switched to yeast-extract free PETC medium and the HRT was kept at 4 days. These conditions were maintained until steady-state was reached (for about 500 h). After about 1500 h, the medium was switched to PETC medium containing 15 mM sodium acetate and the process was run until steady-state was reached. Daily samples were taken throughout the fermentation.

3.11.4 Analytical methods

OD_{600}- and pH-measurements were conducted as described above (Chapter 3.9). Product concentrations were measured *via* HPLC as described previously (Klask, 2021). Sterility was controlled *via* light microscopy with a BX41TF microscope at 40 x magnification (Olympus, Shinjuku, Japan; equipped with a U-TV0.5XC-3 camera). As the MFCs in the supply tower were calibrated to air by Sartorius, the gas flow with CO 100 vol-% was measured with a drum-type gas meter TG0.5 (Ritter, Bochum, Germany). Online measurements of the off-gas composition were monitored with a mass spectrometer (MS) (PrimaBT, ThermoFisher Scientific, Waltham MA, USA). To determine the cell dry weight to OD_{600} correlation of the cultures, a dilution series was performed with PBS. For each dilution, the samples were filtered through a pre-weighed and dried filter paper by vacuum filtration. The cells were dried in a VO 200 Vacuum-Assisted Drying Oven (Memmert, Schwabach, Germany; equipped with a vacuum pump model SD820, VWR, Bruchsal, Germany) at 80°C and ~20 mbar overnight. Filters were weighed and the correlation factor was calculated.

3.12 Safety precautions when working with CO

CO poses serious health threats as it is a colorless and odorless highly toxic gas. Therefore, several safety precautions were taken for all work with CO. All work with CO and storage of CO-containing vessels was performed in a laboratory, which was equipped with a CO gas-warning system. The reactors were placed in a self-built fume hood (built with item materials and designed by Nicolai Kreitli). Additional mobile CO sensors (Tango TX1-1, Industrial Scientific Corporation, Pittsburgh, USA) were placed inside the fume hood, on the CO gas line connectors, and worn on the lab coat in close proximity to the head. An alarm was triggered at ≥ 30 ppm CO. The sensors were calibrated once a month and after alarms.

CHAPTER 4
RESULTS

4.1 Heterologous production of AOR in E. coli

To analyze the specific biochemical properties of the AOR enzymes, anaerobic, cell-free assays with the functional purified protein are required. AOR activity can be measured in photometric assays according to published protocols (Heider *et al.*, 1995; Hiltrud *et al.*, 1991; Huber *et al.*, 1994; Mock *et al.*, 2015) (Chapter 2.4). The assay is based on the reduction of methylviologen, which is a synthetic electron acceptor and examines the reaction from acetaldehyde to acetate. To provide the functional enzyme for this assay, AOR needs to be produced in a system that enables the correct folding of the enzyme and incorporation of the necessary cofactors. Therefore, we established two systems for heterologous (this chapter) and homologous (Chapter 4.2) production of AOR, fused to an affinity tag (StrepTag II) (Chapters 3.4 and 3.5). We cloned the genes for AOR into an expression vector for *E. coli* (Chapter 3.4) and transformed the expression strain *E. coli* BL21 with the constructed plasmids pASK-IBA3C-*aor1* and pASK-IBA3C-*aor2*. The expression of the target gene is controlled by an aTc-inducible promoter in this construct and the empty vector (pASK-IBA3C, no gene inserted) served as control. After cultivation (Chapter 3.9.1), we disrupted the cells and purified the proteins under anaerobic conditions. We found that AOR1 and AOR2 were produced in small quantities (Figure 13, indicated as red boxes), whereas we could see no signal from the empty vector control (data not shown). We used the purified enzyme fractions for an activity assay with *C. ljungdahlii* wt cell extract in a plate reader, but we were not able to obtain meaningful results (Chapter 7 S1).
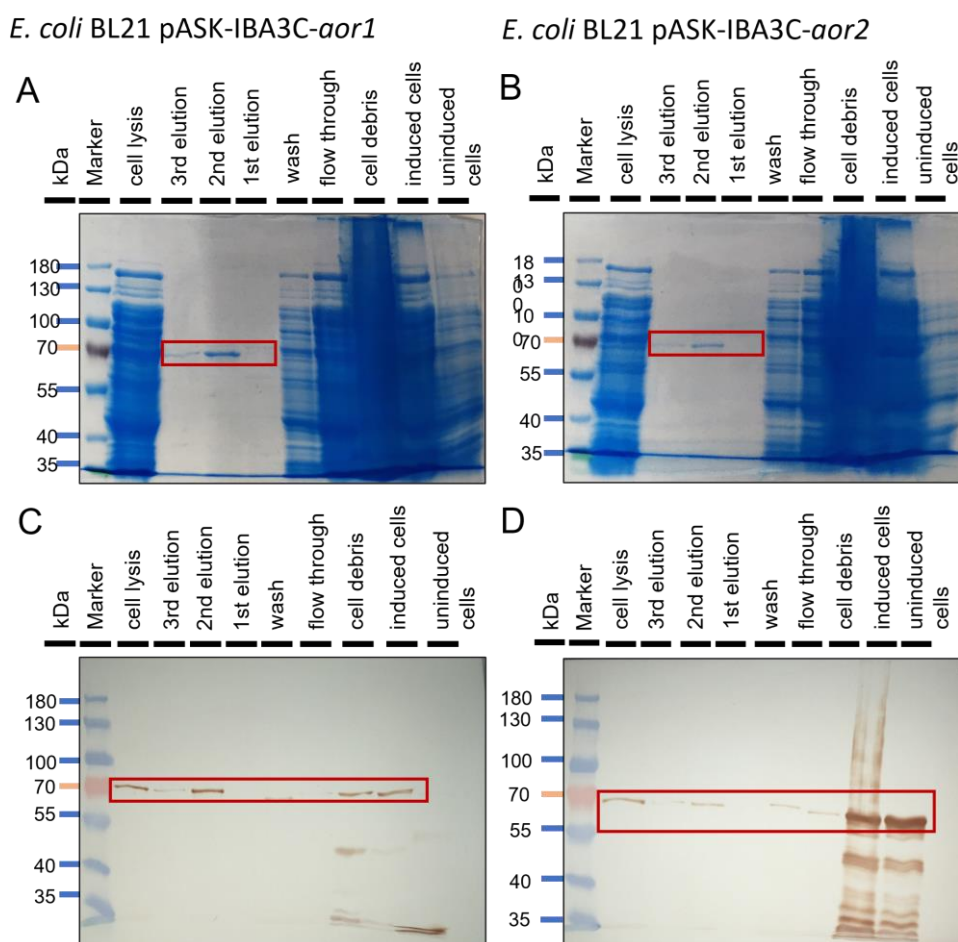
Figure 13: SDS-gels and Western blots of AOR-purification fractions from *E. coli* BL21 pASK-IBA3C-*aor1* (A and C) and *E. coli* BL21 pASK-IBA3C-*aor2* (B and D). A) and B) Coomassie staining of SDS-gels; C) and D) western blots of the gels shown in A) and B), respectively. AOR fraction is highlighted by the red box (the calculated molecular weight of AOR is 68.12 kDa).

4.2 Homologous expression of AOR isoforms in *C. ljungdahlii*

To learn more about the role of the isoforms AOR1 and AOR2 in the metabolism of *C. ljungdahlii,* we constructed plasmids for homologous expression of the respective genes (Chapter 3.5). We transformed *C. ljungdahlii* with the constructed plasmids (Chapter 3.7.2) and verified the strains *via* colony PCR. We performed a preliminary growth experiment (no replicates) with these strains to examine the effect of induction on the cells during growth with fructose. We induced the strains with 100 ng/mL aTc in DMSO or the equivalent amount of DMSO as uninduced controls (Figure 14A and B). We saw that homologous expression of *aor1* led to lower acetate but higher ethanol production compared to the control, while homologous expression of *aor2* showed the opposite behavior (Figure 14C). Both induced strains did not consume the substrate completely (data not shown), which is

probably due to an inhibitory effect of 100 ng/mL aTc on growth and performance. The induced cultures grew slower, but eventually reached the same maximum OD_{600} (Figure 14A and B).
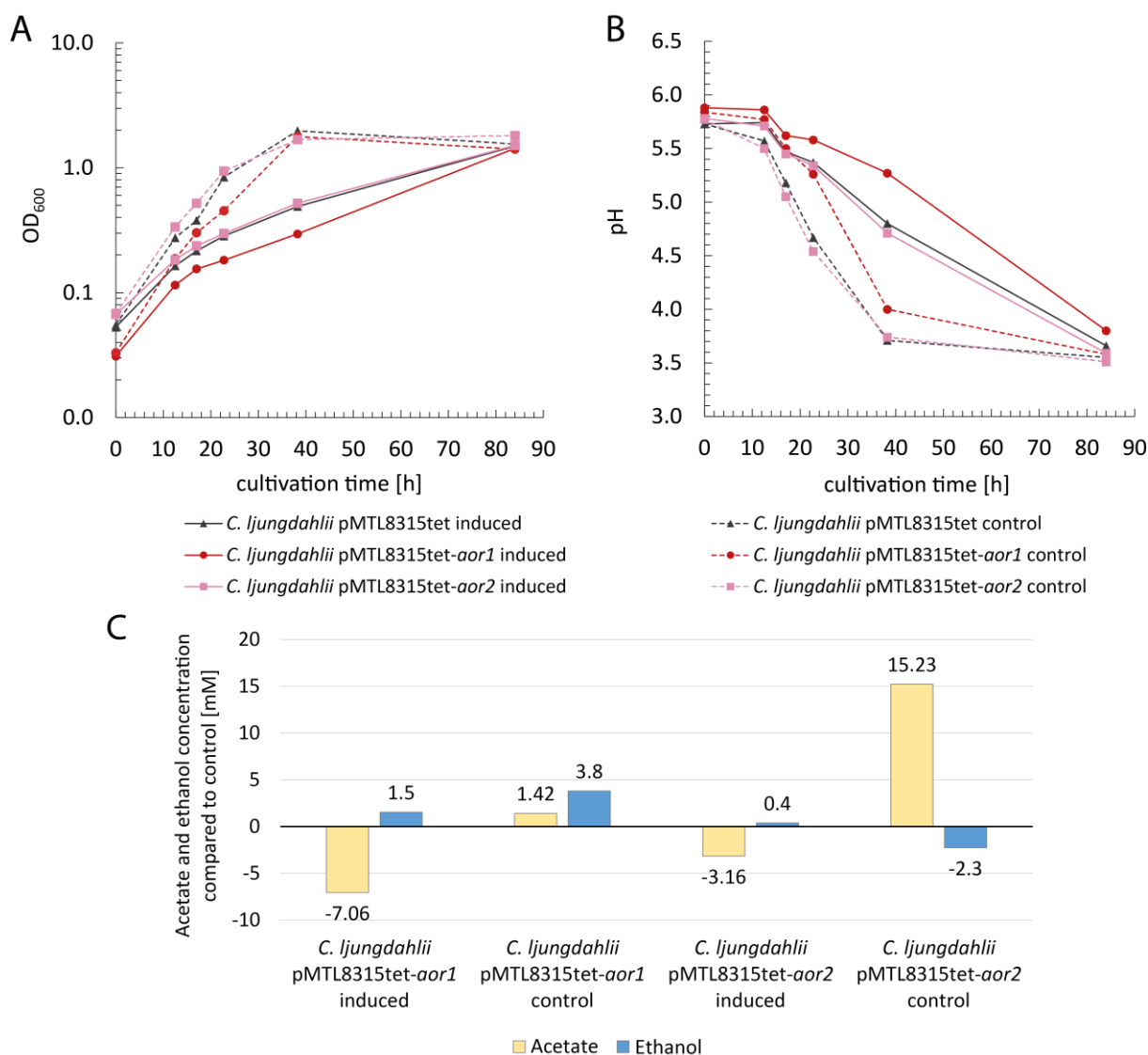
Figure 14: Growth and product formation of *C. ljungdahlii* pMTL8315tet-*aor1* and *C. ljungdahlii* pMTL8315tet-*aor2* compared to *C. ljungdahlii* pMTL8315tet in PETC medium with 5 g/L fructose and 100 ng/mL aTc. A) Growth measured as OD_{600}; B) pH of the cultures. Dashed lines: uninduced cultures (control); grey lines: *C. ljungdahlii* pMTL8315tet (empty-vector control); red lines: *C. ljungdahlii* pMTL8315tet-*aor1*; pink lines: *C. ljungdahlii* pMTL8315tet-*aor2*. N=1. C) Maximum acetate and ethanol concentration [mM]. Black line: *C. ljungdahlii* pMTL8315tet (empty vector control, set as baseline). Yellow: acetate, blue: ethanol. N=1.

As the preliminary experiment was not performed with replicates, we repeated the experiment in triplicates to examine statistical relevance. Due to the inhibitory effect of the aTc, we reduced the inducer concentration to 25 ng/mL aTc for the follow-up experiment (Figure 15). Growth of the control strain *C. ljungdahlii* pMTL8315tet without aTc (0.074 ± 0.006 h^{-1}) was still faster compared to the induced strain (0.059 ± 0.005 h^{-1}), although not significant. The induced cultures of *C. ljungdahlii*

47

pMTL8315tet-*aor1* grew faster by 28.9% (not significant) (0.092 ± 0.017 h⁻¹) compared to the uninduced control strain (0.072 ± 0.017 h⁻¹). The induced and uninduced strains of *C. ljungdahlii* pMTL8315tet-*aor2* did not differ in the growth rate (induced: 0.067 ± 0.007 h⁻¹; control: 0.068 ± 0.010 h⁻¹). We could observe no significant differences in the maximum acetate and ethanol concentration of the induced strains compared to the control strains, except for the empty vector control, which produced significantly less ethanol (-3.8%; control: 15.5 ± 0.5 mM, induced: 14.9 ± 0.5 mM; $P \leq 0.05$). *C. ljungdahlii* pMTL8315tet and *C. ljungdahlii* pMTL8315tet-*aor2*, also did not show different maximum product concentrations. Only *C. ljungdahlii* pMTL8315tet-*aor1* produced 11.8% more acetate (57.3 ± 1.8 mM; $P \leq 0.05$) and 16.3% less ethanol (12.5 ± 0.3 mM; $P \leq 0.05$) than the empty vector control strain (acetate: 51.5 ± 1.9 mM; ethanol: 14.9 ± 0.5 mM) (Figure 15).
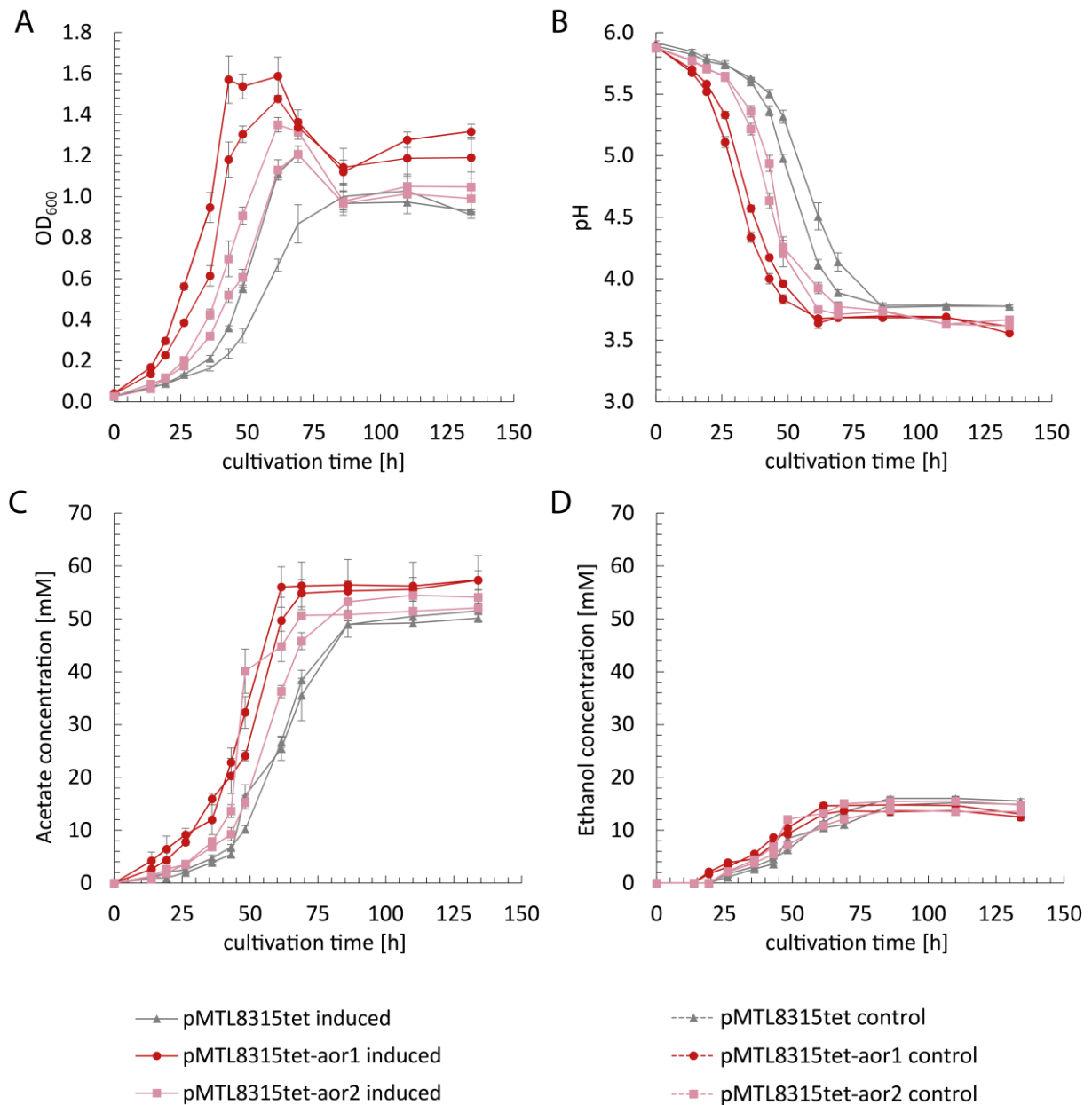
Figure 15: Growth of homologous expression strains in PETC medium with 5 g/L fructose and 25 ng/mL aTc. A) Growth measured as OD_{600}; B) pH of the cultures; C) acetate concentration [mM]; D) ethanol concentration [mM]. Dashed lines: uninduced cultures (control); solid lines: induced cultures (25 ng/mL aTc); grey lines: *C. ljungdahlii* pMTL8315tet (empty vector control); red lines: *C. ljungdahlii* pMTL8315tet-*aor1*; pink lines: *C. ljungdahlii* pMTL8315tet-*aor2*. N=3; error bars represent standard deviation.

To check whether the AOR enzymes were produced in higher concentrations, we analyzed the final sample *via* SDS-PAGE and Western Blot analysis, which showed signals at much smaller sizes than the expected size of 68 kDa for the AORs.

4.3 Deletion of *aor* genes in *C. ljungdahlii*

Gene deletions in acetogenic bacteria can be achieved through several methods. One major drawback of most of the methods is that they produce so-called cloning scars or selective markers on the genome. In recent years, however, new methods for marker-less and scar-free gene deletions have been developed. To delete the genes for *aor1* and *aor2* from the genome of *C. ljungdahlii*, we tested two different methods: **1)** the *Triple-Cross* method developed by LanzaTech (Walker *et al.*, 2015); and **2)** a CRISPR/Cas9 system, which was inspired by the base-editing tool developed in our lab (Xia *et al.*, 2020) and a published CRISPR interference (CRISPRi) system (Woolston *et al.*, 2018).

4.3.1 *Triple-Cross* gene deletion cannot be facilitated by temperature-sensitive plasmid propagation

Our initial plan to delete the *aor* genes in *C. ljungdahlii* was to use the *Triple-Cross* method, developed by LanzaTech (Walker *et al.*, 2015), in combination with a different selection marker, which was the temperature-sensitive origin of replication (ts-ori) pWV01ts from pMTLts (Figure 16) (Molitor *et al.*, 2016a; Schulz, 2018). The idea was to simplify the selection of recombinant strains because it would only require a change of the incubation temperature from 30°C to 37°C. The plasmid pMTLts is an *E. coli – Clostridium* shuttle vector that carries a temperature-sensitive ori for plasmid propagation in Gram[+] bacteria. Contrary to the expectations, the ori also worked in *E. coli* and was dominant over the high-copy ColE1 ori (Molitor *et al.*, 2016a; Schulz, 2018).
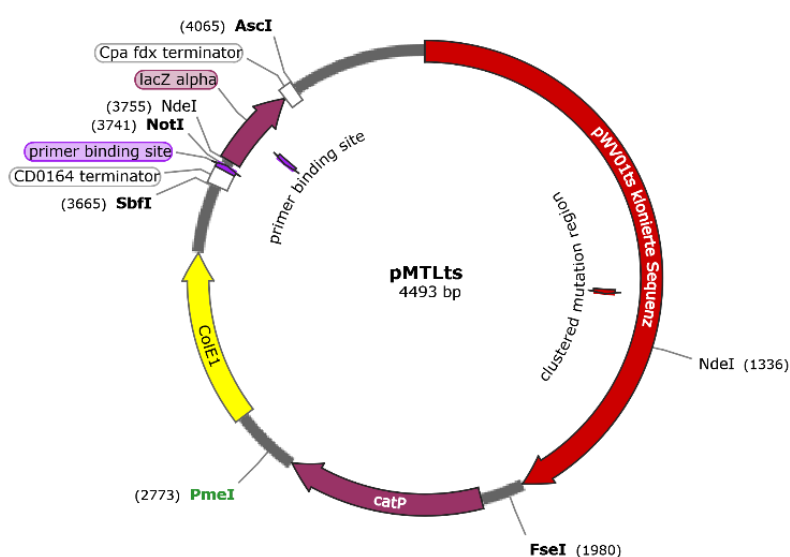
Figure 16: Plasmid map of pMTLts (Molitor *et al.*, 2016a). Shown are the features of the plasmid and the modular restriction sites of the pMTL80000 shuttle vector system (Heap *et al.*, 2009)**.**

In our initial tests with the plasmid during my master's thesis, we found that it underwent unpredictable mutation events, such as an inserted transposable element or different point mutations in the CDS of the ori, during the propagation in *E. coli* (Schulz, 2018). None of the extracted plasmids showed a 100% correct sequence. When we tested the mutated plasmids with *C. ljungdahlii*, none of the plasmids showed functionality. Therefore, we tried to restore the original sequence of pWV01ts by QuikChange mutagenesis (Chapter 3.3.6) at the position of a point mutation in two different clones. While we achieved the desired original sequence at one position, a new mutation occurred at a different position within the CDS of the ori, causing a frameshift mutation. In all the experiments that we performed with pMTLts, the ts-ori was either not present, or not functional due to insertions or point mutations. A detailed description of all attempts to obtain a functional ts-ori can be found in Chapter 7.S3.

4.3.2   Successful gene deletion with a novel CRISPR/Cas9 system

Due to the problems with mutations of the ts-ori, we decided to re-plan the gene deletion strategy using CRISPR/Cas9 technology, which was demonstrated to work in *C. ljungdahlii* (Huang *et al.*, 2016a). This technology requires a plasmid that contains a sequence for an sgRNA to target the genomic DNA, the Cas9 nuclease to cleave the targeted DNA sequence, and homologous repair templates to facilitate the desired edits (Knott *et al.*, 2018). Together, the system enables targeted and efficient genome editing with relatively low effort.

4.3.2.1 Deletion of *aor1*

We constructed and verified plasmid pMTLCas9-*aor1* as described in chapter 3.7 and used it to transform *C. ljungdahlii* by electroporation (Chapter 3.8.2-3) or conjugation as described by Klask *et al.* (2022). Transformation of *C. ljungdahlii* with the *aor*-deletion plasmids was performed but remained unsuccessful in the first round. The recovery culture grew in RCM with fructose and was transferred to selective medium. Unexpectedly, the plasmid-free control reaction was also able to grow under selective pressure. In a second attempt, the transformation with the *aor1*-deletion plasmid was successful and we yielded >60 single colonies on the selective RCM plate from electroporation (1:1000 dilution) and 16 colonies on the selective plate from conjugation (undiluted). We picked 10 clones from each plate and screened the first 12 that grew in liquid selective medium (6 from electroporation, 6 from conjugation) by colony PCR after several transfers in selective medium. All clones showed the correct signals for plasmid presence and strain specificity in the colony PCR, but we could not see signals for genome editing, yet. We repeated the PCR for the genome edit with primers aligning up- and downstream of the target area in the genome (Figure 17) in a bigger reaction volume, purified the amplified DNA from the PCR, and sequenced it *via* Sanger sequencing. We could verify successful, pure, and scar-free deletion of *aor1* from the genome of *C. ljungdahlii* (Figure 17). We achieved plasmid curing by three successive rounds of: **1)** plating; **2)** picking single colonies; and **3)** transferring in liquid medium. We considered the edited strain plasmid-free when it was not able to grow in selective medium and the plasmid screening PCR did not produce a signal. We prepared cryo stocks of the recombinant strain *C. ljungdahlii* Δ*aor1* (Chapter 3.8.5)*.*
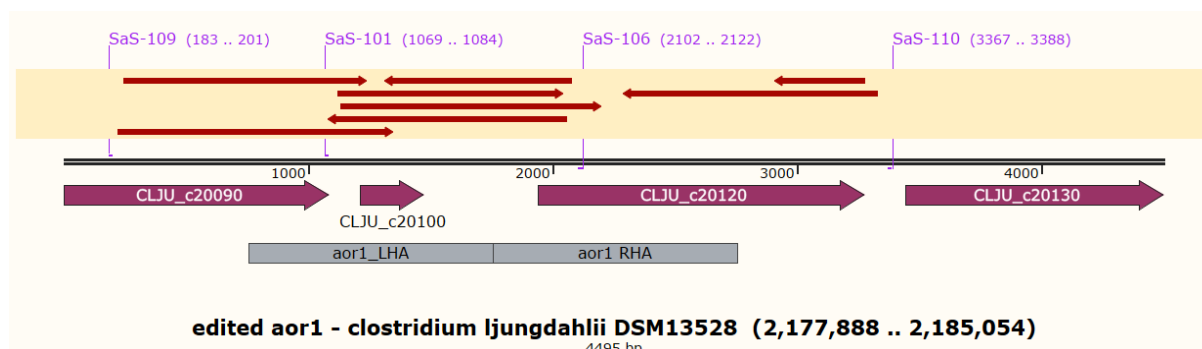
**Figure 17: Deletion of *aor1* from the genome of *C. ljungdahlii.* Genome region up- and downstream of the location of the *aor1* gene. Sequencing data of the edited strain are displayed as arrows. Primers used for verification of the deletion are shown in purple.

4.3.2.2 pMTLCas9-*aor2* for the deletion of the *aor2* gene

We constructed and verified plasmid pMTLCas9-*aor2* as described in chapter 3.7 and used it to transform *C. ljungdahlii* by electroporation (Chapter 3.8.2-3). In our first attempt, the transformants

showed slower growth in the liquid selection (1.5 weeks) and induction medium (2 days). We yielded two candidates from the induction and plated them in a dilution series. We screened 12 clones in total of which 6 showed the correct signal initially. After further PCR screenings, we sequenced one clone and found the correct gene deletion. However, the strain-specific PCR for *C. ljungdahlii* did not work in any of the screened recombinant strains, also not for the sequenced strain. Testing different PCR conditions and new primers remained unsuccessful for the recombinant strains, whereas the controls worked as expected. We repeated this screening with freshly isolated gDNA from the recombinant strains, the wt strain, and the Δ*aor1* culture and observed the same results. Due to the ongoing insecurity about the recombinant strains, we decided to discard the recombinant strains and repeat the transformation.

In our second attempt, we saw very slow growth in the selection (>2 weeks) and induction (several days) medium once again. This time, we repeated the selection and induction step, because the growth in the first induction round was slow and to low OD_{600}. We plated the induced strains in a dilution series on selective and unselective plates immediately after they started to grow. Single colonies took two weeks to grow on the unselective plates and we saw no growth on the selective plates. We picked 6 clones from the plate and isolated gDNA from the two candidates that grew within a few days. The sequencing confirmed the deletion of *aor2* in both candidates and we were able to prove the candidates were *C. ljungdahlii* transformants by strain-specific PCR. We initiated plasmid curing by three successive liquid cultures and plated on RCM plates in a dilution series. After two unsuccessful plating attempts, we were able to yield single colonies on RCM plates again, however, the signal for *aor2* deletion disappeared. Because we were not able to get a wt signal or a mutant signal for the genome area around *aor2*, while all controls worked as expected, we performed whole-genome sequencing with a Oxford Nanopore MinION sequencing platform (Chapter 3.8.5). The results showed that the strain is contaminated with *Sporolactobacillus laevolacticus.*

4.3.2.3 Double deletion of *aor1* and *aor2*

To construct a double deletion mutant of *C. ljungdahlii*, we used *C. ljungdahlii* Δ*aor1* (Chapter 4.3.2.1) as parental strains and transformed it with pMTLCas9-*aor2* by electroporation (Chapter 3.8.2-3). Similar to the transformation of the wt strain with the plasmid, we observed slow growth in the selection (~2 weeks) and induction (2 days) medium. Therefore, as described above, we repeated the selection and induction step to further enrich possible transformants. We plated the induced strains in a dilution series on selective plates immediately after they started to grow and picked 6 clones from the plate after one week. All 6 clones showed the positive signal for deletion of *aor1* and *aor2* and the strain-specific PCR worked well for all candidates. We isolated gDNA from two clones and Sanger

sequencing verified the double deletion in *C. ljungdahlii* (Figure 18). We prepared cryo stocks of the recombinant strain *C. ljungdahlii Δaor1 Δaor2* (Chapter 3.8.5)*.
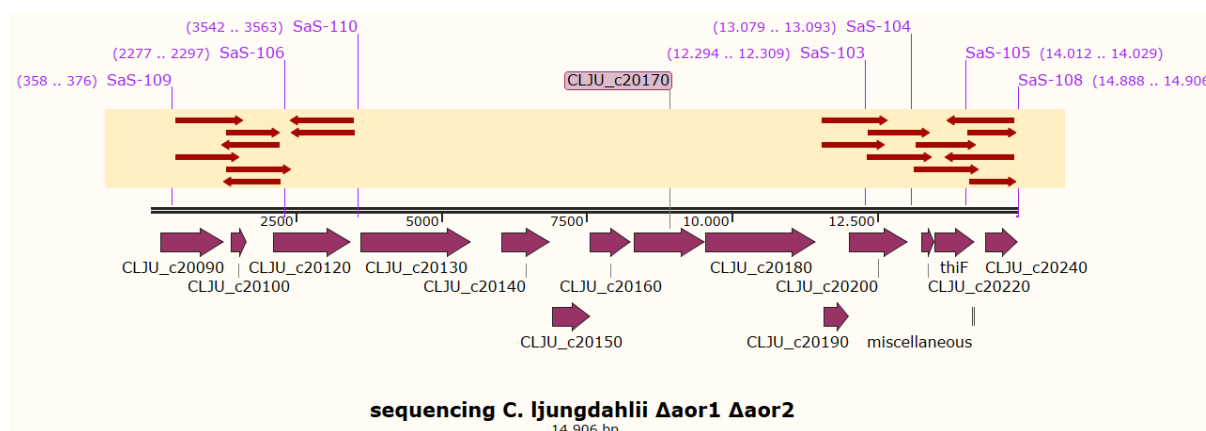
Figure 18: Deletion of *aor1* and *aor2* from the genome of *C. ljungdahlii*. Genome region up- and downstream of the location of the *aor* genes. Sequencing data of the edited strain are displayed as arrows. Primers used for verification of the deletion are shown in purple.

4.4 Phenotypical characterization experiments

4.4.1 CRISPR deletion strains under heterotrophic growth conditions

After successful generation of the *aor* deletion strains *C. ljungdahlii Δaor1* and *C. ljungdahlii Δaor1Δaor2*, we conducted a growth experiment to examine the effect of the deletions. We compared the growth performance and product formation of *C. ljungdahlii, C. ljungdahlii Δaor1*, and *C. ljungdahlii Δaor1Δaor2* in a heterotrophic growth experiment with fructose as substrate. Compared to the wt strain (0.140 ± 0.002 h^{-1}), we saw a reduction in the growth rate of *C. ljungdahlii Δaor1* and *C. ljungdahlii Δaor1Δaor2* by 4.5% (0.133 $h^{-1} \pm 0.004$, not significant) and 35.7% (0.090 $h^{-1} \pm 0.003$, $P \leq 0.001$), respectively. The maximum cell density that we measured in the cultures was significantly reduced by 15.2% (OD_{600} of 1.39 ± 0.04, $P \leq 0.05$) and 32.7% (OD_{600} of 1.10 ± 0.05, $P \leq 0.001$), respectively, compared to the wt (OD_{600} of 1.64 ± 0.06) (Figure 19A). Additionally, we found a considerable reduction in substrate consumption, as both deletion mutants did not consume the substrate completely (Figure 19B). The maximum acetate concentration of *C. ljungdahlii Δaor1* was significantly reduced by 30.8% (40.7 mM, $P \leq 0.001$) compared to the wt (58.8 mM), while the maximum ethanol concentration significantly increased by 118.1% (19.0 mM, $P \leq 0.001$) compared to the wt (8.7 mM) (Figure 19C). We saw similar behavior for *C. ljungdahlii Δaor1Δaor2,* which showed a significantly reduced maximum acetate concentration by 31.7% (40.2 mM, $P \leq 0.001$) and a significantly increased maximum ethanol concentration by 127.3% (19.8 mM, $P \leq 0.001$) (Figure 19C). In fact, the maximum product concentrations of *C. ljungdahlii Δaor1* and *C. ljungdahlii Δaor1Δaor2* did not show significant differences during growth with fructose.
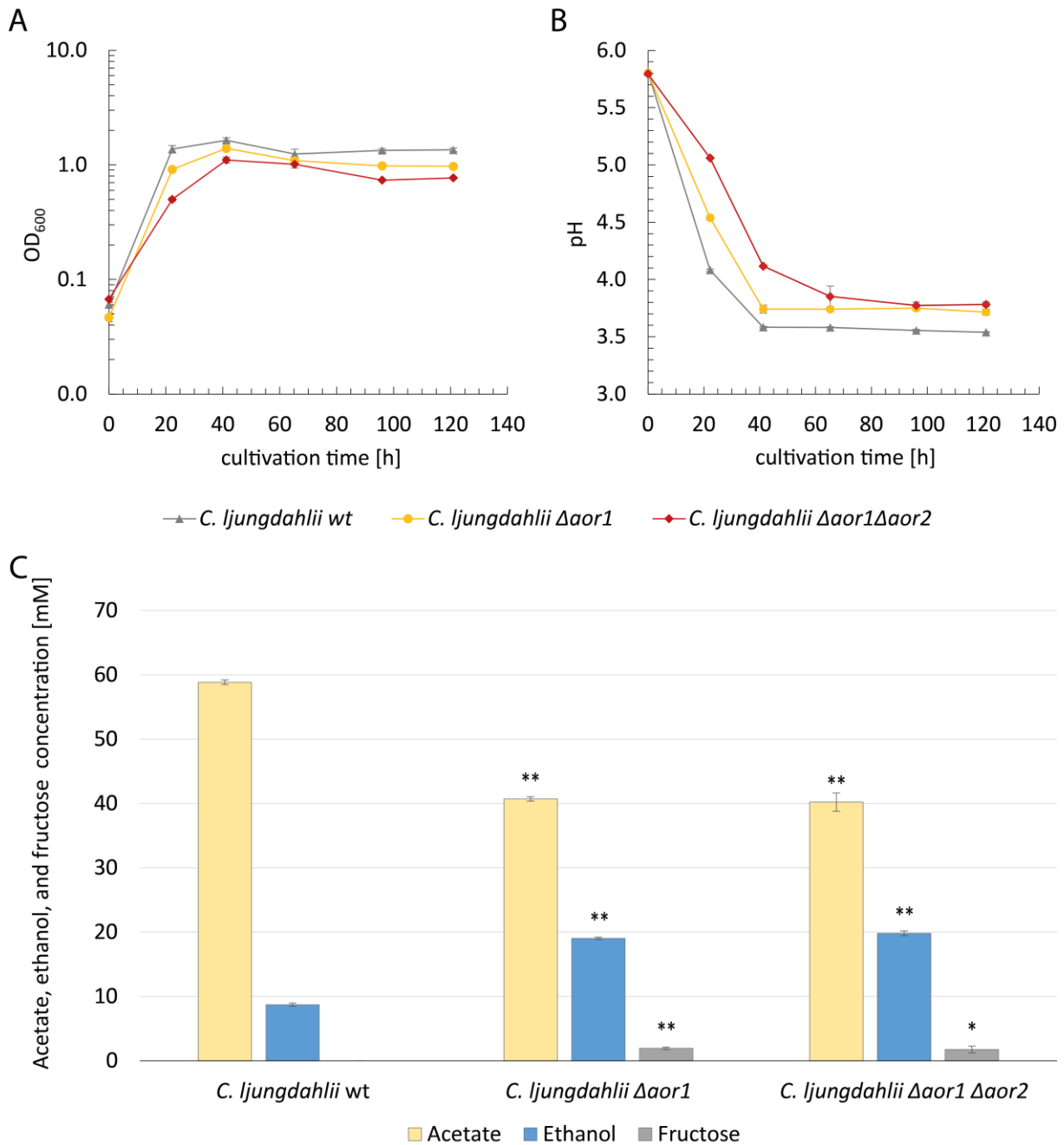
Figure 19: Growth and product formation of *C. ljungdahlii* wt*, C. ljungdahlii* Δ*aor1*, and *C. ljungdahlii* Δ*aor1*Δ*aor2* in PETC medium with 5 g/L fructose. A) Growth measured as OD_{600}; B) pH of the cultures; C) Acetate, ethanol, and fructose concentration [mM]. Yellow: acetate, blue: ethanol. N=3; error bars represent standard deviation; The differences in acetate, ethanol, and fructose concentration were verified by two-tailed Student's t-test with $P < 0.05$ as a significant difference (*) and $P < 0.001$ as a highly significant difference (**).

4.4.2   Base-editing

We successfully applied the base-editing system (Chapter 2.3.4) to generate premature STOP-codons in *adhE1*, *adhE2*, *aor1* (strain designation in Xia *et al.* (2020), QX5), and *aor2* (strain designation in Xia *et al.* (2020), QX6), thus, allowing evaluation of the re-distribution of carbon fluxes in disruption

mutants (Xia *et al.*, 2020). We used the constructed mutants with *aor1* or *aor2* disruption to examine the effect of the AOR isoforms on autotrophic batch fermentations with H_2/CO_2 (Figure 21). Both disruption strains showed impaired growth and substrate consumption. We observed reduced growth rates of QX5 by 55.8% (0.013 h^{-1}, $P \leq 0.001$) and QX6 by 59.6% (0.012 h^{-1}, $P \leq 0.001$), respectively when compared to the growth rate of the wt strain (0.029 h^{-1}). QX5 showed wt-like behavior in terms of acetate and ethanol yield. The maximum acetate and ethanol concentrations were significantly reduced by 21.2% (49.1 ± 0.1 mM, $P \leq 0.001$) and by 23.3% (1.4 ± 0 mM, $P \leq 0.001$), respectively, compared to the wt (acetate = 62.3 ± 0.6 mM, ethanol = 1.9 ± 0.1 mM). QX6 showed impaired ethanol production (ethanol was below our detection limit) and a significant increase in the final acetate yield by 4.6% (0.490 mol/mol CO_2, $P \leq 0.001$) compared to the wt strain (0.468 mol/mol consumed CO_2). The maximum acetate concentration was significantly reduced by 35.6% to 40.1 ± 2.3 mM ($P \leq 0.001$) and the ethanol concentration was below our detection limit.
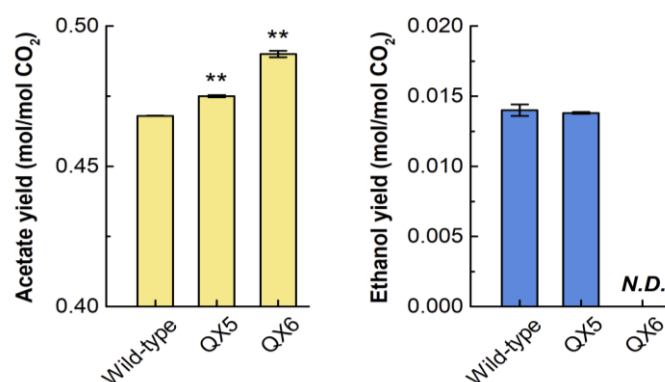
Figure 20: Acetate and ethanol yields of wt, QX5, and QX6 under autotrophic conditions with a gas mixture of H_2/CO_2 (80/20 vol %, 1.5 bar) as the substrate. The fermentation experiments were conducted in triplicate (N=3), and the error bars indicate the standard deviations. The differences in acetate yield and ethanol yield were verified by two-tailed Student's t-test with a $P < 0.001$ as a highly significant difference (**) (Xia *et al.*, 2020).

4.4.3 CRISPR deletion strains under autotrophic growth conditions with H_2/CO_2

To further analyze the effect of the full deletion of *aor1* on autotrophic behavior, we compared the growth performance and product formation of *C. ljungdahlii* wt and *C. ljungdahlii* Δ*aor1* in an autotrophic growth experiment with H_2/CO_2 (80/20 vol-%, 1.5 bar) as substrate. We observed a significant reduction of the growth rate by 72.3% (0.009 h^{-1} ± 0.001, $P \leq 0.001$) and the maximum cell density was reduced by 51.1% (OD_{600} of 0.177 ± 0.002, $P \leq 0.05$) compared to the wt (0.031 ± 0.001 h^{-1}, OD_{600} of 0.362 ± 0.033) (Figure 22A and B). The maximum acetate concentration was significantly reduced by 22.8% in the Δ*aor1* culture (33.3 ± 0.4 mM, $P \leq 0.001$) compared to the wt (44.4 ± 0.9 mM)

(Figure 22C). Contrary, the ethanol concentration significantly increased by 870% (1.9 ± 0.5 mM, $P \leq$ 0.05) compared to the wt (0.217 ± 0.3 mM), although it was still very low (Figure 22C).
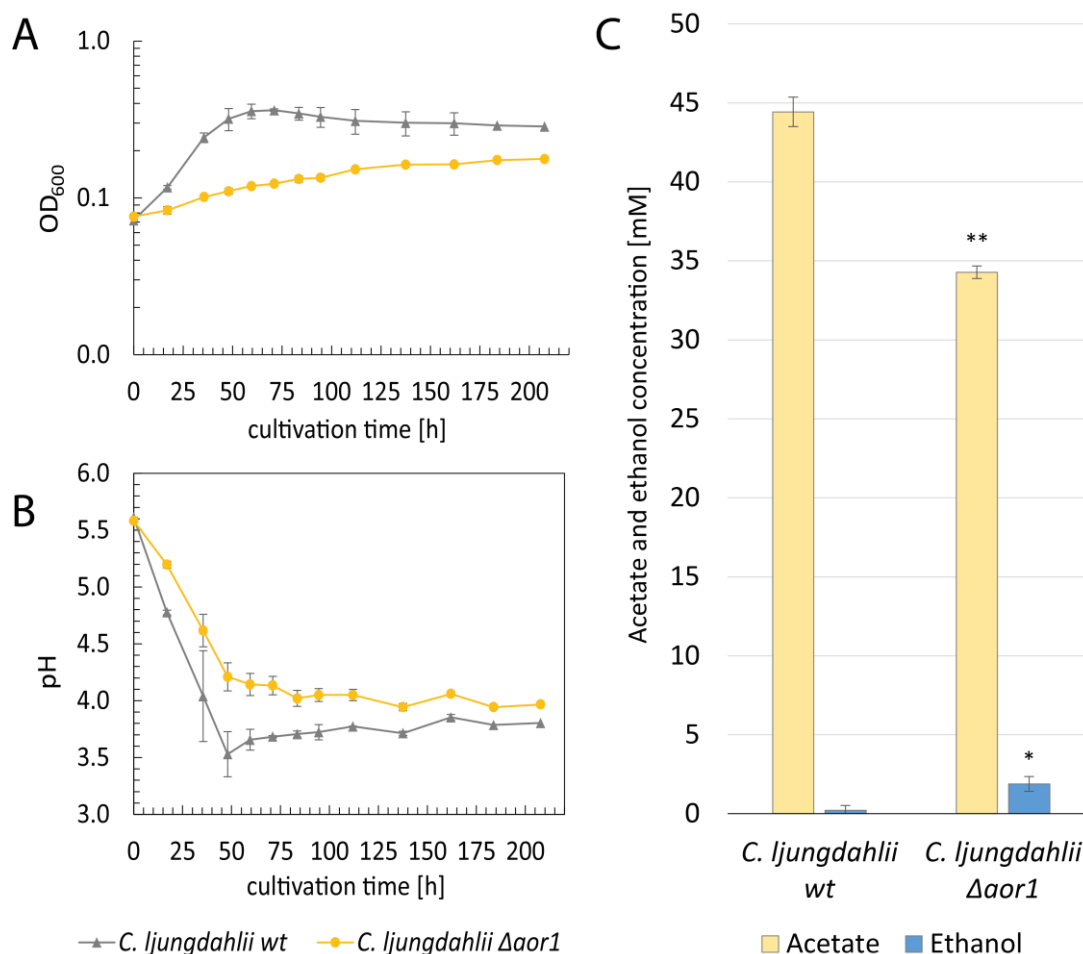
Figure 21: Growth and product formation of *C. ljungdahlii* wt and *C. ljungdahlii* Δ*aor1* in autotrophic conditions with H₂/CO₂. A) Growth measured as OD_{600}; B) pH of the cultures; C) acetate and ethanol concentration [mM]. Yellow: acetate, blue: ethanol. N=3; error bars represent standard deviation; The differences in acetate and ethanol concentration were verified by two-tailed Student's t-test with a $P < 0.001$ as a highly significant difference (**).

4.4.4   CRISPR deletion strains under autotrophic growth conditions with CO

CO is the most energy-dense molecule of the possible substrates of *C. ljungdahlii* and often constitutes a large portion of the off-gas from steel mills, which is a common substrate source for syngas fermentation. During fermentation with CO, the pool of reduced Fd is high, which makes it an ideal substrate for high ethanol production *via* the indirect route (Chapter 2.2). Therefore, to get a better understanding of the behavior under relevant conditions, we compared the growth performance and product formation of *C. ljungdahlii, C. ljungdahlii* Δ*aor1*, and *C. ljungdahlii* Δ*aor1*Δ*aor2* in an autotrophic growth experiment with CO as substrate. We observed a prolonged lag phase for all three

strains. The wt strain started to grow after about 200 h incubation time and reached a maximum OD_{600} of 0.707 ± 0.034 (growth rate 0.034 ± 0.011 h^{-1}) (Figure 23A). *C. ljungdahlii Δaor1* started growing after about 328 h incubation time at a significantly reduced growth rate of 0.004 ± 0.002 h^{-1} (reduced by 89.0%, *P* ≤ 0.05) and reached a maximum cell density of 0.173 ± 0.076 (reduced by 75.5%, *P* ≤ 0.001) (Figure 23A). Compared to the wt strain (34.1 ± 0.2 mM), we found a significant reduction in the maximum acetate concentration by 80.9% (6.5 ± 3.6 mM, *P* ≤ 0.05) in the *C. ljungdahlii Δaor1* culture. The maximum ethanol concentration decreased by 8.7% (9.5 ± 5.0 mM, not significant) compared to the wt (10.4 ± 1.5 mM) (Figure 23C). *C. ljungdahlii Δaor1Δaor2* was not able to grow stably with CO as sole carbon and energy source. Growth was only observed after 355 h incubation time. The growth rate and maximum cell density were significantly reduced by 95.4% (0.002 ± 0.001 h^{-1}, *P* ≤ 0.05) and 94.9% (OD_{600} of 0.036 ± 0.002, *P* ≤ 0.001) (Figure 23A). The acetate concentration of the *C. ljungdahlii Δaor1Δaor2* cultures was below the detection limit and the maximum ethanol concentration was significantly reduced by 97.37% (0.27 ± 0.2 mM, *P* ≤ 0.001) (Figure 23C).
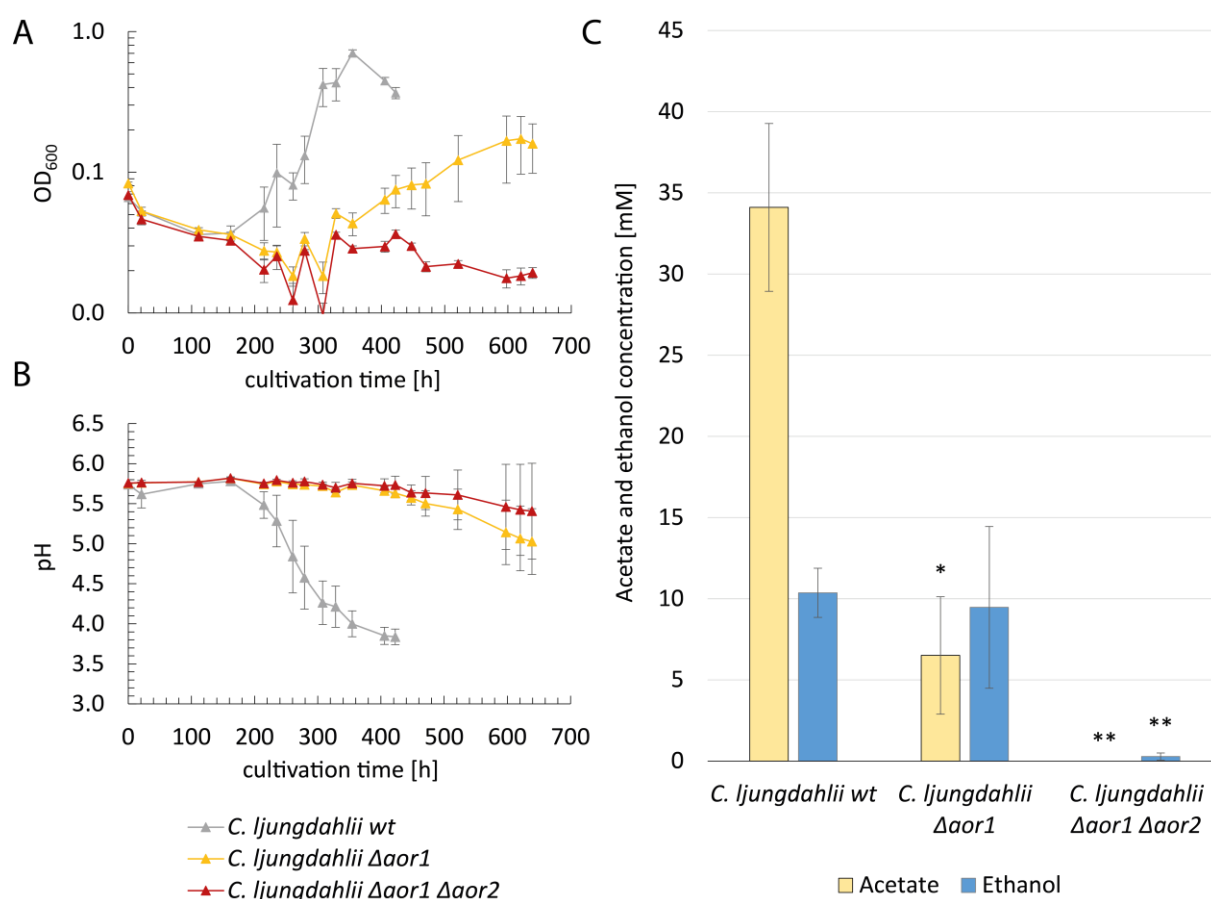

Figure 22: Growth and product formation of *C. ljungdahlii* wt, *C. ljungdahlii Δaor1*, and *C. ljungdahlii Δaor1Δaor2* in autotrophic conditions with CO. A) Growth measured as OD_{600}; B) pH of the cultures; C) acetate and ethanol concentration [mM]. Yellow: acetate, blue: ethanol. N=3; error bars represent standard deviation;

The differences in acetate and ethanol concentration were verified by two-tailed Student's t-test with a $P < 0.05$ as a significant difference (*) and a $P < 0.001$ as a highly significant difference (**).

4.5 *C. ljungdahlii* wt in chemostat fermentation with CO

To gain a better understanding of how *C. ljungdahlii* behaves when grown with CO as sole carbon and energy source, we conducted a long-term chemostat fermentation experiment with *C. ljungdahlii* wt until we achieved steady-state conditions. We ran the fermentation in duplicates and both vessels were simultaneously prepared, sterilized, and made anaerobic as described previously (Chapter 3.11.1). We used PETC medium with 1 g/L yeast extract and without fructose as growth medium for the start-up and batch phase (Chapter 3.11.1-2). The vessels remained anaerobic and sterile over three days after connecting the CO gas feed and starting the process. After initial sampling, we inoculated both bioreactors with 20 mL of the same pre-culture (OD_{600} of 0.770, t = 0 h). We saw a doubling of the OD_{600} within 18 h. However, we had to stop the gassing with CO at that point, because of safety precautions because the ventilation in our laboratory failed and triggered multiple CO gas alarms. During the repair time, we switched the gas supply back to N_2 to keep the reactors anaerobic. During this time, the OD_{600} dropped and while re-starting the CO feed, we were not able to prevent oxygen from entering the bioreactors (t = 180 h) (Figure 24A and B, Phase I). The OD_{600} did not increase over the next days, so we re-inoculated the bioreactors with a fresh pre-culture (OD_{600} of 0.570) after 240 h process time. Over the next days (t = 351 h), the OD_{600} of reactors 1 and 2 (R1 and R2) increased very slowly from 0.068 to 0.103 (R1) and from 0.085 to 0.096 (R2), respectively. To grow in autotrophic batch fermentation during the initial phase of our fermentation, *C. ljungdahlii* requires yeast extract. We suspected that the initial yeast extract in the medium had been used up during the starvation phase without CO. Therefore, we added sterile yeast extract to both bioreactors to a final concentration of 1 g/L to boost growth during the batch phase. After the addition of yeast extract, the microbes in both bioreactors grew to an OD_{600} of 1.97 (R1) and 0.97 (R2) within the next 176 h (Figure 24, A and B, Phase I). At t = 527 h, we started Phase II of the fermentation, which marked the beginning of the continuous mode of operation and reduction of yeast extract in the medium. We started the continuous mode of operation with fresh PETC medium containing 1 g/L yeast extract and at a hydraulic retention time (HRT) of 8 days (Figure 24A and B, Phase II). After 65 h, we lowered the setpoint for the pH control from 5.9 to 5.7. The OD_{600} of the reactors peaked at 4.95 (R1 at t = 592 h) and at 4.08 (R2 at t = 647 h), respectively. Shortly after that (t = 668 h), the acetate production rate peaked at 83.34 mmol $L^{-1} d^{-1}$ (R1) and 82.10 mmol $L^{-1} d^{-1}$ (R2) (Table 16). The ethanol production rate peaked at 61.48 mmol $L^{-1} d^{-1}$ (R1, t = 837 h) and 64.20 mol $L^{-1} d^{-1}$ (R2, t = 885 h), and the 2,3-butanediol (BDO) production rate peaked at 7.08 mmol $L^{-1} d^{-1}$ (R1, t = 592 h) and 5.59 mmol $L^{-1} d^{-1}$ (R2, t = 885 h)

respectively (Table 16). After that, we reduced the HRT to 4 days at t = 932 h. Simultaneously, we slowly started to reduce the concentration of yeast extract in the feed medium, first to 0.5 g/L at t = 932 h, and completely omitted yeast extract after t = 1029 h. It is important to remove the yeast extract from the medium in fully autotrophic chemostat cultures because it represents an additional unaccountable source of carbon, nitrogen, vitamins, and trace elements. During phase III of the fermentation, the bioreactors were kept at the same conditions (HRT 4 days, no yeast extract) until we reached steady-state conditions after 3 HRTs (12 days) (Figure 24A and B, Phase III). During steady-state between t = 1336 h and t = 1527 h, the OD_{600}s of the reactors fluctuated only slightly between 2.3 and 2.5 (R1) and 1.8 and 2.0 (R2), respectively. We achieved acetate production rates of R1 and R2 that averaged at 25.8 ± 4.1 mmol $L^{-1} d^{-1}$ and 30.8 ± 1.9 mmol $L^{-1} d^{-1}$, respectively (Table 16). Ethanol production rates reached 35.0 ± 5.7 mmol $L^{-1} d^{-1}$ (R1) and 21.7 ± 1.2 mmol $L^{-1} d^{-1}$ (R2) and 2,3-BDO was produced at a rate of 0.9 ± 0.1 mmol $L^{-1} d^{-1}$ (R1) and 0.5 ± 0.0 mmol $L^{-1} d^{-1}$ (R2) (Table 16). We achieved an average ratio of ethanol/acetate production of 1.41 in R1 and 0.71 in R2. At t = 1558 h, we started phase IV of the fermentation. We started adding PETC medium containing 15 mM sodium acetate (no yeast extract). Recent research has shown that the addition of acetate to fermentations with CO can improve ethanol production and growth rates (Kwon *et al.*, 2022; Xu *et al.*, 2020). We reached steady-state conditions at t = 1773 h. During phase IV, we saw a different behavior of the two bioreactors, which was caused by problems of oxygen penetration in the feed medium of R1 (Figure 24A and B, Phase IV). While the OD_{600} of R1 increased only marginally to 2.4-2.6, the OD_{600} of R2 fluctuated between 3.3 and 4.0, which is an increase of 92%. We could also see a difference in production rates of the two bioreactors. R1 produced acetate at a rate of 25.1 ± 1.3 mmol $L^{-1} d^{-1}$, ethanol at a rate of 36.4 ± 0.7 mmol $L^{-1} d^{-1}$, and 2,3-BDO at a rate of 0.7 ± 0.1 mmol $L^{-1} d^{-1}$ (Table 16). The average ethanol/acetate ratio was 1.45 and only slightly higher than in phase IV. R2 produced acetate at a rate of 1.4 ± 0.5 mmol $L^{-1} d^{-1}$, ethanol at a rate 120.0 ± 5.9 mmol $L^{-1} d^{-1}$, and 2,3-BDO at a rate of 2.5 ± 0.6 mmol $L^{-1} d^{-1}$ (Table 16). The average ethanol/acetate ratio was 93.0, which is a 131-fold increase. The fermentation was stopped after 1841 h and biomass was collected for long-term storage.

Table 16: Production rates of acetate, ethanol, and 2,3-BDO and the corresponding OD_{600} during different operational phases in R1 and R2. Peak production and OD_{600} values are given for Phase II. Mean production and OD_{600} values are given for Phases III and IV during steady-state conditions.

Reactor	Operating condition	OD_{600}	Acetate production rate [mmol L^{-1} d^{-1}]	Acetate production rate [g L^{-1} h^{-1}]	Ethanol production rate [mmol L^{-1} d^{-1}]	Ethanol production rate [g L^{-1} h^{-1}]	2,3-BDO production rate [mmol L^{-1} d^{-1}]	2,3-BDO production rate [g L^{-1} h^{-1}]	average ethanol/acetate ratio
R1	**Phase II:** YE[1] 1 g/L HRT 8 days	2.64	83.34 (t = 668 h)	0.205 (t = 668 h)	61.48 (t = 837 h)	0.118 (t = 837 h)	7.08 (t = 592 h)	0.027 (t = 592 h)	-
	Phase III: No YE HRT 4 days	2.3-2.5	25.8 ± 4.1	0.063 ± 0.010	35.0 ± 5.7	0.067 ± 0.011	0.9 ± 0.1	0.004 ± 0.000	1.41
	Phase IV: NaAc[2] 15 mM[*3]	2.4-2.6	25.1 ± 1.3	0.062 ± 0.003	36.4 ± 0.7	0.070 ± 0.001	0.7 ± 0.1	0.003 ± 0.000	1.45
R2	**Phase II:** YE 1 g/L HRT 8 days	3.54	82.10 (t = 668 h)	0.202 (t = 668 h)	64.20 (t = 885 h)	0.123 (t = 885 h)	5.59 (t = 885 h)	0.021 (t = 885 h)	-
	Phase III: No YE HRT 4 days	1.8-2.0	30.8 ± 1.9	0.076 ± 0.005	21.7 ± 1.2	0.042 ± 0.002	0.5 ± 0.0	0.009 ± 0.002	0.71
	Phase IV: NaAc 15 mM[*]	3.3-4.0	1.4 ± 0.5	0.004 ± 0.001	120.0 ± 5.9	**0.230 ± 0.011**	2.5 ± 0.6	0.009 ± 0.002	93.0

[1] Yeast extract
[2] Sodium acetate
[3] Only changes in the operating conditions displayed
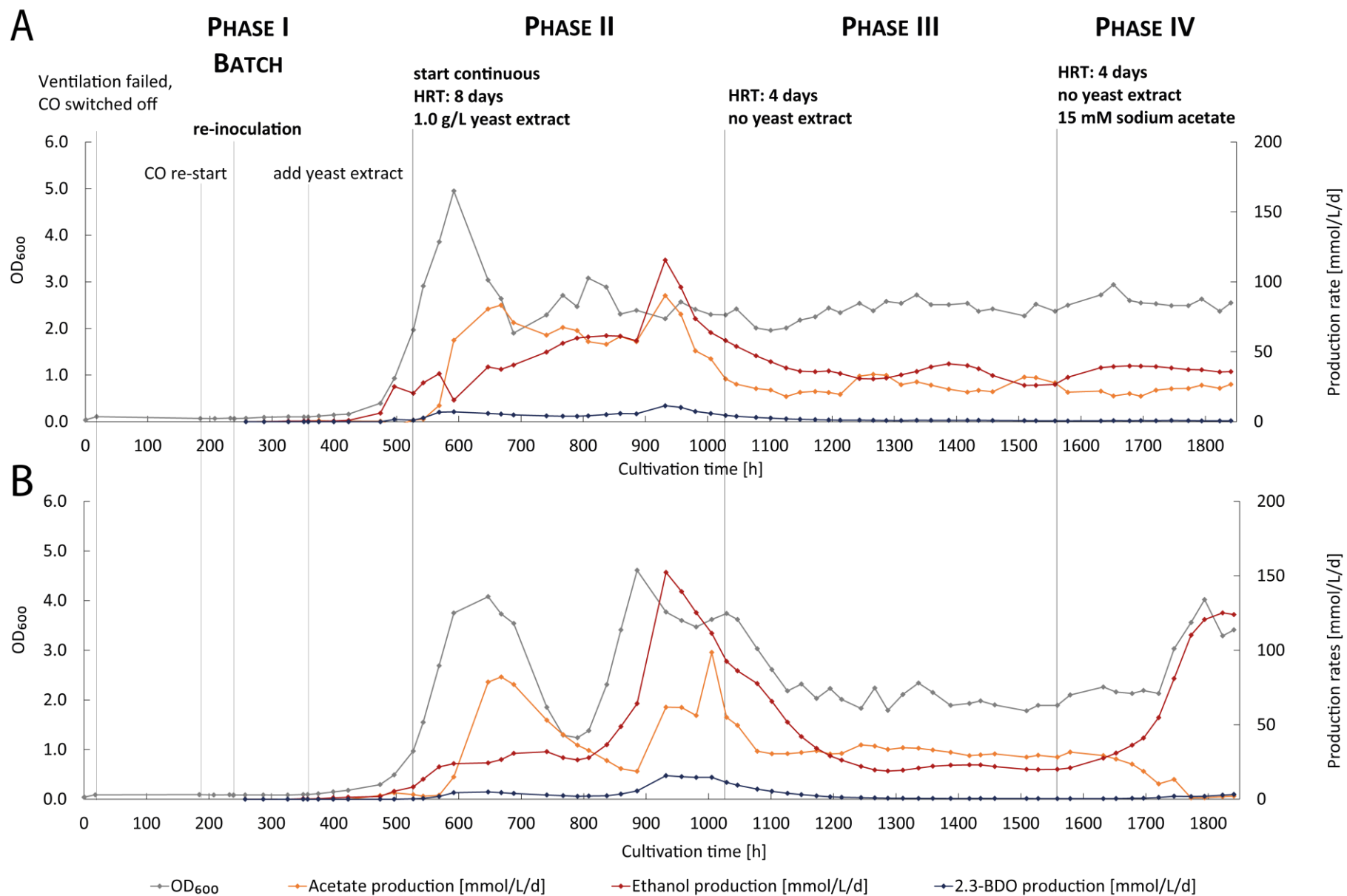
Figure 23: Growth of *C. ljungdahlii* wt in chemostat fermentations with CO. A) Bioreactor 1; B) Bioreactor 2. Process parameter: Temp. 37°C; stirring at 500 rpm; pH 5.9 (t = 0 h until t = 592 h) or pH 5.7 (after t = 592 h); gassing rate (CO 100 vol-%) 0.061 L/min; automated foam and level control; 65 mbar overpressure; working volume 2 L (Chapter 3.11**)**. Phase I: Preparation and batch phase; Phase II: Reduction of yeast extract in the medium and ramping up HRT; Phase III: Steady-state conditions; Phase IV: Addition of 15 mM sodium acetate. Growth was measured as OD_{600} (grey). Acetate (yellow), ethanol (red), and 2,3-BDO (blue) were calculated from HPLC results. HRT: hydraulic retention time; BDO: 2,3-butanediol.

CHAPTER 5
DISCUSSION

In this dissertation, we report attempts to produce clostridial proteins heterologously in *E. coli* and homologously in *C. ljungdahlii.* We present a robust CRISPR/Cas9 system for genome editing in *C. ljungdahlii.* We applied this system for the clean and stable deletion of *aor* genes. The effects of these gene deletions were examined and presented in detail under various representative growth conditions. Lastly, we assessed the growth behavior of *C. ljungdahlii* wt during chemostat fermentation with CO as the sole carbon and energy source. We report that the addition of external acetate to the growth medium can enhance ethanol production rates during steady-state conditions.

5.1   Production of clostridial proteins

Here, we report the purification of clostridial AOR proteins heterologously in *E. coli*, while the current system does not yield active enzymes (Chapters 4.1). After producing AOR enzymes, fused to a StrepTag II in *E. coli* BL21, we were able to detect the correct size fraction for both proteins, AOR1 and AOR2, in an SDS-PAGE. The western blots showed the correct signal in all samples, except for the sample from the uninduced cells (Chapter 4.1, Figure 13). Thus, we produced AOR proteins in *E. coli*. When comparing the purification of AOR1 and AOR2, however, the purification procedure seemed to be less efficient for AOR2, because the signal in the fractions of cell debris and induced cells are much stronger than those of the eluted fractions. This might be due to conformational differences in the AOR structure, which might influence the binding of the protein to the column resin.

After successful purification of the enzyme fractions, we analyzed their AOR-specific activity in an anaerobic activity assay in a plate reader (Chapter 7, S1). The assay showed that the purified enzyme was not active. Mock *et al.* (2015) have reported a specific AOR activity of 1.5 U/mg with cell extract from *C. ljungdahlii* grown with fructose. They measured considerably higher activities of 8 U/mg and 20 U/mg from cells grown in autotrophic conditions with H_2/CO_2 or CO, respectively. The inactivity of our heterologous enzyme preparation can be explained, because others have shown that *E. coli* is lacking certain genes for enzymes involved in the production of cofactors of a variety of anaerobic enzymes (Huang *et al.*, 2016b; Keßler, 2021; Nakamura *et al.*, 1999; Petschak, 2019). This might be a reason for the lack of AOR activity in our assay, as *E. coli* might not be able to produce functional AOR in general. We achieved similar results when we attempted to produce Fd from *C. ljungdahlii* heterologously in *E. coli*. The *C. ljungdahlii* Fd will be required for the AOR activity assay. Because Fd also contains iron-sulfur clusters, we used the same system for heterologous expression of genes, encoding Fd as we had used for the AORs (Keßler, 2021) (Chapter 7, S2). It was demonstrated before, that by co-expression of additional genes for FeS-cluster generation the functionality of the

heterologously produced Fd proteins can be ensured (Huang *et al.*, 2016b), but additional systems might be required for correct incorporation of cofactors into the AOR proteins. Production of clostridial ferredoxins was generally possible for us, though only in small amounts. Consequently, we postulate that for the efficient production of larger quantities of clostridial proteins in *E. coli,* additional improvements to the production systems are critical.

An alternative approach would be to produce AOR for activity assays homologously in the native host, *C. ljungdahlii*, to circumvent these hindrances*.* This would allow for production under the most representative conditions (autotrophic growth with CO or syngas) and ensure correct folding and cofactor incorporation. Therefore, we established a production system in *C. ljungdahlii* based on the modular shuttle-vector system pMTL80000 (Heap *et al.*, 2009). We used the aTc- inducible promoter $P_{tetR-01}$ (Dong *et al.*, 2012) to control the expression of the *aor* genes, fused to the affinity tag StrepTag II. The plasmid-based system required the addition of thiamphenicol to the medium to prevent plasmid loss in addition to the inducer aTc. Our pre-experiment showed that the addition of these two agents influenced the growth of *C. ljungdahlii* considerably, which is why we reduced the concentration of the inducer by 75% in the successive growth experiment. Here, the differences in growth performance were significantly reduced compared to the previous experiment, and we did not report significant differences between the induced and uninduced empty vector control strain anymore. We analyzed the final sample of the growth experiment for AOR presence *via* SDS-PAGE and western blot analysis, which showed that the protein was already degraded. To use the recombinant strains to produce the enzymes for the activity assay, we postulate that the cultures should be induced in the early-exponential phase and harvested in the late-exponential phase. Additionally, to achieve high amounts of protein, the culture volume should be scaled-up and the cell density should be maximized. This could be achieved by cultivating the respective strains in bioreactors, such as the MBS system (Klask *et al.*, 2020), and harvesting the cells during steady-state conditions.

Another important factor for the efficient purification of enzymes from cells is the effective disruption of the cells. For Gram[+] microbes, such as *C. ljungdahlii*, this is especially crucial due to their thick cell wall. We have tested different protocols and methods to disrupt the cells, including sonication (Petschak, 2019), enzymatic lysis with lysozyme (Petschak, 2019), ultrasonic bath (Petschak, 2019), and bead beating in a FastPrep (Keßler, 2021). Our results show that the most efficient cell disruption can be achieved by bead beating in a FastPrep, although at the expense of risking oxygen exposure.

5.2 Deletion of *aor* genes in *C. ljungdahlii*

To adapt a robust system for gene deletions in *C. ljungdahlii*, we first planned to apply the *Triple-Cross* method developed by LanzaTech (Walker *et al.*, 2015), using the temperature-sensitive pWV01ts ori as a selective tool. The pWV01ts ori had previously been shown to facilitate stable plasmid propagation at 30 °C in *C. ljungdahlii* and the plasmid could be cured from the microbe by incubation at 37°C (Molitor *et al.*, 2016a). Contrary to the expectations, however, the ori also seemed to be active in *E. coli* (Molitor *et al.*, 2016a; Schulz, 2018). When aiming to use the ori in our *Triple-Cross* design, we experienced a multitude of mutations and problems with the ori (Chapters 4.3.1 and 7.S3). Table S1 (Chapter 7.S3) summarizes the mutations that occurred during cloning attempts with pMTLts, ranging from silent mutations to the complete loss of the ori, and insertion of the IS*10* related transposable element. The entirety of the unsuccessful attempts led us to the conclusion that the presence of two functional oris on the plasmid results in mutations of the ts-ori. It is well known that plasmid oris can be grouped into different incompatibility groups (Novick, 1987). This means that two (or more) plasmids with oris belonging to the same group in one cell will block the replication of each other, resulting in impaired plasmid segregation during cell division. Although it is unsure whether the two oris on pMTLts, ColE1 and pWV01ts, belong to the same incompatibility group, they both replicate *via* a rolling circle mechanism (Leenhouts *et al.*, 1991; Maguin *et al.*, 1992; Novick, 1987; Shintani *et al.*, 2015). It seems that the two oris on the plasmid indeed influence the functionality of one another, which is why the bacterium produces escape mutations to render one ori unfunctional. Our hypothesis is supported by our attempts to restore the functionality of pWV01ts in pMTLts during which we saw new mutations when we were able to recover the original sequence during site-directed mutagenesis (Chapter 4.3.1). We saw a similar effect in a different plasmid, pMUT2ts, which also carried both oris (Chapter 7.S3). Lastly, we tried to get the pWV01ts ori synthesized and cloned into an ori-free vector by a company (Chapter 7.S3).

Owing to these instability issues, we decided to switch our strategy for gene deletion in *C. ljungdahlii* to a CRISPR/Cas9-based system. A previously published system for CRISPR/Cas9 in *C. ljungdahlii* applied constitutive expression of *cas9* and the sgRNA controlled by P_{thl} and P_{araE}, respectively (Huang *et al.*, 2016a). The authors successfully deleted four genes (*pta, adhE1, ctf,* and *pyre*) and achieved efficiencies between 50 and 100%. Nagaraju *et al.* (2016) used a CRISPR/Cas9 system based on inducible expression to delete *adh* and *2,3-bdh* in *C. autoethanogenum*. They fine-tuned the expression of *cas9* by creating promoter libraries of $P_{tetR-01}$ derivatives, achieving more stringent and higher expression. Xu *et al.* (2015) reported that expression of a wildtype *cas9* was not possible in *C. cellulolyticum*, requiring the use of an engineered nickase to produce genome edits. Wasels *et al.* (2017) also used the aTc-inducible promoter for the expression of *cas9* in *C. acetobutylicum*, but they

used a two-plasmid system. These results hint at the fact that higher expression of *cas9* can be toxic for acetogenic bacteria, possibly by introducing nicks that are not repaired efficiently. Therefore, we designed a system based on the inducible production of the Cas9 protein in combination with constitutive expression of the sgRNA and a repair DNA template on the same plasmid. To avoid Cas9 toxicity, we used the $P_{tetR-01}$ promoter for the successful generation of our editing plasmid pMTLCas9-*aor1* (*cas9* controlled by $P_{tetR-01}$). A simultaneous attempt to use the constitutive promoter P_{thl} to control the expression of *cas9* was unsuccessful and the *cas9* gene contained escape mutations, probably due to the toxicity of Cas9 in *E. coli* (Chapter 7.S4.1). We achieved pure, and scar-free deletion of *aor1* in all analyzed clones with low effort using pMTLCas9-*aor1* (Chapter 4.3.2).

The construction of pMTLCas9-*aor2* was more complicated. After initially constructing pMTLCas9-*aor2* with sgRNA2.1 and sgRNA2.2, we could not generate recombinant strains that carry the plasmids, while our positive controls yielded colonies on selective plates as expected (Chapter 7.S4.2). Neither transformation by electroporation, nor by conjugation yielded colonies with the plasmids, so we re-evaluated them *via* sequencing. Sequencing revealed a point mutation in LHA, potentially leading to an unfunctional gene product of the locus CLJU_c20200, a predicted σ^{54}-interacting transcription regulator. We suspected that this mutation might be lethal in the transformants, which would explain the various unsuccessful attempts of transforming *C. ljungdahlii* with the plasmid thus far. After reconstruction of the plasmid the mutation did not appear again. This time, the transformation of *C. ljungdahlii* was successful in our first attempt, supporting our hypothesis that the point mutation introduced a lethal mutation in CLJU_c20200. We achieved deletion of *aor2*, but after several transfers in unselective medium, the signal for the gene deletion disappeared (Chapter 7.S4.2). We concluded that the gene deletion of *aor2* with this target sequence might not be efficient enough and decided to construct a new plasmid with sgRNA2.3 and sgRNA2.4 (Chapter 3.7). We assembled this plasmid in a two-step strategy after several unsuccessful attempts to assemble it in a one-step strategy. During these failed attempts, a large part of LHA, containing the locus CLJU_c20200, was not present in the assembled products. We were able to avoid these mutations presumably caused by read-through from promoters on the plasmid, by sub-cloning the fused repair DNA (LHA and RHA) and flipping the direction of the sequence in our final plasmid, pMTLCas9-*aor2.3* (Chapter 3.7). We enriched possible transformants by sub-culturing in liquid selective medium before plating (Chapter 4.3.2.2) to increase the probability of obtaining successful deletion mutants. Thus, we generated *C. ljungdahlii Δaor2* and confirmed the strain *via* sequencing and strain-specific PCR. During plasmid curing, however, the signal for the gene deletion disappeared again, similar to what we saw during our first strain construction. Whole-genome sequencing revealed that the mutant strain was overgrown by *S. laevolavticus* in unselective medium.

We also used the plasmid pMTLCas9-*aor2* to generate the double deletion mutant *C. ljungdahlii* *Δaor1Δaor2* using *C. ljungdahlii Δaor1* as the parental strain. During the generation of this strain, we observed the same impaired growth behavior and applied the same enrichment strategy as for the generation of *C. ljungdahlii Δaor2.* Here, we were able to generate the clean deletion of *aor2* and successfully generate the PCR signal. The signal also remained stable after multiple transfers and growth experiments.

5.3 Investigation of the effects of *aor* alterations in *C. ljungdahlii*

There are different ways to analyze the effect of a gene product in the host microbe's metabolism, such as: **1)** increasing the number of gene products, and **2)** deleting the gene from the genome. Closely examining the effects of these alterations can give a good overview of the importance of the gene for growth behavior, substrate consumption, and product formation. Therefore, we constructed strains for plasmid-based expression of *aor1* and *aor2* and deletion mutants to examine the role of two AOR isozymes*.*

Plasmid-based expression of *aor* genes did not significantly influence the growth behavior during growth with fructose (Chapter 4.2), but we could see that high concentrations of the inducing agent aTc negatively influenced the growth of *C. ljungdahlii* strains. Overexpressing *aor1* led to increased growth rates, although this was not significant. The growth boost was accompanied by significantly higher maximum acetate concentrations (+11.8%, 57.3 ± 1.8 mM) and significantly lower ethanol concentrations (-16.3%, 12.5 ± 0.3 mM) (Chapter 4.2). These results suggest that a higher AOR1 abundance leads to increased catalysis from acetaldehyde to acetate. However, it is unclear whether the overproduction construct led to higher levels of active enzymes, as we were not able to obtain a signal for AOR in the western blot of the final sample. To attribute the different acetate and ethanol concentrations, which we measured in the cultures, to an increase in AOR1 activity, we would have to be able to confirm an increase in the AOR abundance in the SDS-PAGE and western blot compared to the wt. Furthermore, enzyme activity assays would be possible to analyze differences in the overproducing strains compared to the wt. However, the overexpression of *aor2* had no significant impact on the growth behavior of the strain compared to the wt strain.

We also examined the effects of the deletions of *aor1* and the double deletion of *aor1* and *aor2* in *C. ljungdahlii* during growth under different conditions, including heterotrophic growth with fructose and autotrophic growth with H_2/CO_2 or CO. During heterotrophic growth with fructose, we observed reduced growth rates and maximum cell densities of both mutant strains. The strains also did not consume the substrate completely during the heterotrophic batch. Both mutant strains produced significantly less acetate (30.8% and 31.7%) and significantly more ethanol (118.1% and 127.3%)

compared to the wt strain. Interestingly, even though the growth behavior of *C. ljungdahlii* Δ*aor1* and *C. ljungdahlii* Δ*aor1*Δ*aor2* differed both in the growth rate, as well as the maximum cell density, the maximum product concentrations did not differ significantly from each other during growth with fructose. The deletion of *aor1* leads to improved ethanol production during growth with fructose, leading to the deduction that *aor1* is not important for ethanol production during heterotrophic growth. The observation that the additional deletion of *aor2* in the *C. ljungdahlii* Δ*aor1* does not significantly influence ethanol production, leads to the conclusion that it does not pose an important metabolic rearrangement under these conditions. Our results are in accordance with the findings of Lo *et al.* (2020) (Table 17), who found that deletion of *aor2* and double deletion of *aor1* and *aor2* in a *pta*-deficient strain resulted in decreased ethanol production. It seems that the AOR enzymes are not important for ethanol production during these conditions and might, indeed, be involved in the re-assimilation of ethanol towards acetate. Others have shown that ethanol is mostly produced *via* the bifunctional AdhE1/2 under heterotrophic conditions, as the double deletions of these genes have caused reduced ethanol production in *C. ljungdahlii* (Leang *et al.*, 2013; Liu *et al.*, 2020) (Table 17). Contradicting to that, the deletions of *adhE* genes did not impair ethanol production in *C. autoethanogenum* under heterotrophic conditions (Liew *et al.*, 2017). The differences between the two microbes, although small, become apparent here. Others have reported differences between the microbes before, including ethanol production (Brown *et al.*, 2014; Liew *et al.*, 2016b; Marcellin *et al.*, 2016; Martin *et al.*, 2016). Liew *et al.* (2017) attributed the differences in ethanol production in the *adhE* deletion strains to differences in the amino acid sequence, which could possibly influence cofactor binding.

We analyzed the behavior of *aor* mutants during autotrophic growth with H_2/CO_2, using strains with truncated genes, which were constructed *via* base-editing (Xia *et al.*, 2020), and strains with clean gene deletions, which were constructed *via* CRISPR/Cas9 editing (Chapter 4.3.2). All strains showed significantly reduced growth rates and decreased maximum cell densities. However, the behavior concerning product formation of the *aor*-disruption strains, constructed by base-editing, differs from the behavior of the *aor*-deletion strain, constructed *via* CRISPR/Cas9. Both, the base-editing strain QX5 (*aor1* disruption) and *C. ljungdahlii* Δ*aor1* produced significantly less acetate (21.2% and 22.8%, respectively). Contrary to that, however, the maximum ethanol concentration decreased significantly in QX5 by 23.3%, while *C. ljungdahlii* Δ*aor1* produced significantly more ethanol (870% increase). The difference between the production performances of the disruption and deletion mutants could be attributed to the partial or complete deletion of the gene. While in the base-editing strain only a single base pair was exchanged to introduce a premature STOP-codon in the gene, the gene was deleted from the genome completely in the CRISPR/Cas9-edited strain. The truncated and still present part of

the gene might still influence the strain's behavior. Besides that, the missense mutation in *aor1*, or the deletion of the full gene, might influence the translation of downstream genes by polar effects (Margolin, 1967). The promoter of the *aor* gene is still present and might be a promoter for more than one gene. Thus, by introducing a premature STOP codon in a polycistronic mRNA, translation of the downstream genes could be inhibited as well. The *aor2* disruption strain (QX6) showed impaired ethanol production (ethanol was below our detection limit) and a significant increase in the final acetate yield. Due to the ongoing issues with the verification of the *aor2* CRISPR/Cas9-deletion strain, we cannot compare QX6 to other strains, yet. Upon successful verification of the *aor2* deletion, further growth experiments and comparisons will have to be conducted.

When growing *C. ljungdahlii* in autotrophic batch experiments with CO as the sole carbon and energy source, we observed prolonged lag phases from all strains. *C. ljungdahlii* Δ*aor1* started growing after about 128 h later than the wt, and reached a significantly reduced growth rate and maximum cell density. Both the maximum acetate concentration and maximum ethanol concentration (not significant) decreased in the *aor1* deletion mutant, while the ratio of ethanol/acetate shifted from 0.3 for the wt to 1.46 in *C. ljungdahlii* Δ*aor1.* This is contradictory to the findings of Liew *et al.* (2017), who reported a shift toward more acetate production by deleting *aor1* in *C. autoethanogenum* (Table 17). The differences between the produced ethanol concentration of the wt and the *aor1* deletion strains appeared not to be statistically significant though, thus more work is necessary to understand the effect of this deletion. Analysis in chemostat fermentations would help to understand the behavior better.

The double deletion strain *C. ljungdahlii* Δ*aor1*Δ*aor2* was not able to grow stably. We observed a slight increase in optical density after more than two weeks, but the strains were not able to grow well. Besides that, acetate concentration remained below the detection limit and the maximum ethanol concentration was significantly reduced. These findings are in accordance with the findings of Liew *et al.* (2017), who observed the same effect in *C. autoethanogenum.*

Table 17: Effect of genetic engineering of *aor* and *adh* genes in *C. ljungdahlii* and closely related *C. autoethanogenum*.

Strain	Genetic variant	Growth condition	Effect	Reference
C. ljungdahlii pMTL8315tet-*aor1*	Homologous production of AOR1	Fructose (+Tm5[4], +aTc25[5]), batch	Increased Ac[6], decreased EtOH[7]	This study
C. ljungdahlii pMTL8315tet-*aor2*	Homologous production of AOR2	Fructose (+Tm5, +aTc25), batch	wt-like behavior	This study
C. ljungdahlii QX5 (*aor1* Gln267*)	Premature STOP-codon in *aor1*	H_2/CO_2 (80/20 vol-%, 1.5 bar), batch	wt-like behavior	(Xia *et al.*, 2020)
C. ljungdahlii QX6 (*aor2* Gln267*)	Premature STOP-codon in *aor2*	H_2/CO_2 (80/20 vol-%, 1.5 bar), batch	No EtOH detectable, higher Ac yield	(Xia *et al.*, 2020)
C. ljungdahlii Δ*aor1*	Deletion of *aor1*	Fructose, batch	Increased EtOH production (compared to wt)	This study
C. ljungdahlii Δ*aor1* Δ*aor2*	Deletion of *aor1* and *aor2*	Fructose, batch	Increased EtOH production (compared to wt), no significant difference to Δ*aor1*	This study
C. ljungdahlii Δ*aor1*	Deletion of *aor1*	H_2/CO_2 (80/20 vol-%, 1.5 bar), batch	Decreased Ac, increased EtOH	This study
C. ljungdahlii Δ*aor1*	Deletion of *aor1*	CO, batch	Decreased Ac, decreased EtOH Product ratio EtOH/Ac increased	This study

---

[4] Thiamphenicol was added for plasmid stability (working concentration in the medium: 5 µg/mL)
[5] Anhydrotetracycline was added to induce production of AOR (working concentration in the medium: 5 µg/mL)
[6] Acetate
[7] Ethanol

C. ljungdahlii Δaor1 Δaor2	Deletion of *aor1* and *aor2*	CO, batch	No stable growth, no product formation	This study
C. ljungdahlii Δpta	Deletion of *pta*	Fructose, batch	Similar growth and production as wt strain	(Lo *et al.*, 2020)
C. ljungdahlii Δpta ΔadhE1 ΔadhE2	Deletion of *pta*, *adhE1,* and *adhE2*	Fructose, batch	Increased EtOH production (compared to *C. ljungdahlii Δpta*)	(Lo *et al.*, 2020)
C. ljungdahlii Δpta Δaor2	Deletion of *pta* and *aor2*	Fructose, batch	Increased EtOH production (compared to *C. ljungdahlii Δpta*)	(Lo *et al.*, 2020)
C. ljungdahlii Δpta Δaor2	Deletion of *pta* and *aor2*	CO, batch	Increased EtOH production, decreased Ac (compared to *C. ljungdahlii Δpta*)	(Lo *et al.*, 2020)
C. ljungdahlii Δpta Δaor1 Δaor2	Deletion of *pta*, *aor1,* and *aor2*	Fructose, batch	Increased EtOH production, decreased Ac production (compared to *C. ljungdahlii Δpta Δaor2*)	(Lo *et al.*, 2020)
C. ljungdahlii Δpta Δaor1 Δaor2	Deletion of *pta*, *aor1,* and *aor2*	CO, batch	No growth	(Lo *et al.*, 2020)
C. autoethanogenum ΔadhE1/2	Deletion of *adh*E genes individually	CO, batch	Decreased EtOH titer by 154-183 %, respectively	(Liew *et al.*, 2017)
C. autoethanogenum Δaor1	Deletion of *aor1*	CO, batch	Decreased growth, decreased EtOH titer by 43 %	(Liew *et al.*, 2017)
C. autoethanogenum Δaor2	Deletion of *aor2*	CO, batch	Increased EtOH titer by 170 %	(Liew *et al.*, 2017)
C. autoethanogenum Δaor1Δaor2	Deletion of *aor1* and *aor2*	CO, batch	Decreased EtOH titer, loss of ability to reduce carboxylic acids to their corresponding alcohols	(Liew *et al.*, 2017)
C. ljungdahlii ΔadhE1	Deletion of *adhE1*	Fructose, batch	Decreased EtOH production, increased Ac production	(Leang *et al.*, 2013)

C. ljungdahlii Δ*adhE1* Δ*adhE2*	Deletion of *adhE1* and *adhE2*	Fructose, batch	Decreased EtOH production, increased Ac production	(Leang *et al.*, 2013)
C. ljungdahlii Δ*adhE1*	Deletion of *adhE1*	Fructose, batch	Increased EtOH production	(Liu *et al.*, 2020)
C. ljungdahlii Δ*adhE1* Δ*adhE2*	Deletion of *adhE1* and *adhE2*	Fructose, batch	Decreased growth and substrate consumption, no EtOH production	(Liu *et al.*, 2020)
C. ljungdahlii Δ*adhE1* Δ*adhE2*	Deletion of *adhE1* and *adhE2*	Syngas, fed-batch	EtOH production during exponential phase, re-oxidization during stationary phase; strong up-regulation of *aor2* during stationary phase	(Liu *et al.*, 2020)
C. ljungdahlii **wt**	-	CO	AOR2 catalyzed acetate to acetaldehyde	(Zhu *et al.*, 2020)
C. ljungdahlii **wt**	-	H_2/CO_2	AOR2 catalyzed acetaldehyde to acetate	(Zhu *et al.*, 2020)

5.4 Directionality of AOR in different conditions; a hypothesis

As described previously, the AOR does not have an impact on the ethanol production pathway during heterotrophic growth (Table 18), which has been reported by others previously (Leang *et al.*, 2013; Richter *et al.*, 2016). It is known, however, that the AOR plays a critical role in the ethanol production pathway during autotrophic growth (Richter *et al.*, 2016). Other clostridia strains that lack genes for AOR, produced significantly less ethanol in a comparison of several industrially relevant strains (Bengelsdorf *et al.*, 2016; Martin *et al.*, 2016). The role of the two isoforms AOR1 and AOR2 for this pathway remained unknown thus far. Our results suggest, that AOR1 and AOR2 catalyze reverse reactions under different fermentation conditions (Table 18). During autotrophic growth, the gas mixture of the substrate plays a vital role for the microbes. Flux balance analysis revealed that fermentation with CO as the sole carbon and energy source leads to the highest ATP gain compared to H_2/CO_2 and syngas (Hermann *et al.*, 2020). A stoichiometric calculation of ATP gains from different gas mixtures estimated an ATP yield of 0.75 mol ATP per 1 mol produced acetate during growth with H_2/CO_2, compared to an ATP yield of 10 mol while producing 1 mol acetate, 1 mol 2,3-butanediol, and 4 mol ethanol (Zhu *et al.*, 2020). When H_2/CO_2 or syngas (CO:CO_2 80:20 vol-%) is used as the growth substrate, the microbes grow more slowly and to lower maximum cell densities. Besides that, the fermentation products are generally less reduced with acetate as the dominant product (Zhu *et al.*, 2020).

An absolute proteome quantification revealed that AOR1 plays a vital role in the production of ethanol *via* acetate in *C. autoethanogenum* during all tested fermentation conditions (CO, H_2/CO_2, and syngas) (Valgepea *et al.*, 2022). Furthermore, they were able to determine Adh4 (CAETHG_RS08920, previously characterized as butanol dehydrogenase (Tan *et al.*, 2014)) to be responsible for reducing acetaldehyde to ethanol contrary to what has been suspected before that AdhE was responsible (Valgepea *et al.*, 2018; Valgepea *et al.*, 2022). Adh4 shares 100 % sequence identity with Adh2 (CLJU_c39950), annotated as a predicted NADPH-dependent butanol dehydrogenase in the genome of *C. ljungdahlii*. Richter *et al.* (2016) found Adh2 to be the most abundant alcohol dehydrogenase in the proteomics analysis and concluded it must be responsible for acetaldehyde conversion to ethanol. AOR1 was also among the most expressed genes of *C. ljungdahlii* during fed-batch fermentation with CO/CO_2 (Xie *et al.*, 2015). The addition of acetic acid to the fermentation increased the expression level of *aor1* during this fermentation (Xie *et al.*, 2015), which highlights the importance of AOR1 for reducing acetic acid. Deletion of *aor1* in *C. autoethanogenum* led to decreased ethanol concentrations during growth with CO, whereas deletion of *aor2* led to increased ethanol concentrations, clearly indicating that AOR1 is catalyzing the reduction towards acetaldehyde (Liew *et al.*, 2017). Lo *et al.*

(2020) reported increased ethanol concentrations that were produced by *C. ljungdahlii Δpta Δaor2* during growth with CO, supporting the results of Liew *et al.* (2017) that AOR1 catalyzes towards acetaldehyde. However, it should be noted that the strain also harbors the deletion of *pta.* PTA is responsible for the conversion of acetyl-CoA to acetyl-P, the first step in acetate formation. The deletion of this gene can, thus, influence the catalysis of AOR even more and create a bias. Our results from the autotrophic growth experiments contradict these results, indicating that AOR1 would preferentially catalyze the oxidation of acetaldehyde towards acetate during autotrophic fermentations with H_2/CO_2 as well as CO (Table 18). As discussed in Chapter 5.3 already, these results need further investigation, such as chemostat fermentations to examine the phenotype during steady-state conditions. Due to the poor growth behavior during batch fermentation, it is hard to estimate the phenotypical changes of the gene deletions under relevant conditions. Additionally, analyzing the *aor2* deletion mutant will give more insight into the role of AOR1. For AOR2, the direction of catalysis seems to be reversed when *C. ljungdahlii* is growing with CO, compared to growth with H_2/CO_2 (Table 18). Our results indicate, that AOR2 is responsible for oxidizing acetaldehyde to acetate during growth with CO, which is in accordance with previous reports (Lo *et al.*, 2020; Zhu *et al.*, 2020). Liew *et al.* (2017) have reported the same results for *C. autoethanogenum.* Comparative transcriptomic analysis during a batch fermentation with *C. ljungdahlii* grown with CO has shown that AOR2 and AdhE1 can re-oxidize ethanol during the stationary phase (Liu *et al.*, 2020).

In summary, our results support the current opinion in the literature that the AOR is not the key enzyme for ethanol formation during heterotrophic growth but plays a vital role during autotrophic growth (Tables 17 and 18). We hypothesize that AOR2 is responsible for oxidizing acetaldehyde to acetate during growth of *C. ljungdahlii* with H_2/CO_2 and CO, although further experiments with the *aor2* deletion strain will contribute more insights. The results of Liew *et al.* (2017), Lo *et al.* (2020), Valgepea *et al.* (2022), and Xie *et al.* (2015) indicated that AOR1 is responsible for ethanol formation *via* acetate, however, our experiments contradict these findings. Future experiments should put special emphasis on elucidating the role of AOR1 during autotrophic fermentation, especially during growth with CO-containing gases.

Table 18: Directionality of AOR1 and AOR2 in *C. ljungdahlii* in different growth conditions.

Isoform	Growth condition	Directionality	Reference
AOR1	Fructose	Acetaldehyde to acetate Ethanol production *via adhE*	This study (Lo *et al.*, 2020) (Leang *et al.*, 2013)
	H$_2$/CO$_2$	Acetaldehyde to acetate	This study (Xia *et al.*, 2020)
	CO	Acetate to acetaldehyde	(Lo *et al.*, 2020) (Zhu *et al.*, 2020) (Valgepea *et al.*, 2022) (Xie *et al.*, 2015)
	CO	Acetaldehyde to acetate?[8]	This study
	CO (*C. autoethanogenum*)	Acetate to acetaldehyde	(Liew *et al.*, 2017)
AOR2	Fructose	Acetaldehyde to acetate Ethanol production *via adhE*	This study (Lo *et al.*, 2020) (Leang *et al.*, 2013)
	H$_2$/CO$_2$	Acetate to acetaldehyde	(Xia *et al.*, 2020)
	CO	Acetaldehyde to acetate	(Lo *et al.*, 2020) (Zhu *et al.*, 2020)
	CO (*C. autoethanogenum*)	Acetaldehyde to acetate	(Liew *et al.*, 2017)

5.5 Chemostat fermentation with CO as the sole carbon and energy source

To our knowledge, this study represents the first fully continuous chemostat fermentation with *C. ljungdahlii* using CO as the sole carbon and energy source. Our data prove feasibility and reproducibility. We achieved a process time of more than 75 days and steady-state conditions during full autotrophy without any yeast extract for more than 21 days. We observed that during the batch phase with continuous CO supply, yeast extract was essential to obtain stable growth in the bioreactors. After reaching a high OD$_{600}$ in both bioreactors, we started the continuous mode of operation and continuously decreased the concentration of yeast extract that was added to the medium until we were able to omit it completely. Simultaneously, we increased the medium exchange rate. During steady-state conditions with no yeast extract and an HRT of 4 days, we achieved stable

---

[8] unclear result

production rates of acetate, ethanol, and 2,3-BDO. In average, bioreactors 1 and 2 produced acetate at a rate of 0.063 ± 0.010 g L^{-1} h^{-1} and 0.076 ± 0.005 g L^{-1} h^{-1} (25.8 ± 4.1 mmol L^{-1} d^{-1}. and 30.8 ± 1.9 mmol L^{-1} d^{-1}), ethanol at a rate of 0.067 ± 0.011 g L^{-1} h^{-1} and 0.042 ± 0.002 g L^{-1} h^{-1} (35.0 ± 5.7 mmol L^{-1} d^{-1} and 21.7 ± 1.2 mmol L^{-1} d^{-1}), and 2,3-BDO at a rate of 0.004 ± 0.000 g L^{-1} h^{-1} and 0.002 ± 0.000 g L^{-1} h^{-1} (0.9 ± 0.1 mmol L^{-1} d^{-1} and 0.5 ± 0.0 mmol L^{-1} d^{-1}), respectively (Table 16). The bioreactors achieved an average ratio of ethanol/acetate production of 1.41 and 0.71, respectively. We assume the difference between the product ratios is due to marginal oxygen penetration in bioreactor 2. At t = 1528 h, the ethanol production rates of bioreactors 1 and 2 settled at 0.050 g L^{-1} d^{-1} (26.01 mmol L^{-1} d^{-1}) and 0.038 g L^{-1} h^{-1} (19.88 mmol L^{-1} d^{-1}), respectively. In a comparable setup using H_2/CO_2, we achieved an ethanol production rate of 0.02 g L^{-1} h^{-1} (Klask *et al.*, 2020), which shows that CO is a much more suitable substrate when aiming for maximum ethanol production. Valgepea *et al.* (2018) conducted a chemostat fermentation with *C. autoethanogenum* growing with CO (CO/Ar 60/40 vol-%, gas flow rate = 0.0465 L/min, HRT = 1 d, agitation 510 rpm, pH 5) and they achieved an ethanol concentration of 0.6 g L^{-1} (value estimated from Fig. S1 (Valgepea *et al.*, 2018)). We achieved higher concentrations of 2.5 g L^{-1} (R1) and 1.9 g L^{-1} (R2) under similar conditions at pH 5.7 and higher HRT (4 d). Valgepea *et al.* (2018) were able to significantly shift their carbon flux towards ethanol (~ 4.5 g L^{-1}) by adding H_2 to the feed gas (CO/H_2/Ar 15/45/40 vol-%), which coincided with a higher re-assimilation of CO_2 from the off-gas. Previous reports have shown that the addition of external acetate can shift the product ratio further to ethanol. Xie *et al.* (2015) have shown that acids induce expression of *aor1*, while *aor2* was down-regulated (fed-batch with CO/CO_2). This effect was strongest when acetic acid (20 mM) was used. The results highlight the importance of AOR1 for the ethanol production pathway, as well as for the detoxification of acids. During batch experiments with *C. autoethanogenum* grown with CO (100-vol %), the addition of external acetate to the medium led to increased ethanol concentrations and expression levels of *aor* genes (Xu *et al.*, 2015). Xu *et al.* (2015) reported the best results for an addition of 15 mM acetate, while the expression of *aor1* dramatically decreased during the addition of 20 mM acetate. Kwon *et al.* (2022) used a novel species, *Clostridium* sp. AWRP (Lee *et al.*, 2019), in a batch fermentation with 40 mM external acetate. They achieved 2.9-fold higher ethanol production, increased growth rate, and a shortened lag phase during growth with CO. Kwon *et al.* (2022) postulated that the electrons gained from CO oxidation are used for the reduction of acetate to acetaldehyde. During the last phase of our fermentation, we, therefore, added 15 mM sodium acetate to the medium to observe the effect of external acetate on the metabolism of *C. ljungdahlii* during steady-state with CO. We experienced some difficulties with oxygen penetration in the feed medium of bioreactor 1, which led to no statistically relevant changes of the performance compared to the performance with no acetate in the medium. For bioreactor 2, we observed a dramatic increase in the ethanol production

rate and selectivity four days after starting the feed of the acetate-containing medium (1 HRT). The ethanol production rate increased by more than 230% from 0.042 g $L^{-1} h^{-1}$ (21.7 mmol $L^{-1} d^{-1}$) to 0.230 g $L^{-1} h^{-1}$ (120.0 mmol $L^{-1} d^{-1}$, marked in bold in Table 16). The ratio of ethanol/acetate increased from 0.71 to 92.96. This is, to our knowledge, the highest ethanol selectivity achieved during fermentation with CO.

Richter *et al.* (2016) were the first to hypothesize that ethanol production is controlled by thermodynamics rather than on a transcriptional or translational level. Recent results intensify this understanding. The group of Esteban Marcellin at the Australian Institute for Bioengineering and Nanotechnology (University of Queensland) is doing intensive work to produce omics data and use this data to constrain metabolic models for *C. autoethanogenum* (Heffernan *et al.*, 2020; Mahamkali *et al.*, 2020; Valgepea *et al.*, 2018; Valgepea *et al.*, 2017). In a chemostat fermentation with syngas, Valgepea *et al.* (2017) reported a shift towards ethanol production in correlation to increased biomass concentrations, which were not caused by transcriptional changes. They were the first to report periodic crashes of the biomass concentration and they attributed this to the depletion of internal acetyl-CoA concentration. This observation was further characterized in their following work (Mahamkali *et al.*, 2020). Mahamkali *et al.* (2020) showed that oscillations of chemostat fermentations of *C. autoethanogenum* with CO/H_2 are caused by thermodynamics, as they did not find differentially expressed proteins that would explain the metabolic rearrangements. Valgepea *et al.* (2017) propose a model that explains the biomass crashes (Figure 25): **1)** During high biomass concentration fermentations, high acetate production causes a high extracellular acetic acid concentration, which leads to increased uncoupling of the proton motive force (PMF)**; 2)** Consequently, ATP demand is increasing and additional ATP is generated through substrate level phosphorylation *via* PTA and ACK; **3)** The produced acetate is reduced to ethanol, which is in turn causing a higher Fd_{red} demand; **4)** CO oxidation provides additional Fd_{red} for ATP and ethanol generation; **5)** Due to carbon dissipation as CO_2, less carbon is available for biomass production, resulting in decreasing biomass concentrations; **6)** This effect is intensified, as the increased ATP production *via* the AOR pathway eventually depletes the acetyl-CoA pool supplied by the WLP.
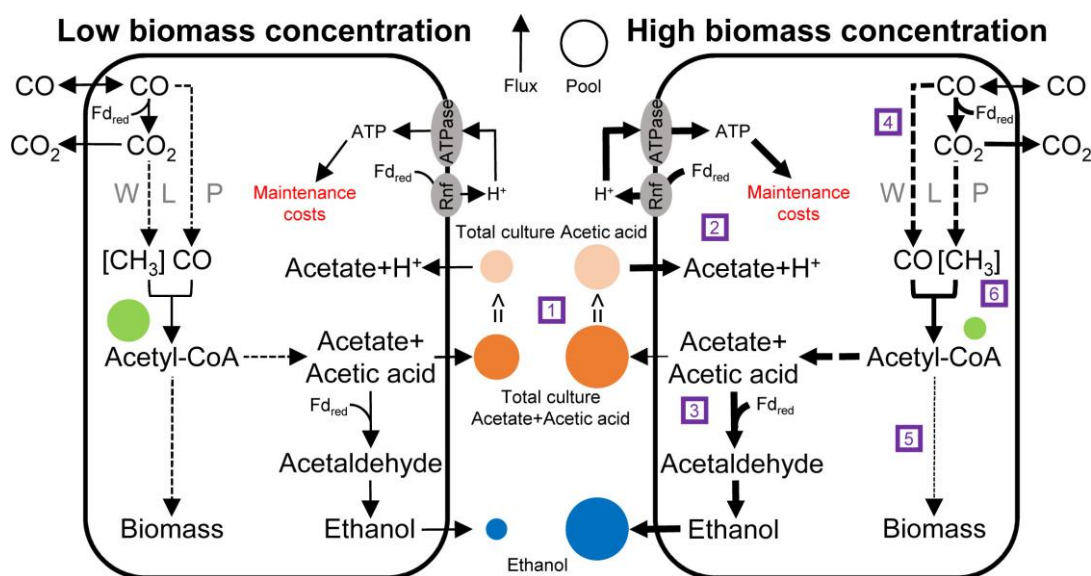
Figure 24: Regulation of carbon distribution and ATP metabolism through extracellular acetate levels during autotrophic growth of *C. autoethanogenum* with syngas (Figure and legend adapted from (Valgepea *et al.*, 2017). Thickness of arrows and size of circles illustrate the relative difference of the magnitude of fluxes and metabolite pools, respectively, between high- and low-biomass conditions. Purple numbered squares indicated phases of the described model, for details refer to the text above (Valgepea *et al.*, 2017).

During our fermentation with *C. ljungdahlii*, growing on CO as the sole carbon and energy source, we did not observe oscillations of biomass as described by Valgepea *et al.* (2017) and Mahamkali *et al.* (2020). We postulate the lack of oscillations is due to the following behavior: **1)** the external addition of acetate and the resulting increase in intracellular acetic acid concentration act as an increased driving force for the AOR; **2)** due to the high pool of Fd_{red} from the oxidation of CO, acetic acid is used as an electron sink; **3)** the increased NADH demand for the successive thermodynamically favorable alcohol-dehydrogenase reaction is met *via* the Rnf; **4)** this simultaneously increases ATP production *via* the generated PMF; **5)** which enables increased growth rates as reported in chapter 4.5. Additionally, it must be noted that our biomass concentration was comparable to the biomass concentration reported as "low-biomass concentration" by Valgepea *et al.* (2017) (0.25 gDCW L^{-1} compared to 0.5 gDCW L^{-1}), so we cannot predict the behavior during high-biomass concentrations. To further analyze our hypothesis, metabolic modeling of the presented growth conditions could provide vital insights into the metabolism.

CHAPTER 6
SUMMARY AND FURTHER RECOMMENDATIONS

My work tempted to give valuable new insights into the metabolism of the model acetogen *C. ljungdahlii*. We have put a major focus on elucidating the role of the AOR in the autotrophic metabolism, with special emphasis on the role of the two tungsten-containing isoforms AOR1 and AOR2. Furthermore, we examined the growth behavior of *C. ljungdahlii* during fully autotrophic steady-state growth with pure CO. In chapter 4.1 we present a preliminary production system for heterologous production of AOR enzymes in *E. coli*. We established an efficient protocol for cell disruption and a protein purification system for *E. coli*. We demonstrated that AOR enzymes can be produced in *E. coli*, but the enzymes were not active in an enzyme activity assay. We assume, that to produce functional AORs in *E. coli*, the expression of further genes for helper enzymes, such as chaperones and enzymes for cofactor assembly, will be necessary. Consequently, we designed a system for homologous production of AORs in *C. ljungdahlii*. The benefit of this system will be, that all enzymes that are required to produce functional AOR are already present and expressed naturally. We learned, that minimizing the concentration of the inducing agent aTc is crucial to reduce the metabolic burden for the recombinant strains during overproduction experiments. We established an efficient protocol for cell disruption of Gram$^+$ cells and purified proteins from the cell extract. However, we saw that the AORs had been degraded in our sample from stationary cells. We suggest harvesting clostridial cells during late-exponential growth and to increase the sample volume for efficient purification of AOR enzymes. An ideal set-up to generate suitable cultures would be the MBS system developed by Klask *et al.* (2020).

In chapter 3, we present a novel CRISPR/Cas9 system for efficient genome editing in *C. ljungdahlii*. Cloning of the plasmid for deletion of *aor1* was straightforward, while the assembly of the plasmid for *aor2* deletion was more complicated. We learned that the expression of an adjacent gene locus for a predicted σ^{54}-interacting transcription regulator (CLJU_c20200) in *E. coli* produces a toxic effect leading to escape mutations. These mutations render the gene unfunctional, which causes the transformation of *C. ljungdahlii* with the plasmid to fail, as they are lethal in *C. ljungdahlii*. Preventing these mutations and switching the directionality of the respective area in the plasmid to prevent read-through in *E. coli* circumvented this effect. After correct assembly of both deletion plasmids, we successfully generated two deletion strains, *C. ljungdahlii Δaor1* and the double deletion mutant *C. ljungdahlii Δaor1Δaor2*. Deletion of *aor2* individually and subsequent plasmid curing has not yet been confirmed. After the successful generation and verification of the deletion mutant, the PCR signal for the deletion disappeared during the plasmid curing process. Our whole-genome sequencing revealed that the

mutant strain was overgrown by *S. laevolacticus*. We will repeat the construction of *C. ljungdahlii Δaor2* to ensure the stability of the strain and conduct further research on the effect of the gene deletion. During the work on deletions of *aor* genes, we tried to establish the pWV01ts ori as a selective marker for gene deletion *via* the *Triple-Cross* method. We demonstrate that the ori was not applicable for this system, as it was unstable and produced numerous different escape mutations.

In chapter 4.4, we examine the effects of the gene deletions in *C. ljungdahlii* under different fermentation conditions. Our results support the consensus in the literature that the AOR is not the key enzyme for ethanol production during heterotrophic growth of *C. ljungdahlii.* Deletion of *aor* genes led to increased ethanol production, indicating that AOR might be involved in re-oxidizing ethanol during these conditions. During autotrophic growth with CO and H_2/CO_2, all deletion mutants showed impaired growth behavior and reduced maximum OD_{600}. During growth with H_2/CO_2, we compared the base-editing strains QX5 and the CRISPR-deletion strain *C. ljungdahlii Δaor1*. Surprisingly to us, we observed reduced maximum acetate concentrations in both strains, while the maximum ethanol concentration decreased significantly in QX5 but increased significantly in *C. ljungdahlii Δaor1*. The differences between the strains indicate, that the truncated gene still affects the strains' behavior, possibly due to polar effects. A more detailed comparison between the two strains will be necessary to fully understand the differences, ideally under steady-state conditions in chemostat fermentations. When growing *C. ljungdahlii* with CO, we observed a prolonged lag phase and reduced growth rates with all strains. *C. ljungdahlii Δaor1* produced less acetate and less ethanol, compared to the wt, although the difference in acetate production was not significant. We observed a shift in the ethanol/acetate ratio from 0.3 to 1.46. These results contradict previous results by Liew *et al.* (2017), who reported that the deletion of *aor1* in *C. autoethanogenum* reduces ethanol production. The double deletion mutant *C. ljungdahlii Δaor1Δaor2* was not able to grow stably, which is in accordance with previous findings (Liew *et al.*, 2017). From our phenotypical characterizations (Tables 16 and 17), we hypothesize that: **1)** AOR1 and AOR2 are important for ethanol generation *via* acetate **only** during autotrophic growth conditions; **2)** AOR2 is mainly responsible for oxidizing acetaldehyde to acetate during autotrophic growth with H_2/CO_2 and CO; **3)** AOR1 is responsible for ethanol formation *via* acetate during autotrophic growth with CO (Liew *et al.*, 2017; Lo *et al.*, 2020; Valgepea *et al.*, 2022; Xie *et al.*, 2015), but catalyzes the reverse reaction during growth with H_2/CO_2 (this study, (Xia *et al.*, 2020)). Further experiments with the *aor2* deletion strain will contribute more insights. Our experiments partly contradict the third hypothesis, so we suggest future experiments should put special emphasis on elucidating the role of AOR1 during autotrophic growth with CO.

In this dissertation, we present the first fully autotrophic chemostat fermentation of *C. ljungdahlii* with CO as the sole carbon and energy source. We achieved stable growth and production rates in

duplicates. By adding 15 mM sodium acetate to the feed medium, we were able to increase the ethanol production rate drastically by 230%. This increase was not observed when the medium feed was slightly aerobic (R1). Contrary to what others have reported, we did not observe fluctuations in the biomass concentration during this fermentation. We hypothesize that the external acetate acts as an electron sink. The produced acetaldehyde is reduced to ethanol using NADH, which is produced through increased flux through the Rnf complex to recycle the increased pool of Fd_{red} originated from the oxidation of CO. For industrial applications, it is crucial to increase product selectivity and production rates, because it simplifies the downstream processing. We could show, that the addition of external acetate can increase selectivity to ethanol immensely. Nevertheless, it is necessary to further improve the autotrophic ethanol production of *C. ljungdahlii*. The AOR enzymes have been shown to play a vital role during autotrophic ethanol production (Chapter 5.4). Therefore, we suggest targeting the AOR for further engineering strategies. In this dissertation, we initially attempted to rationally designed improved AORs or perform random mutagenesis on the enzyme (Chapter 7.S5). However, for a rational enzyme engineering approach, extensive knowledge about the confirmation and catalytic activity is a fundamental prerequisite. However, so far, the AOR enzyme from *C. ljungdahlii* or other closely related acetogens has not been characterized in detail. Additionally, a stable and reproducible activity assay in the physiological direction is required to efficiently characterize possible candidates. Both these requirements for rationally engineering the AOR are not met, yet. Alternatively, random mutagenesis does not require extensive knowledge of the enzyme, but a high-throughput screening system would be needed to analyze the mutated candidates. Due to the lack of techniques for rational and random engineering of the AOR, we propose to use an adaptive laboratory evolution (ALE) approach to target improvements in the AOR. ALE is a synthetic biology tool, that exploits the microbes' natural evolution and selection of beneficial mutations. In this process, selective pressure is applied during the growth of the microbe, which pushes the metabolism toward the desired phenotype (Dragosits *et al.*, 2013; Portnoy *et al.*, 2011; Sandberg *et al.*, 2019). The tool has been used since 1880, when William Dallinger conducted the first ALE experiment to adapt monads to higher temperatures (from 23°C to 70°C) (Dallinger, 1887; Haas, 2000). Since then, ALE has been used to adapt microbes to new substrates, increase stress tolerance, improve general fitness, increase product yields, and optimize growth rates (Sun *et al.*, 2018). By analyzing adapted microbes *via* whole genome sequencing (WGS), causal mutations of the observed phenotypes can be determined. Introducing these mutations in the parental strains, termed reverse engineering, helps to confirm the causality of the mutations (Sandberg *et al.*, 2019). ALE has already been applied in acetogens for example to: **1)** enhance tolerance of *C. saccharoperbutylacetonicum* to acetic acid and 5-hydroxymethyl (Alves *et al.*, 2021); **2)** improve general robustness and oxygen tolerance of *Sporomusa ovata* during microbial

electrosynthesis (Shi *et al.*, 2021); **3)** achieve faster substrate conversion and autotrophic growth of *Sporomusa ovata* (Tremblay *et al.*, 2015); **4)** improve production of *n*-butanol with *C. cellulovorans* (Wen *et al.*, 2019); and **5)** adapt *Eubacterium limosum* to CO and reduce CO inhibition of the hydrogenases (Kang *et al.*, 2020). ALE cannot only be performed in successive batch fermentations with increasing selective pressure (Alves *et al.*, 2021; Tremblay *et al.*, 2015; Zhang *et al.*, 2018), but it is also possible during chemostat fermentations (Holwerda *et al.*, 2020) or can be combined with rational strain engineering (Wen *et al.*, 2019). For ALE of *C. ljungdahlii* for improved ethanol production, we propose to use chemostat fermentations with pure CO and increase concentrations of external acetate. High CO availability will maintain a high Fd_{red} pool, which will be used by the AOR to reduce the supplied acetate to acetaldehyde. We hypothesize that the increasing concentration of acetate, in combination with access CO and Fd_{red}, will lead to increased AOR activity and accumulation of beneficial mutations. After further characterization of the *aor* deletion mutants, choosing the best ethanol-producing mutant as the parental strain for the ALE experiment will be possible. It is likely that this will also affect other enzymes involved in the ethanol production pathway. By using WGS and reverse engineering, we will be able to trace the phenotype change back to the mutations and analyze AOR variants in more detail. To this end, it is also crucial to further improve the AOR activity assay and optimize the production of Fd in *E. coli* to provide sufficient electron carries for the physiological direction of the assay.

In conclusion, further research is needed to unravel the role of the two isoforms of AOR. Further analysis of the *aor* deletion mutants can fill this knowledge gap and guide future strain engineering for industrially relevant production strains. Additionally, improvement of the critical enzymes in the AOR-pathway for ethanol production by ALE and chemostat fermentations will contribute immensely. The knowledge gained from this dissertation will be of high value for future research and the use of acetogenic bacteria in biotechnological applications.

CHAPTER 7
Supplemental

S1   Enzyme activity assay with AOR from heterologous production in *E.coli* BL21

To determine the activity of heterologously produced AOR, we cultivated *E. coli* BL21 pASK-IBA3C, *E. coli* BL21 pASK-IBA3C-*aor1,* and *E. coli* BL21 pASK-IBA3C-*aor2* and purified the enzymes *via* affinity chromatography (Petschak, 2019). We used the purified enzyme fractions for the anaerobic activity assay in a VICTOR Nivo Multimode Microplate Reader (PerkinElmer, Waltham, USA) placed in an anaerobic workbench. The assay was set up according to protocols previously described (Heider *et al.*, 1995; Huber *et al.*, 1995; Mock *et al.*, 2015; Petschak, 2019; Wang *et al.*, 2013a; Whitham *et al.*, 2015). We used a total reaction volume of 200 µL with varying acetaldehyde concentrations in a 96-well plate. The plate was heated to 28 °C and agitated at 300 rpm. The reaction was initiated by the addition of the enzyme or cell lysate and the catalyzed reaction was monitored by measuring the change in absorption at $\lambda=395$ nm. In this assay, we compared the purified samples (including the empty vector control) to cell extract from a culture of *C. ljungdahlii* wt. The substrate for the reaction was acetaldehyde, and methylviologen served as the reducing equivalent. It was clearly visible that the assay needs further improvement because we saw AOR activity in our controls without substrate (Figure S1). Thus, it is not possible to draw meaningful conclusions from the assay. As I learned during my literature research, the heterologous production of AOR can be challenging in *E. coli*, especially under aerobic conditions (Ayala-Castro *et al.*, 2008; Huang *et al.*, 2016b). The maturation of the enzyme requires a set of cofactors such as tungstopterin and iron-sulphur clusters. *E. coli* is not able to produce the entity of the required cofactors and assemble the enzyme correctly (unpublished data, personal communication with Prof. Dr. Soucaille). Therefore, the introduction of genes encoding for additional pathways would be necessary to produce functional AOR with *E. coli*.
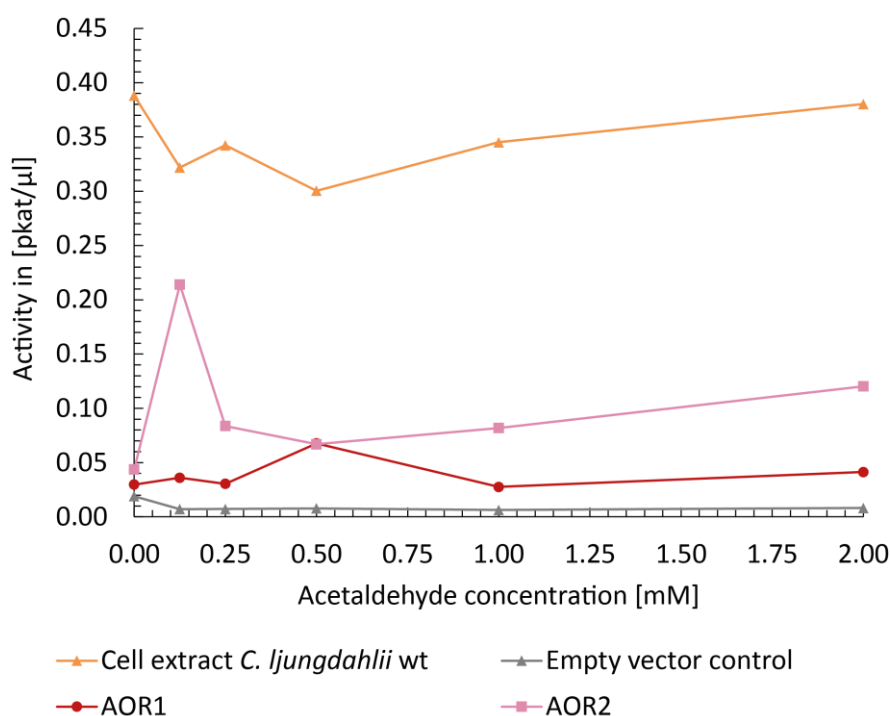
Figure S1: Enzyme activity assay with AOR from heterologous production in *E.coli* BL21. Grey line: empty vector control; red line: purified AOR1 enzyme fraction; pink lines: purified AOR2 enzyme fraction; orange line: cell extract from *C. ljungdahlii* wt. N=1.

To further improve the activity assay, we planned to investigate the activity of the AOR in the direction that is important under physiological conditions for *C. ljungdahlii* (reduction of acetic acid to acetaldehyde). However, due to the thermodynamic relationships, this assay is less trivial compared to the non-physiological direction. It is necessary to keep the concentration of the product of the AOR reaction (acetaldehyde) low, to make the reaction thermodynamically feasible, and to allow for the determination of the AOR-specific enzyme parameters. For this purpose, the acetaldehyde can be reacted to ethanol in a favorable reaction either with purified alcohol dehydrogenase (ADH) or with AOR-free *C. ljungdahlii* cell extract, which also contains ADH and NAD(P)H. To keep the co-substrate level (Fd$_{red}$) high, the reduction of Fd is achieved using CODH or *C. ljungdahlii* cell extract and CO in a separate or coupled reaction, as described by Wang *et al.* (2013a) and Demmer *et al.* (2015). Appropriate controls cover parameters, such as the background activity of ferredoxin in the cell extract. The ADH reaction is thermodynamically favorable and occurs at a significantly higher rate. Therefore, the AOR reaction can be considered the rate-determining step. Establishing this assay will be crucial to analyzing purified AOR under physiological conditions and is the subject of future work in our group. The assay will also be crucial to compare the wt AOR enzymes to possible altered versions from the ALE experiment (Chapter 6).

S2   Production of clostridial holo ferredoxins in *E. coli*

To achieve representative conditions in the design of the improved enzyme assay, it will be necessary to exchange the methylviologen with the physiological enzyme carrier ferredoxin. To produce sufficient amounts of this small iron-sulphur cluster-containing protein, we designed production plasmids for heterologous production of *fd1* (CLJU_c01820) and *fd2* (CLJU_c01440) from *C. ljungdahlii* in *E. coli*. However, *E. coli* lacks certain maturation systems for the production of functional clostridial proteins *in vivo* (Petschak, 2019). Consequently, we extended our system according to the findings of Huang *et al.* (2016b) and Nakamura *et al.* (1999), who found that co-expression of iron-sulphur cluster producing operons can support the production of holo-ferredoxins. We successfully purified both ferredoxins from *E. coli* carrying both the ferredoxin-production system (pASK-IBA3C-*fd1*/*fd2*) and the plasmids containing the iron-sulphur cluster production operon (pRKISC_*kanR* or pRKSUF_*kanR*) (Keßler, 2021). However, the quantity of the protein gained from the recombinant strains is still not sufficient and further work is necessary to improve protein yields.

S3   Temperature-sensitive ori pWV01ts in pMTLts and pMUT2ts

For the deletion of *aor1* and *aor2,* we originally planned to apply the *Triple-Cross* method developed by Lanzatech (Walker *et al.*, 2015) using pWV01ts as a selective tool. As described in Chapter 4.3.1, we faced multiple difficulties with the plasmid pMTLts harboring both the temperature-selective ori pWV01ts and the high-copy ori ColE1. We analyzed a variety of different plasmid stocks from our plasmid collection and the plasmid stocks from the Rosenbaum Lab in Aachen, where the plasmid had been constructed (Molitor *et al.*, 2016a). Sequencing of the different stocks revealed silent mutations at different locations, but also other mutations with more severe effects were found (Table S1). We found the mutation G212A in almost all clones, which led us to the conclusion that the annotation of the plasmid might be faulty. Similarly, we found the silent mutation T913C in all clones. We found an inserted G in a non-coding area at position 1927 in all clones. In clone 5, an inserted A in the *repA* gene in the pWV01ts led to a premature STOP codon. We found an amino acid exchange from Thr to Ile at position 557 (clone 2) and a Tyr to Cys exchange at position 1056 (clone 4). We found a frameshift mutation due to an insertion of a TATTGA motif at position 1434 in clone 3. During my master's thesis, we analyzed other stocks that showed mutations, such as the insertion of an IS*10* related transposable element at position 581, the complete lack of the pWV01ts ori, and 11 bp deletion of a repetitive 5'-AATCGCCAACG-3' motif at position 661, which all rendered the ori unfunctional (Schulz, 2018). As clones 2 and 4 showed the least effective mutations (Table S1), we decided to test them for functionality in *C. ljungdahlii.* We transformed *C. ljungdahlii* with the two plasmids from clones 2 and 4 and pMTL83151 as a positive control. The transformation with the positive control worked well while

we were not able to generate colonies from the transformations with the plasmids from clones 2 and 4. Therefore, we concluded the amino acid exchanges rendered the pWV01ts unfunctional.

Table S1: Mutations in pWV01ts in different plasmid stocks of pMTLts.

Mutation	Effect	Clones	Reference
G212A	Found many clones, annotation in the plasmid map different, G to A	2, 3, 4, 5	This study
T913C	Silent mutation; TAT now TAC: both code for Tyr	2, 3, 4, 5	This study
1927G	Insertion of a G in the non-coding region at the end of pWV01ts sequence	2, 3, 4, 5	This study
1150A	Insertion of an A leads to premature STOP codon, inside *repA* gene	5	This study
C557T	ACA to ATA leads to amino acid exchange from Thr to Ile	2	This study
1434	TATTGA insertion at position 1434	3	This study
A1056G	Amino acid exchange from Tyr to Cys	4	This study
661	11 bp deletion of a repetitive 5'-AATCGCCAACG-3' motif	Aachen	(Schulz, 2018)
1	Deletion of pWV01ts	Aachen	(Schulz, 2018)
581	Insertion of an IS*10* related transposable element	1	(Schulz, 2018)

The plasmid pMUT2ts, which I have previously used in my bachelor thesis also harbors the pWV01ts ori. In our first analysis of the stocks that were sent to us, the plasmid digest showed the correct size of the bands. Sequencing revealed a few point mutations of which some led to amino acid exchanges similar to the mutations in pMTLts. We tested the plasmid for functionality in *C. ljungdahlii* and again were unable to obtain any transformants.

To obtain a functional pWV01ts ori, we tried to restore the ori with different strategies: First, we tried to restore the functionality of the ori in clones 2 and 4 by site-directed mutagenesis with the QuikChange method (Chapter 3.3.6). After multiple unsuccessful attempts, we were able to obtain successful transformants with the QuikChange product in *E. coli* NEB stable. Sequencing showed that we had successfully restored the point mutation at position 557 in clones 2. However, a new mutation causing a frameshift appeared, so the functionality of the ori could not be restored. Second, we aimed to exchange the ColE1 ori on pMTLts with the low-copy ori p15a. The oris ColE1 and p15a belong to different incompatibility groups. It is known, that the presence of two oris of the same incompatibility group on the same plasmid can cause problems and mutations causing one of them to lose functionality. We intended to avoid an incompatibility by using an ori from a different group. However, removing the ColE1 and exchanging it with the p15a with restriction ligation cloning was not successful.

Lastly, we tried to synthesize pWV01ts in a plasmid without another ori and flanked by *Asc*I and *Fse*I restriction sites to facilitate easy cloning into the *Triple-Cross* plasmid. However, the company was unable to synthesize the ori in various attempts and canceled our order. During the different attempts to restore pWV01ts, we worked with different *E. coli* cloning strains and did all incubations at 30°C, but we did not see any differences from these alterations. Therefore, we decided to stop working with the temperature-sensitive system and switched to a CRISPR/Cas9-based method for deletion of *aor1* and *aor2.*

S4 Problems with the design of CRISPR/Cas9 system for deletion of *aor* genes

S4.1 Toxicity of Cas9 causes problems during plasmid cloning

When designing the CRISPR/Cas9 system for gene deletions in *C. ljungdahlii*, we had some initial difficulties with cloning target and repair sequences into the plasmid containing the aTc-inducible promoter for the expression of *cas9*. Therefore, we designed a second set of plasmids in which the *cas9* gene would be inserted downstream of the P_{thl} promoter in pMTL83152. This promoter is a strong constitutive promoter from *C. acetobutylicum* ATCC 824 (Girbal *et al.*, 2003). Both cloning strategies were carried out simultaneously and the inducible system was finished earlier. In fact, the expression of *cas9* controlled by P_{thl} seemed to be too strong to construct a functional CRISPR deletion system due to the toxicity of Cas9. Cloning the gene for Cas9 downstream of the promoter led to escape mutations in the gene, creating different mutations at the beginning of the gene (amino acid exchanges).

S4.2 Cloning difficulties during construction of the CRISPR/Cas9 system for the deletion of *aor2*

The first strategy to construct pMTLCas9-*aor2* was identical to the strategy for the plasmid for *aor1* deletion. After assembly of the plasmid, the sequencing results showed that the wrong sequence was amplified from gDNA as repair template DNA. Detailed analysis of the primer revealed that 11 bp of the primers can also anneal in an off-target region. Therefore, the primers for the homologous repair templates for *aor2* were re-designed, making sure to avoid off-target annealing. Assembly of the new components was successful for the plasmids for *aor2* deletion with a protospacer that targets a sequence at the beginning of the gene. We used the constructed plasmids for the transformation of *C. ljungdahlii* wt. The transformation was performed in triplicates using the plasmids for *aor1* and *aor2* deletion, pMTL83151 as a positive control, and without a plasmid as a negative control. As described in Chapter 4.3.2.1, the transformants were discarded because the negative control failed. In the second attempt in triplicates, we were not able to obtain transformants with the plasmid pMTLCas9-*aor2*. We

tried a conjugation approach with *E. coli* HB101 pRK2013 that had successfully been applied for the transformation of *C. ljungdahlii* with a CRISPR-Cas12a system (Klask, 2021), but we did not obtain recombinant clones. Sequencing analysis of the plasmid showed that a point mutation in LHA might have led to an unfunctional gene product of the locus CLJU_c20200, a predicted σ[54]-interacting transcription regulator. We suspected that this mutation might be lethal in the transformants, which would explain the various unsuccessful attempts of CRISPR editing thus far. Consequently, we constructed the plasmid again and the mutation did not occur again. We achieved successful editing of *C. ljungdahlii* at first, but after several transfers of the culture in unselective medium, we lost the signal for deletion of *aor2.* We, therefore, decided to construct a new plasmid for deletion of *aor2*, using new sgRNAs (sgRNA2.3 and sgRNA2.4, Table 15 Chapter 3.7). The plasmid was constructed as described in Chapter 3.7 and used for the successful transformation of *C. ljungdahlii* wt (Chapter 4.3.2.2).

S5   Enzyme engineering

S5.1   Computational tools for rational protein design

To improve the efficiency of the AOR, modification towards a higher substrate affinity is a possible target. Improving the catalytic properties (K_m, k_{cat}) is hypothesized to increase the rate of the AOR reaction at lower substrate concentrations. To achieve this, individual amino acids are replaced by point mutations in the gene. This method is generally referred to as site-directed mutagenesis. To find suitable targets, several computational tools have been developed for rational protein design (Lutz, 2010). One of which is the HotSpot Wizard (Pavelka *et al.*, 2009; Sumbalova *et al.*, 2018), a free web-based software. It was used, for example, to plan the modification of a haloalkane halase from *Rhodococcus rhodochrous*, achieving a 32-fold higher activity (Pavelka *et al.*, 2009). The HotSpot Wizard draws information from the protein sequence and various databases to develop a mutability map for possible targets of single amino acid exchanges. For this purpose, putative active centers or binding pockets are investigated. In the protein database PDB, published 3D structures of proteins are stored and can be used for comparisons (Rose *et al.*, 2016; Rose *et al.*, 2015). The structure of an AOR from the hyperthermophilic organism *P. furiosus* (see above) has already been solved (Chan *et al.*, 1995). With the help of this structure and after comparison with the sequence of the AOR from *C. ljungdahlii*, possible targets for protein changes can also be identified in the structure of the *C. ljungdahlii* enzyme. As a further method, the Rosetta modeling software allows energetic and kinetic parameters to be considered (Das *et al.*, 2008). The Max-Planck Institute offers a bioinformatic toolkit for protein sequence analysis, which allows a combination of various tools to gain a more thorough

understanding of the protein and its structure (Alva *et al.*, 2016; Biegert *et al.*, 2006). For instance, this tool could be used to analyze the *C. ljungdahlii* AOR structure and comparison to other AORs.

S5.2   Methods of acquiring enzyme variants

Another method to modify enzymes is to use error-prone PCR to produce random gene mutations. This method involves heavy screening, as all generated mutants need to be tested. Based on undirected mutagenesis, a technique called directed evolution has been developed, which emulates the process of natural selection. Libraries of randomly mutated versions of one gene are expressed in a host, such as *E. coli*, and promising candidates are isolated (Kuchner *et al.*, 1997; Woycechowsky *et al.*, 2007; Zhang *et al.*, 1999). These candidates are then subjected to the same cycle to enhance the effect of the mutation. Pavlova *et al.* (2009) have successfully applied this technique to improve a dehalogenase from *R. rhodochrous* to a 32-fold higher activity toward a toxic anthropogenic compound 1,2,3-trichloropropane (TCP) after identifying target sites with the help of the HotSpot Wizard. This showed that combining rational protein design with directed evolution can be an efficient method for enzyme engineering.

CHAPTER 8

LITERATURE

Al-Hinai, M. A., Fast, A. G., & Papoutsakis, E. T. (2012). Novel system for efficient isolation of *Clostridium* double-crossover allelic exchange mutants enabling markerless chromosomal gene deletions and DNA integration. *Applied and Environmental Microbiology, 78*(22), 8112-8121.

Alva, V., Nam, S. Z., Soding, J., & Lupas, A. N. (2016). The MPI bioinformatics Toolkit as an integrative platform for advanced protein sequence and structure analysis. *Nucleic Acids Research, 44*(W1), W410-415.

Alves, R. F., Zetty-Arenas, A. M., Demirci, H., Dias, O., Rocha, I., Basso, T. O., & Freitas, S. (2021). Enhancing acetic acid and 5-hydroxymethyl furfural tolerance of *C. saccharoperbutylacetonicum* through adaptive laboratory evolution. *Process Biochemistry, 101*, 179-189.

Andreesen, J. R., Gottschalk, G., & Schlegel, H. G. (1970). *Clostridium formicoaceticum* nov. spec. isolation, description and distinction from *C. aceticum* and *C. thermoaceticum*. *Archives of Microbiology, 72*(2), 154-174.

Ayala-Castro, C., Saini, A., & Outten, F. W. (2008). Fe-S cluster assembly pathways in bacteria. *Microbiology and Molecular Biology Reviews, 72*(1), 110-125, table of contents.

Banerjee, A., Leang, C., Ueki, T., Nevin, K. P., & Lovley, D. R. (2014). Lactose-inducible system for metabolic engineering of *Clostridium ljungdahlii*. *Applied and Environmental Microbiology, 80*(8), 2410-2416.

Bengelsdorf, F. R., Poehlein, A., Linder, S., Erz, C., Hummel, T., Hoffmeister, S., Daniel, R., & Durre, P. (2016). Industrial acetogenic biocatalysts: A comparative metabolic and genomic analysis. *Frontiers in Microbiology, 7*, 1036.

Biegert, A., Mayer, C., Remmert, M., Soding, J., & Lupas, A. N. (2006). The MPI Bioinformatics Toolkit for protein sequence analysis. *Nucleic Acids Research, 34*(Web Server issue), W335-339.

Brown, S. D., Nagaraju, S., Utturkar, S., De Tissera, S., Segovia, S., Mitchell, W., Land, M. L., Dassanayake, A., & Kopke, M. (2014). Comparison of single-molecule sequencing and hybrid approaches for finishing the genome of *Clostridium autoethanogenum* and analysis of CRISPR systems in industrial relevant Clostridia. *Biotechnology for Biofuels, 7*, 40.

Chan, M. K., Mukund, S., Kletzin, A., Adams, M. W., & Rees, D. C. (1995). Structure of a hyperthermophilic tungstopterin enzyme, aldehyde ferredoxin oxidoreductase. *Science, 267*(5203), 1463-1469.

Dallinger, W. H. (1887). The President's Address. *Journal of the Royal Microscopical Society, 7*(2), 185-199.

Daniell, J., Kopke, M., & Simpson, S. D. (2012). Commercial biomass syngas fermentation. *Energies, 5*(12), 5372-5417.

Das, R., & Baker, D. (2008). Macromolecular modeling with rosetta. *Annual Review of Biochemistry, 77*, 363-382.

Demmer, J. K., Huang, H., Wang, S., Demmer, U., Thauer, R. K., & Ermler, U. (2015). Insights into flavin-based electron bifurcation via the NADH-dependent reduced ferredoxin:NADP oxidoreductase structure. *Journal of Biological Chemistry, 290*(36), 21985-21995.

Diekert, G. B., & Thauer, R. K. (1978). Carbon monoxide oxidation by *Clostridium thermoaceticum* and *Clostridium formicoaceticum*. *Journal of Bacteriology, 136*(2), 597-606.

Diner, B. A., Fan, J., Scotcher, M. C., Wells, D. H., & Whited, G. M. (2018). Synthesis of heterologous mevalonic acid pathway enzymes in *Clostridium ljungdahlii* for the conversion of fructose and of syngas to mevalonate and isoprene. *Applied and Environmental Microbiology, 84*(1), e01723-01717.

Dong, H., Tao, W., Zhang, Y., & Li, Y. (2012). Development of an anhydrotetracycline-inducible gene expression system for solvent-producing *Clostridium acetobutylicum*: A useful tool for strain engineering. *Metabolic Engineering, 14*(1), 59-67.

Doudna, J. A., & Charpentier, E. (2014). Genome editing. The new frontier of genome engineering with CRISPR-Cas9. *Science, 346*(6213), 1258096.

Dragosits, M., & Mattanovich, D. (2013). Adaptive laboratory evolution - principles and applications for biotechnology. *Microbial Cell Factories, 12*, 64.

Fink, C. (2021). Establishment of tools for genetic modification of the thermophilic methanogenic archaeon *Methanothermobacter thermautotrophicus* ΔH*.* (Dissertation), Eberhard Karls Universität Tübingen, Tübingen.

Gaddy, J. L., Arora, D. K., Ko, C.-W., Phillips, J. R., Basu, R., Wikstrom, C. V., & Clausen, E. C. (2014) Methods for increasing the production of ethanol from microbial fermentation. US 8,647,851 B2.

Girbal, L., Mortier-Barriere, I., Raynaud, F., Rouanet, C., Croux, C., & Soucaille, P. (2003). Development of a sensitive gene expression reporter system and an inducible promoter-repressor system for *Clostridium acetobutylicum*. *Applied and Environmental Microbiology, 69*(8), 4985-4988.

Girbal, L., von Abendroth, G., Winkler, M., Benton, P. M., Meynial-Salles, I., Croux, C., Peters, J. W., Happe, T., & Soucaille, P. (2005). Homologous and heterologous overexpression in *Clostridium acetobutylicum* and characterization of purified clostridial and algal Fe-only hydrogenases with high specific activities. *Applied and Environmental Microbiology, 71*(5), 2777-2781.

Haas, J. W. (2000). The reverend Dr. William Henry Dallinger, F.R.S. (1839-1909). *Notes and Records The Royal Society Journal of the History of Science, 54*(1), 53-65.

Hartman, A. H., Liu, H., & Melville, S. B. (2011). Construction and characterization of a lactose-inducible promoter system for controlled gene expression in *Clostridium perfringens*. *Applied and Environmental Microbiology, 77*(2), 471-478.

Heap, J. T., Kuehne, S. A., Ehsaan, M., Cartman, S. T., Cooksley, C. M., Scott, J. C., & Minton, N. P. (2010). The ClosTron: Mutagenesis in *Clostridium* refined and streamlined. *Journal of Microbiological Methods, 80*(1), 49-55.

Heap, J. T., Pennington, O. J., Cartman, S. T., Carter, G. P., & Minton, N. P. (2007). The ClosTron: A universal gene knock-out system for the genus *Clostridium*. *Journal of Microbiological Methods, 70*(3), 452-464.

Heap, J. T., Pennington, O. J., Cartman, S. T., & Minton, N. P. (2009). A modular system for *Clostridium* shuttle plasmids. *Journal of Microbiological Methods, 78*(1), 79-85.

Heffernan, J. K., Valgepea, K., de Souza Pinto Lemgruber, R., Casini, I., Plan, M., Tappel, R., Simpson, S. D., Kopke, M., Nielsen, L. K., & Marcellin, E. (2020). Enhancing CO_2-Valorization using *Clostridium autoethanogenum* for sustainable fuel and chemicals production. *Frontiers in Bioengineering and Biotechnology, 8*(204), 204.

Heider, J., Ma, K., & Adams, M. W. (1995). Purification, characterization, and metabolic function of tungsten-containing aldehyde ferredoxin oxidoreductase from the hyperthermophilic and proteolytic archaeon *Thermococcus* strain ES-1. *Journal of Bacteriology, 177*(16), 4757-4764.

Hermann, M., Teleki, A., Weitz, S., Niess, A., Freund, A., Bengelsdorf, F. R., Durre, P., & Takors, R. (2021). Identifying and engineering bottlenecks of autotrophic isobutanol formation in recombinant *C. ljungdahlii* by systemic analysis. *Frontiers in Bioengineering and Biotechnology, 9*, 647853.

Hermann, M., Teleki, A., Weitz, S., Niess, A., Freund, A., Bengelsdorf, F. R., & Takors, R. (2020). Electron availability in CO_2 , CO and H_2 mixtures constrains flux distribution, energy management and product formation in *Clostridium ljungdahlii*. *Microbial Biotechnology, 13*(6), 1831-1846.

Hiltrud, W., Richard, F., Claudia, H., Friedrich, L., & Helmut, S. (1991). Purification and some properties of the tungsten-containing carboxylic acid reductase from *Clostridium formicoaceticum*. In *Biological chemistry Hoppe-Seyler* (Vol. 372, pp. 999).

Hoffmeister, S., Gerdom, M., Bengelsdorf, F. R., Linder, S., Fluchter, S., Ozturk, H., Blumke, W., May, A., Fischer, R. J., Bahl, H., & Durre, P. (2016). Acetone production with metabolically engineered strains of *Acetobacterium woodii*. *Metabolic Engineering, 36*, 37-47.

Holwerda, E. K., Olson, D. G., Ruppertsberger, N. M., Stevenson, D. M., Murphy, S. J. L., Maloney, M. I., Lanahan, A. A., Amador-Noguez, D., & Lynd, L. R. (2020). Metabolic and evolutionary responses of *Clostridium thermocellum* to genetic interventions aimed at improving ethanol production. *Biotechnology for Biofuels, 13*, 40.

Huang, H., Chai, C., Li, N., Rowe, P., Minton, N. P., Yang, S., Jiang, W., & Gu, Y. (2016a). CRISPR/Cas9-based efficient genome editing in *Clostridium ljungdahlii*, an autotrophic gas-fermenting bacterium. *ACS Synthetic Biology, 5*(12), 1355-1361.

Huang, H., Chai, C., Yang, S., Jiang, W., & Gu, Y. (2019). Phage serine integrase-mediated genome engineering for efficient expression of chemical biosynthetic pathway in gas-fermenting *Clostridium ljungdahlii*. *Metabolic Engineering, 52*, 293-302.

Huang, H., Hu, L., Yu, W., Li, H., Tao, F., Xie, H., & Wang, S. (2016b). Heterologous overproduction of 2[4Fe4S]- and [2Fe2S]-type clostridial ferredoxins and [2Fe2S]-type agrobacterial ferredoxin. *Protein Expression and Purification, 121*, 1-8.

Huang, H., Wang, S., Moll, J., & Thauer, R. K. (2012). Electron bifurcation involved in the energy metabolism of the acetogenic bacterium *Moorella thermoacetica* growing on glucose or H_2 plus CO_2. *Journal of Bacteriology, 194*(14), 3689-3699.

Huber, C., Caldeira, J., Jongejan, J. A., & Simon, H. (1994). Further characterization of two different, reversible aldehyde oxidoreductases from *Clostridium formicoaceticum*, one containing tungsten and the other molybdenum. *Archives of Microbiology, 162*(5), 303-309.

Huber, C., Skopan, H., Feicht, R., White, H., & Simon, H. (1995). Pterin cofactor, substrate-specificity, and observations on the kinetics of the reversible tungsten-containing aldehyde oxidoreductase from *Clostridium thermoaceticum* - preparative reductions of a series of carboxylates to alcohols. *Archives of Microbiology, 164*(2), 110-118.

Humphreys, C. M., & Minton, N. P. (2018). Advances in metabolic engineering in the microbial production of fuels and chemicals from C1 gas. *Current Opinion in Biotechnology, 50*, 174-181.

Jiang, Y., Chen, B., Duan, C., Sun, B., Yang, J., & Yang, S. (2015). Multigene editing in the *Escherichia coli* genome via the CRISPR-Cas9 system. *Applied and Environmental Microbiology, 81*(7), 2506-2514.

Jinek, M., Chylinski, K., Fonfara, I., Hauer, M., Doudna, J. A., & Charpentier, E. (2012). A programmable dual-RNA-guided DNA endonuclease in adaptive bacterial immunity. *Science, 337*(6096), 816-821.

Kang, S., Song, Y., Jin, S., Shin, J., Bae, J., Kim, D. R., Lee, J. K., Kim, S. C., Cho, S., & Cho, B. K. (2020). Adaptive laboratory evolution of *Eubacterium limosum* ATCC 8486 on carbon monoxide. *Frontiers in Microbiology, 11*, 402.

Keßler, D. (2021). Production and characterization of clostridial holo ferredoxins in *Escherichia coli.* (Bachelor's Thesis), Eberhard Karls Universität Tübingen, Tübingen.

Klask, C.-M., Jäger, B., Casini, I., Angenent, L. T., & Molitor, B. (2022). Genetic evidence reveals the indispensable role of the *rseC* gene for autotrophy and the importance of a functional electron balance for nitrate reduction in *Clostridium ljungdahlii*. *Frontiers in Microbiology, 13*.

Klask, C. M. (2021). Interrogating the energy conservation of *Clostridium ljungdahlii* by genetic manipulation and bench-scale fermentation. (Dissertation), Eberhard Karls Universität Tübingen, Tübingen.

Klask, C. M., Kliem-Kuster, N., Molitor, B., & Angenent, L. T. (2020). Nitrate feed improves growth and ethanol production of *Clostridium ljungdahlii* with CO_2 and H_2, but results in stochastic inhibition events. *Frontiers in Microbiology, 11*, 724.

Kletzin, A., Mukund, S., Kelley-Crouse, T. L., Chan, M. K., Rees, D. C., & Adams, M. W. (1995). Molecular characterization of the genes encoding the tungsten-containing aldehyde ferredoxin

oxidoreductase from *Pyrococcus furiosus* and formaldehyde ferredoxin oxidoreductase from *Thermococcus litoralis*. *Journal of Bacteriology, 177*(16), 4817-4819.

Knott, G. J., & Doudna, J. A. (2018). CRISPR-Cas guides the future of genetic engineering. *Science, 361*(6405), 866-869.

Köpke, M., Held, C., Hujer, S., Liesegang, H., Wiezer, A., Wollherr, A., Ehrenreich, A., Liebl, W., Gottschalk, G., & Durre, P. (2010). *Clostridium ljungdahlii* represents a microbial production platform based on syngas. *Proceedings of the National Academy of Sciences of the United States of America, 107*(29), 13087-13092.

Kramer, S. P., Johnson, J. L., Ribeiro, A. A., Millington, D. S., & Rajagopalan, K. V. (1987). The structure of the molybdenum cofactor. Characterization of di-(carboxamidomethyl)molybdopterin from sulfite oxidase and xanthine oxidase. *Journal of Biological Chemistry, 262*(34), 16357-16363.

Kuchner, O., & Arnold, F. H. (1997). Directed evolution of enzyme catalysts. *Trends in Biotechnology, 15*(12), 523-530.

Kwon, S. J., Lee, J., & Lee, H. S. (2022). Acetate-assisted carbon monoxide fermentation of *Clostridium* sp. AWRP. *Process Biochemistry, 113*, 47-54.

Latif, H., Zeidan, A. A., Nielsen, A. T., & Zengler, K. (2014). Trash to treasure: production of biofuels and commodity chemicals *via* syngas fermenting microorganisms. *Current Opinion in Biotechnology, 27*, 79-87.

Leang, C., Ueki, T., Nevin, K. P., & Lovley, D. R. (2013). A genetic system for *Clostridium ljungdahlii*: A chassis for autotrophic production of biocommodities and a model homoacetogen. *Applied and Environmental Microbiology, 79*(4), 1102-1109.

Lee, J., Lee, J. W., Chae, C. G., Kwon, S. J., Kim, Y. J., Lee, J. H., & Lee, H. S. (2019). Domestication of the novel alcohologenic acetogen *Clostridium* sp. AWRP: From isolation to characterization for syngas fermentation. *Biotechnology for Biofuels, 12*, 228.

Leenhouts, K. J., Tolner, B., Bron, S., Kok, J., Venema, G., & Seegers, J. F. (1991). Nucleotide sequence and characterization of the broad-host-range lactococcal plasmid pWVO1. *Plasmid, 26*(1), 55-66.

Li, L., Wei, K., Zheng, G., Liu, X., Chen, S., Jiang, W., & Lu, Y. (2018). CRISPR-Cpf1-assisted multiplex genome editing and transcriptional repression in *Streptomyces*. *Applied and Environmental Microbiology, 84*(18), e00827-00818.

Li, Q., Chen, J., Minton, N. P., Zhang, Y., Wen, Z., Liu, J., Yang, H., Zeng, Z., Ren, X., Yang, J., Gu, Y., Jiang, W., Jiang, Y., & Yang, S. (2016). CRISPR-based genome editing and expression control systems in *Clostridium acetobutylicum* and *Clostridium beijerinckii*. *Biotechnology Journal, 11*(7), 961-972.

Li, Q., Seys, F. M., Minton, N. P., Yang, J., Jiang, Y., Jiang, W., & Yang, S. (2019). CRISPR-Cas9(D10A) nickase-assisted base editing in the solvent producer *Clostridium beijerinckii*. *Biotechnology and Bioengineering, 116*(6), 1475-1483.

Liew, F., Henstra, A. M., Kpke, M., Winzer, K., Simpson, S. D., & Minton, N. P. (2017). Metabolic engineering of *Clostridium autoethanogenum* for selective alcohol production. *Metabolic Engineering, 40*, 104-114.

Liew, F., Henstra, A. M., Winzer, K., Kopke, M., Simpson, S. D., & Minton, N. P. (2016a). Insights into CO_2 fixation pathway of *Clostridium autoethanogenum* by targeted mutagenesis. *MBio, 7*(3).

Liew, F., Martin, M. E., Tappel, R. C., Heijstra, B. D., Mihalcea, C., & Kopke, M. (2016b). Gas fermentation - a flexible platform for commercial scale production of low-carbon-fuels and chemicals from waste and renewable feedstocks. *Frontiers in Microbiology, 7*(694), 694.

Liew, F. E., Nogle, R., Abdalla, T., Rasor, B. J., Canter, C., Jensen, R. O., Wang, L., Strutz, J., Chirania, P., De Tissera, S., Mueller, A. P., Ruan, Z., Gao, A., Tran, L., Engle, N. L., Bromley, J. C., Daniell, J., Conrado, R., Tschaplinski, T. J., Giannone, R. J., Hettich, R. L., Karim, A. S., Simpson, S. D., Brown, S. D., Leang, C., Jewett, M. C., & Kopke, M. (2022). Carbon-negative production of acetone and isopropanol by gas fermentation at industrial pilot scale. *Nature Biotechnology, 40*(3), 335-344.

Liu, Z. Y., Jia, D. C., Zhang, K. D., Zhu, H. F., Zhang, Q., Jiang, W. H., Gu, Y., & Li, F. L. (2020). Ethanol metabolism dynamics in *Clostridium ljungdahlii* grown on carbon monoxide. *Applied and Environmental Microbiology, 86*(14).

Lo, J., Jack, J., Urban, C., Magnusson, L., Xiong, W., Gu, Y., Ren, J., & Maness, P. C. (2020). The metabolism of *Clostridium ljungdahlii* in phosphotransacetylase negative strains and development of an ethanologenic strain. *Frontiers in Bioengineering and Biotechnology, 8*, 560726.

Lutz, S. (2010). Beyond directed evolution - semi-rational protein engineering and design. *Current Opinion in Biotechnology, 21*(6), 734-743.

Lux, M. F., & Drake, H. L. (1992). Re-examination of the metabolic potentials of the acetogens *Clostridium aceticum* and *Clostridium formicoaceticum*: chemolithoautotrophic and aromatic-dependent growth. *FEMS Microbiology Letters, 74*(1), 49-56.

Maguin, E., Duwat, P., Hege, T., Ehrlich, D., & Gruss, A. (1992). New thermosensitive plasmid for gram-positive bacteria. *Journal of Bacteriology, 174*(17), 5633-5638.

Mahamkali, V., Valgepea, K., de Souza Pinto Lemgruber, R., Plan, M., Tappel, R., Kopke, M., Simpson, S. D., Nielsen, L. K., & Marcellin, E. (2020). Redox controls metabolic robustness in the gas-fermenting acetogen *Clostridium autoethanogenum*. *Proceedings of the National Academy of Sciences of the United States of America, 117*(23), 13168-13175.

Marcellin, E., Behrendorff, J. B., Nagaraju, S., DeTissera, S., Segovia, S., Palfreyman, R. W., Daniell, J., Licona-Cassani, C., Quek, L. E., Speight, R., Hodson, M. P., Simpson, S. D., Mitchell, W. P., Kopke, M., & Nielsen, L. K. (2016). Low carbon fuels and commodity chemicals from waste gases - systematic approach to understand energy metabolism in a model acetogen. *Green Chemistry, 18*(10), 3020-3028.

Margolin, P. (1967). Genetic polarity in bacteria. *American Naturalist, 101*(920), 301-&.

Martin, M. E., Richter, H., Saha, S., & Angenent, L. T. (2016). Traits of selected *Clostridium* strains for syngas fermentation to ethanol. *Biotechnology and Bioengineering, 113*(3), 531-539.

Mearls, E. B., Olson, D. G., Herring, C. D., & Lynd, L. R. (2015). Development of a regulatable plasmid-based gene expression system for *Clostridium thermocellum*. *Applied Microbiology and Biotechnology, 99*(18), 7589-7599.

Mock, J., Zheng, Y., Mueller, A. P., Ly, S., Tran, L., Segovia, S., Nagaraju, S., Kopke, M., Durre, P., & Thauer, R. K. (2015). Energy conservation associated with ethanol formation from H_2 and CO_2 in *Clostridium autoethanogenum* involving electron bifurcation. *Journal of Bacteriology, 197*(18), 2965-2980.

Molitor, B., Kirchner, K., Henrich, A. W., Schmitz, S., & Rosenbaum, M. A. (2016a). Expanding the molecular toolkit for the homoacetogen *Clostridium ljungdahlii*. *Nature Scientific Reports, 6*, 31518.

Molitor, B., Marcellin, E., & Angenent, L. T. (2017). Overcoming the energetic limitations of syngas fermentation. *Current Opinion in Chemical Biology, 41*, 84-92.

Molitor, B., Richter, H., Martin, M. E., Jensen, R. O., Juminaga, A., Mihalcea, C., & Angenent, L. T. (2016b). Carbon recovery by fermentation of CO-rich off gases - turning steel mills into biorefineries. *Bioresource Technology, 215*, 386-396.

Mordaka, P. M., & Heap, J. T. (2018). Stringency of synthetic promoter sequences in *Clostridium* revealed and circumvented by tuning promoter library mutation rates. *ACS Synthetic Biology, 7*(2), 672-681.

Nagarajan, H., Sahin, M., Nogales, J., Latif, H., Lovley, D. R., Ebrahim, A., & Zengler, K. (2013). Characterizing acetogenic metabolism using a genome-scale metabolic reconstruction of *Clostridium ljungdahlii*. *Microbial Cell Factories, 12*, 118.

Nagaraju, S., Davies, N. K., Walker, D. J., Kopke, M., & Simpson, S. D. (2016). Genome editing of *Clostridium autoethanogenum* using CRISPR/Cas9. *Biotechnology for Biofuels, 9*, 219.

Nakamura, M., Saeki, K., & Takahashi, Y. (1999). Hyperproduction of recombinant ferredoxins in *Escherichia coli* by coexpression of the ORF1-ORF2-*iscS-iscU-iscA-hscB-hscA-fdx*-ORF3 gene cluster. *Journal of Biochemistry, 126*(1), 10-18.

Nariya, H., Miyata, S., Kuwahara, T., & Okabe, A. (2011). Development and characterization of a xylose-inducible gene expression system for *Clostridium perfringens*. *Applied and Environmental Microbiology, 77*(23), 8439-8441.

Novick, R. P. (1987). Plasmid incompatibility. *Microbiol Rev, 51*(4), 381-395.

Oppinger, C., Kremp, F., & Muller, V. (2022). Is reduced ferredoxin the physiological electron donor for MetVF-type methylenetetrahydrofolate reductases in acetogenesis? A hypothesis. *International Microbiology, 25*(1), 75-88.

Pavelka, A., Chovancova, E., & Damborsky, J. (2009). HotSpot Wizard: A web server for identification of hot spots in protein engineering. *Nucleic Acids Research, 37*(Web Server issue), W376-383.

Pavlova, M., Klvana, M., Prokop, Z., Chaloupkova, R., Banas, P., Otyepka, M., Wade, R. C., Tsuda, M., Nagata, Y., & Damborsky, J. (2009). Redesigning dehalogenase access tunnels as a strategy for degrading an anthropogenic substrate. *Nature Chemical Biology, 5*(10), 727-733.

Petschak, S. (2019). Homologous and heterologous overproduction of AOR-Enzymes in *Clostridium ljungdahlii* and *Escherichia coli.* (Master Thesis), Eberhard Karls University Tuebingen, Germany.

Philipps, G., de Vries, S., & Jennewein, S. (2019). Development of a metabolic pathway transfer and genomic integration system for the syngas-fermenting bacterium *Clostridium ljungdahlii*. *Biotechnology for Biofuels, 12*, 112.

Phillips, J. R., Klasson, K. T., Clausen, E. C., & Gaddy, J. L. (1993). Biological production of ethanol from coal synthesis gas - medium development studies. *Applied Biochemistry and Biotechnology, 39*(1), 559-571.

Portnoy, V. A., Bezdan, D., & Zengler, K. (2011). Adaptive laboratory evolution - harnessing the power of biology for metabolic engineering. *Current Opinion in Biotechnology, 22*(4), 590-594.

Purdy, D., O'Keeffe, T. A., Elmore, M., Herbert, M., McLeod, A., Bokori-Brown, M., Ostrowski, A., & Minton, N. P. (2002). Conjugative transfer of clostridial shuttle vectors from *Escherichia coli* to *Clostridium difficile* through circumvention of the restriction barrier. *Molecular Microbiology, 46*(2), 439-452.

Ragsdale, S. W., & Pierce, E. (2008). Acetogenesis and the Wood-Ljungdahl pathway of CO_2 fixation. *Biochimica Et Biophysica Acta-Proteins and Proteomics, 1784*(12), 1873-1898.

Richter, H., Martin, M. E., & Angenent, L. T. (2013). A two-stage continuous fermentation system for conversion of syngas into ethanol. *Energies, 6*(8), 3987-4000.

Richter, H., Molitor, B., Wei, H., Chen, W., Aristilde, L., & Angenent, L. T. (2016). Ethanol production in syngas-fermenting *Clostridium ljungdahlii* is controlled by thermodynamics rather than by enzyme expression. *Energy & Environmental Science, 9*(7), 2392-2399.

Rose, A. S., Bradley, A. R., Valasatava, Y., Duarte, J. M., Prlić, A., & Rose, P. W. (2016). *Web-based molecular graphics for large complexes*. Paper presented at the Proceedings of the 21st International Conference on Web3D Technology.

Rose, A. S., & Hildebrand, P. W. (2015). NGL Viewer: A web application for molecular visualization. *Nucleic Acids Research, 43*(W1), W576-579.

Sambrook, J., Fritsch, E., & Maniatis, T. (1989). Molecular cloning: A laboratory manual. *Cold spring harbor laboratory press*.

Sandberg, T. E., Salazar, M. J., Weng, L. L., Palsson, B. O., & Feist, A. M. (2019). The emergence of adaptive laboratory evolution as an efficient tool for biological discovery and industrial biotechnology. *Metabolic Engineering, 56*, 1-16.

Schlake, T., & Bode, J. (1994). Use of mutated FLP recognition target (FRT) sites for the exchange of expression cassettes at defined chromosomal loci. *Biochemistry, 33*(43), 12746-12751.

Schmidt, T. G., & Skerra, A. (2007). The Strep-tag system for one-step purification and high-affinity detection or capturing of proteins. *Nature Protocols, 2*(6), 1528-1535.

Schmitz, R., Sabra, W., Arbter, P., Hong, Y., Utesch, T., & Zeng, A. P. (2019). Improved electrocompetence and metabolic engineering of *Clostridium pasteurianum* reveals a new regulation pattern of glycerol fermentation. *Engineering in Life Sciences, 19*(6), 412-422.

Schuchmann, K., Chowdhury, N. P., & Muller, V. (2018). Complex multimeric [FeFe] hydrogenases: Biochemistry, physiology and new opportunities for the hydrogen economy. *Frontiers in Microbiology, 9*, 2911.

Schuchmann, K., & Muller, V. (2012). A bacterial electron-bifurcating hydrogenase. *Journal of Biological Chemistry, 287*(37), 31165-31171.

Schuchmann, K., & Muller, V. (2014). Autotrophy at the thermodynamic limit of life: A model for energy conservation in acetogenic bacteria. *Nature Reviews: Microbiology, 12*(12), 809-821.

Schulz, S. (2015). Characterization of the rapid mutagenesis strain *Clostridium ljungdahlii* pMUT2ts under autotrophic growh conditions and generation of auxotrophic mutants. (Bachelor's Thesis), RWTH Aachen University, Aachen.

Schulz, S. (2018). Engineering the metabolism of *Clostridium ljungdahlii* by altering the availability of the aldehyde:ferredoxin oxidoreductase (AOR), a key enzyme in ethanol formation during syngas fermentation*.*), RWTH Aachen University, Aachen.

Shi, X. C., Tremblay, P. L., Wan, L., & Zhang, T. (2021). Improved robustness of microbial electrosynthesis by adaptation of a strict anaerobic microbial catalyst to molecular oxygen. *Science of the Total Environment, 754*, 142440.

Shintani, M., Sanchez, Z. K., & Kimbara, K. (2015). Genomics of microbial plasmids: Classification and identification based on replication and transfer systems and host taxonomy. *Frontiers in Microbiology, 6*, 242.

Sumbalova, L., Stourac, J., Martinek, T., Bednar, D., & Damborsky, J. (2018). HotSpot Wizard 3.0: Web server for automated design of mutations and smart libraries based on sequence input information. *Nucleic Acids Research, 46*(W1), W356-W362.

Sun, X. M., Ren, L. J., Zhao, Q. Y., Ji, X. J., & Huang, H. (2018). Microalgae for the production of lipid and carotenoids: A review with focus on stress regulation and adaptation. *Biotechnology for Biofuels, 11*, 272.

Tan, Y., Liu, J., Liu, Z., & Li, F. (2014). Characterization of two novel butanol dehydrogenases involved in butanol degradation in syngas-utilizing bacterium *Clostridium ljungdahlii* DSM 13528. *Journal of Basic Microbiology, 54*(9), 996-1004.

Tanner, R. S., Miller, L. M., & Yang, D. (1993). *Clostridium ljungdahlii* sp. nov., an acetogenic species in clostridial rRNA homology group I. *International Journal of Systematic Bacteriology, 43*(2), 232-236.

Teng, L., Wang, K., Xu, J., & Xu, C. (2015). Flavin mononucleotide (FMN)-based fluorescent protein (FbFP) as reporter for promoter screening in *Clostridium cellulolyticum*. *Journal of Microbiological Methods, 119*, 37-43.

Tremblay, P. L., Hoglund, D., Koza, A., Bonde, I., & Zhang, T. (2015). Adaptation of the autotrophic acetogen *Sporomusa ovata* to methanol accelerates the conversion of CO_2 to organic products. *Nature Scientific Reports, 5*, 16168.

Tremblay, P. L., Zhang, T., Dar, S. A., Leang, C., & Lovley, D. R. (2012). The Rnf complex of *Clostridium ljungdahlii* is a proton-translocating ferredoxin:NAD^+ oxidoreductase essential for autotrophic growth. *MBio, 4*(1), e00406-00412.

Ueki, T., Nevin, K. P., Woodard, T. L., & Lovley, D. R. (2014). Converting carbon dioxide to butyrate with an engineered strain of *Clostridium ljungdahlii*. *MBio, 5*(5), e01636-01614.

Valgepea, K., de Souza Pinto Lemgruber, R., Abdalla, T., Binos, S., Takemori, N., Takemori, A., Tanaka, Y., Tappel, R., Kopke, M., Simpson, S. D., Nielsen, L. K., & Marcellin, E. (2018). H_2 drives metabolic rearrangements in gas-fermenting *Clostridium autoethanogenum*. *Biotechnology for Biofuels, 11*, 55.

Valgepea, K., de Souza Pinto Lemgruber, R., Meaghan, K., Palfreyman, R. W., Abdalla, T., Heijstra, B. D., Behrendorff, J. B., Tappel, R., Kopke, M., Simpson, S. D., Nielsen, L. K., & Marcellin, E. (2017).

Maintenance of ATP homeostasis triggers metabolic shifts in gas-fermenting acetogens. *Cell Systems, 4*(5), 505-515 e505.

Valgepea, K., Talbo, G., Takemori, N., Takemori, A., Ludwig, C., Mahamkali, V., Mueller, A. P., Tappel, R., Kopke, M., Simpson, S. D., Nielsen, L. K., & Marcellin, E. (2022). Absolute proteome quantification in the gas-fermenting acetogen *Clostridium autoethanogenum*. *mSystems, 7*(2), e0002622.

Walker, D. J. F., & Köpke, M. (2015) Method of producing a recombinant microorganism. WO 2015/116734 Al.

Wang, S., Huang, H., Kahnt, J., Mueller, A. P., Kopke, M., & Thauer, R. K. (2013a). NADP-specific electron-bifurcating [FeFe]-hydrogenase in a functional complex with formate dehydrogenase in *Clostridium autoethanogenum* grown on CO. *Journal of Bacteriology, 195*(19), 4373-4386.

Wang, S., Huang, H., Kahnt, J., & Thauer, R. K. (2013b). A reversible electron-bifurcating ferredoxin- and NAD-dependent [FeFe]-hydrogenase (HydABC) in *Moorella thermoacetica*. *Journal of Bacteriology, 195*(6), 1267-1275.

Wang, Y., Zhang, Z. T., Seo, S. O., Lynn, P., Lu, T., Jin, Y. S., & Blaschek, H. P. (2016). Gene transcription repression in *Clostridium beijerinckii* using CRISPR-dCas9. *Biotechnology and Bioengineering, 113*(12), 2739-2743.

Wasels, F., Jean-Marie, J., Collas, F., Lopez-Contreras, A. M., & Lopes Ferreira, N. (2017). A two-plasmid inducible CRISPR/Cas9 genome editing tool for *Clostridium acetobutylicum*. *Journal of Microbiological Methods, 140*, 5-11.

Wen, Z., Ledesma-Amaro, R., Lin, J., Jiang, Y., & Yang, S. (2019). Improved n-butanol production from *Clostridium cellulovorans* by integrated metabolic and evolutionary engineering. *Applied and Environmental Microbiology, 85*(7).

Westphal, L., Wiechmann, A., Baker, J., Minton, N. P., & Muller, V. (2018). The Rnf complex is an energy-coupled transhydrogenase essential to reversibly link cellular NADH and ferredoxin pools in the acetogen *Acetobacterium woodii*. *Journal of Bacteriology, 200*(21), JB. 00357-00318.

White, H., Feicht, R., Huber, C., Lottspeich, F., & Simon, H. (1991). Purification and some properties of the tungsten-containing carboxylic-acid reductase from *Clostridium formicoaceticum*. *Biological chemistry Hoppe-Seyler, 372*(11), 999-1005.

White, H., Huber, C., Feicht, R., & Simon, H. (1993). On a reversible molybdenum-containing aldehyde oxidoreductase from *Clostridium formicoaceticum*. *Archives of Microbiology, 159*(3), 244-249.

Whitham, J. M., Tirado-Acevedo, O., Chinn, M. S., Pawlak, J. J., & Grunden, A. M. (2015). Metabolic response of *Clostridium ljungdahlii* to oxygen exposure. *Applied and Environmental Microbiology, 81*(24), 8379-8391.

Woolston, B. M., Emerson, D. F., Currie, D. H., & Stephanopoulos, G. (2018). Rediverting carbon flux in *Clostridium ljungdahlii* using CRISPR interference (CRISPRi). *Metabolic Engineering, 48*, 243-253.

Woycechowsky, K. J., Vamvaca, K., & Hilvert, D. (2007). Novel enzymes through design and evolution. *Advances in Enzymology & Related Areas of Molecular Biology, 75*, 241.

Xia, P. F., Casini, I., Schulz, S., Klask, C. M., Angenent, L. T., & Molitor, B. (2020). Reprogramming acetogenic bacteria with CRISPR-targeted base editing *via* deamination. *ACS Synthetic Biology, 9*(8), 2162-2171.

Xie, B. T., Liu, Z. Y., Tian, L., Li, F. L., & Chen, X. H. (2015). Physiological response of *Clostridium ljungdahlii* DSM 13528 of ethanol production under different fermentation conditions. *Bioresource Technology, 177*, 302-307.

Xu, H. J., Liang, C. Y., Chen, X. Y., Xu, J. L., Yu, Q., Zhang, Y., & Yuan, Z. H. (2020). Impact of exogenous acetate on ethanol formation and gene transcription for key enzymes in *Clostridium autoethanogenum* grown on CO. *Biochemical Engineering Journal, 155*.

Xu, T., Li, Y., Shi, Z., Hemme, C. L., Li, Y., Zhu, Y., Van Nostrand, J. D., He, Z., & Zhou, J. (2015). Efficient genome editing in *Clostridium cellulolyticum via* CRISPR-Cas9 nickase. *Applied and Environmental Microbiology, 81*(13), 4423-4431.

Yi, J., Huang, H., Liang, J., Wang, R., Liu, Z., Li, F., & Wang, S. (2021). A heterodimeric reduced-rerredoxin-dependent methylenetetrahydrofolate reductase from syngas-fermenting *Clostridium ljungdahlii*. *Microbiology Spectrum, 9*(2), e0095821.

Zhang, H. Y., Kong, X. D., & Zhang, J. (1999). New strategies of protein engineering - directed evolution of enzyme in *vitro*. *Chinese Science Bulletin, 44*(18), 1641-1648.

Zhang, J., Liu, Y. J., Cui, G. Z., & Cui, Q. (2015). A novel arabinose-inducible genetic operation system developed for *Clostridium cellulolyticum*. *Biotechnology for Biofuels, 8*, 36.

Zhang, T., & Tremblay, P. L. (2018). An adaptive laboratory evolution method to accelerate autotrophic metabolism. *Methods in Molecular Biology, 1671*, 149-161.

Zhao, R., Liu, Y., Zhang, H., Chai, C., Wang, J., Jiang, W., & Gu, Y. (2019). CRISPR-Cas12a-mediated gene deletion and regulation in *Clostridium ljungdahlii* and its application in carbon flux redirection in synthesis gas fermentation. *ACS Synthetic Biology, 8*(10), 2270-2279.

Zhu, H. F., Liu, Z. Y., Zhou, X., Yi, J. H., Lun, Z. M., Wang, S. N., Tang, W. Z., & Li, F. L. (2020). Energy conservation and carbon flux distribution during fermentation of CO or H_2/CO_2 by *Clostridium ljungdahlii*. *Frontiers in Microbiology, 11*(416), 416.